

SYNCRUDE CANADA LTD.  
PROFESSIONAL PAPER 1978-1

A. Kumar, Ph.D.  
Syncrude Canada Ltd.

POLLUTANT DISPERSION IN THE  
PLANETARY BOUNDARY LAYER

Syncrude Canada Ltd., Professional Paper 1978-1

Syncrude's Professional Paper series consists of reports which are not scheduled for publication as Environmental Research Monographs, but which would be of interest to researchers working in related fields outside Syncrude.

## ABSTRACT

Problems associated with the prediction of dispersion of pollutants in the Planetary Boundary Layer (PBL) are investigated using numerical modelling and the available experimental data:

(a) A general model to estimate atmospheric dispersion coefficients for elevated releases and for varying atmospheric stability conditions is presented. The velocity field (PBL model) for the model is either empirically specified or numerically computed from a simplified form of the equations of motion. A set of "new" K-profiles is proposed to model atmospheric turbulence, based on recent experimental evidence and theoretical developments. Finite-difference schemes are used for simulation of the flow on a digital computer.

Results for numerical sigmas compared very well with available experimental curves (such as ASME/BNL, Pasquill-Gifford, Sutton and TVA) and agree qualitatively with previous theoretical studies. However, there are important quantitative differences due to the use of atmospheric stability as a parameter and to the use of variable K-profiles. The sigmas given in this report incorporate effects of elevated releases, cross-wind shear and surface roughness. The results provide a physically realistic extension of the available (experimentally based)  $\sigma$ -graphs and clearly indicate the need for their modifications. The height of the PBL is also introduced as a parameter in the model: this is important if the release height is comparable to the PBL height.

The study indicates that

- (i) cross-wind shear effects on  $\sigma_y$  can not be ignored beyond 4-5km downwind for elevated releases (the numerical value of this depends on atmospheric stability and release height - in general, the

effects are felt much earlier during stable conditions as compared to unstable cases).

- (ii) crosswind shear effects on  $\sigma_y$  are much larger under stable conditions than under unstable conditions.
- (iii) at large downwind distances ( $\sim 100\text{km}$ ) the stable plume disperses more than the unstable plume (for shear cases).
- (iv) increasing surface roughness effects are similar to that of increasing atmospheric instability.

(b) The PBL model uses the same K-profiles as the  $\sigma$ -model and produces independently useful information about the PBL velocity field. The results are compared with the Wangara data. The values of the parameters  $A(\mu)$  and  $B(\mu)$  which arise in the Rossby-number similarity theory are evaluated and found to lie within the limits of experimental data. The model effectively generates the desired velocity profiles.

(c) A numerical analysis of various approximations used in current plume rise theories of wet and dry plume is given. The results show:

- (i) the use of the Boussinesq approximation leads to an overestimate of the plume path and the plume rise, and underestimates the plume radius. An approximate analytical solution showed that this is due to enhanced entrainment (i.e. greater value of entrainment coefficient) in the no Boussinesq approximation case as compared to the Boussinesq approximation.

- (ii) the maximum effect of the Boussinesq approximation on the visible plume length is under unstable and humid atmospheric conditions.
- (iii) horizontal drag effects ( $c_d$ ) have a negligible influence on plume variables.
- (iv) solid particulate matter should not be ignored if the plume is "heavy" ( $\psi > .03$  gm/gm) and the temperature difference between the atmosphere and the plume is small.
- (v) Briggs form of the energy equation is preferred over the Slawson and Csanady form if an approximate form of the Energy equation is used.

(d) An alternative method (referred to as the "area source matching technique") to treat the source term in the numerical solution of convective-diffusion (C-D) equation is proposed and is found to yield results closer to the Gaussian model than the conventional method of using source = source strength (mass/unit time)/(volume of grid).

Main aim of this study was to produce sigmas for elevated releases and to improve our understanding of atmospheric dispersion especially the effects of : (i) elevated releases, (ii) cross-wind shear and (iii) surface roughness.

## ACKNOWLEDGEMENTS

The author wishes to express his sincere, gratitude to Dr. T.M.L. Wigley (Climatic Research Unit, University of East Anglia, Norwich, England), whose suggestions and critical comments were extremely valuable for this work.

This report was cheerfully typed by Miss V. Brecht, Mrs. B. Chiang and Mrs. D. Penney.

## CONTENTS

	<u>PAGE</u>
<i>Abstract</i>	<i>(iv)</i>
<i>Acknowledgements</i>	<i>(vii)</i>
<i>Contents</i>	<i>(viii)</i>
<i>List of Figures</i>	<i>(xi)</i>
<i>List of Tables</i>	<i>(xiv)</i>
<i>Nomenclature</i>	<i>(xv)</i>
 <i>Chapter</i>	
1. <i>Introduction</i>	1
1.1 <i>Scope</i>	1
1.2 <i>General solution methods</i>	2
1.3 <i>Nature of this investigation</i>	4
1.3.1 <i>Comments on the organization of the report</i>	8
1.4 <i>Summary</i>	9
2. <i>Wind Structure in the Planetary Boundary Layer</i>	10
2.1 <i>Literature survey</i>	10
2.2 <i>Numerical model for wind structure</i>	13
2.3 <i>Numerically computed velocity field</i>	23
2.3.1 <i>Comparison with observations</i>	23
2.3.2 <i>Analysis of A and B in Rossby-number similarity theory</i>	28
2.3.3 <i>Numerically generated profiles</i>	32
2.3.4 <i>Comparison of variation of A and B with stability to Wangara data</i>	32
2.3.5 <i>Closure</i>	39
3. <i>Plume rise theory</i>	40
3.1 <i>Literature review</i>	40
3.2 <i>Flow regimes of a plume</i>	41
3.3 <i>Entrainment theory with no Boussinesq Approximation (B.A.)</i>	43
3.4 <i>Approximate forms of energy equations</i>	46
3.5 <i>A simple analytical solution for the NBA case</i>	47

3.6	<i>Numerical results</i>	51
3.6.1	<i>Effects of B.A. on plume growth and on visible plume length</i>	52
3.6.2	<i>Effects of B.A. on the maximum plume rise</i>	56
3.6.3	<i>Effect of horizontal drag coefficients</i>	61
3.6.4	<i>Effects of solid particulate matter</i>	66
3.6.5	<i>Calculation of plume variables using Briggs and Slawson &amp; Csanady forms of the flux of buoyancy</i>	68
4.	<i>Atmospheric diffusion</i>	73
4.1	<i>Literature survey</i>	73
4.1.1	<i>Theoretical approach</i>	73
4.1.2	<i>Current methods for determination of sigmas</i>	77
4.1.3	<i>Wind shear effects</i>	80
4.1.4	<i>Experimental studies</i>	82
4.1.5	<i>Conclusions from literature survey</i>	83
4.2	<i>General background</i>	84
4.2.1	<i>Analysis of Gaussian Dispersion models</i>	84
4.2.2	<i>Calculations for critical concentration</i>	88
4.3	<i>Evaluation of sigmas for elevated continuous releases</i>	91
4.3.1	<i>Mathematical formulation of the problem</i>	91
4.3.2	<i>Numerical scheme</i>	95
4.3.3	<i>Source term as a boundary condition</i>	98
4.3.4	<i>Velocity Profiles</i>	98
	4.3.4.1 <i>Use of empirical relationships</i>	99
	4.3.4.2 <i>Numerical profiles</i>	100
4.3.5	<i>The computer model</i>	101
	4.3.5.1 <i>Input data required for running the computer program</i>	101
4.3.6	<i>Numerical results for sigmas using empirical velocity profiles</i>	102
	4.3.6.1 <i>BNL/ASME dispersion parameters vrs. numerical results</i>	112
	4.3.6.2 <i>Pasquill curves vrs. numerical results</i>	113
	4.3.6.3 <i>TVA dispersion coefficients vrs. numerical curves</i>	114
	4.3.6.4 <i>Sutton coefficients vrs. numerical curves</i>	115

4.3.6.5	Conclusion of 4.3.6.1 to 4.3.6.4	116
4.3.6.6	Predicted sigmas for arbitrary release height	116
4.3.6.7	Cross-Wind shear effects	123
4.3.7	Numerical results for sigmas using numerically computed velocity field	125
4.3.7.1	Numerical and experimental sigmas	126
4.3.7.2	The effect of release height on dispersion coefficients	135
4.3.7.3	Effects of surface roughness, $z_0$	140
4.3.7.4	Application of $\sigma$ -curves to buoyant and non-buoyant plumes, and to limited mixing conditions	146
4.3.7.5	General Assessment of experimental data and numerical results	148
4.3.8	Solution of C - D equation	150
4.3.8.1	Current method of treating source term Q	150
4.3.8.2	Proposed method to treat source term Q	151
4.3.8.3	Comparison of numerical solutions and Gaussian model	151
5.	Concluding Remarks	155
Appendix - A	An Inclined model for a neutral atmosphere for maximum ground level concentration	159
Appendix - B	Thomas Algorithm	161
Appendix - C	Comparison of sigmas for constant diffusivity and constant with field case	162
Appendix - D	A discussion on abrupt slope changes in numerically computed $\sigma_y$ curves	163
Appendix - E	Numerical scheme for the solution of 3-D C-D equation	167
References		173

## LIST OF FIGURES

		Page
1.1	An overview of the research problem	5
2.1	Eddy viscosity profiles used for the solution	16
2.2	Band structure matrix	22
2.3	Comparison of Wangara data and numerical solution for a near-neutral atmosphere ( $(u_{.15}-u)/u_*$ )	25
2.4	Comparison of Wangara data and numerical solution for a near-neutral atmosphere ( $(v-v_{.15})/u_*$ )	26
2.5	Comparison of Wangara data and analytical solutions (from Misra 1976)	27
2.6	Velocity profiles for a baroclinic boundary layer (near-neutral case)	33
2.7	Velocity profiles for an unstable baroclinic atmosphere	34
2.8	Velocity profiles for a stable baroclinic atmosphere	35
2.9	Wind hodograph for varying surface roughness	37
3.1	Flow regimes of a plume	42
3.2	Comparison of plume trajectories in BA and NBA cases (Volcano)	54
3.3	Comparison of plume trajectories in BA and NBA cases (Cooling tower and industrial stack)	55
3.4	Ratio of maximum plume rise for wet and dry plumes for varying atmospheric stability (Industrial stack)	59
3.5	Ratio of maximum plume rise for wet and dry plumes for varying atmospheric stability (Cooling tower)	60

3.6	Variation of ratio of the downwind distances to the maximum rise of wet plume ( $x_{ms}$ ) and a corresponding dry plume ( $x_{md}$ ) with atmospheric stability	62
3.7	Variation of $C_d$ on plume trajectory	63
3.8	Nature of error term in S & C form	71
4.0	Plume element under a typical cross-wind shear condition	94
4.1	Comparison of numerical and experimental $\sigma_y$ curves for a near-neutral atmosphere	103
4.2	Comparison of numerical and experimental $\sigma_z$ curves for a near-neutral atmosphere	104
4.3	Comparison of numerical and experimental $\sigma_y$ curves for a unstable atmosphere	105
4.4	Comparison of numerical and experimental $\sigma_y$ curves for a stable atmosphere	106
4.5	Comparison of numerical and experimental $\sigma_z$ curves for a unstable atmosphere	107
4.6	Comparison of numerical and experimental $\sigma_z$ curves for a stable atmosphere	108
4.7	$\sigma_y$ for elevated releases in a unstable atmosphere	119
4.8	$\sigma_y$ for elevated releases in a stable atmosphere	120
4.9	$\sigma_y$ for elevated releases in a neutral atmosphere	121
4.10	$\sigma_z$ for elevated releases	122
4.11	Velocity profiles for numerical $\sigma$ -calculations	127
4.12	Comparison of experimental and numerical $\sigma_y$ using numerical velocity profiles (near-neutral atmosphere)	128
4.13	Comparison of experimental and numerical $\sigma_z$ using numerical velocity profiles (near-neutral atmosphere)	129

4.14	Comparison of experimental and numerical velocity profiles (unstable atmosphere)	$\sigma_y$ using numerical	130
4.15	Comparison of experimental and numerical velocity profiles (stable atmosphere)	$\sigma_y$ using numerical	131
4.16	Comparison of experimental and numerical velocity profiles (stable atmosphere)	$\sigma_z$ using numerical	131
4.17	Comparison of experimental and numerical velocity profiles (unstable atmosphere)	$\sigma_z$ using numerical	133
4.18	$\sigma_y$ for elevated releases using numerical velocity profiles (near-neutral atmosphere)		136
4.19	$\sigma_y$ for elevated releases using numerical velocity profiles (unstable atmosphere)		137
4.20	$\sigma_y$ for elevated releases using numerical velocity profiles (stable atmosphere)		138
4.21	$\sigma_z$ for elevated releases using numerical velocity profiles		139
4.22	Effect of surface roughness on $\sigma_y$ for a 50 m release height (near-neutral atmosphere)		141
4.23	Effect of surface roughness on $\sigma_y$ for a 500 m release height (near-neutral atmosphere)		142
4.24	$\sigma_z$ for varying surface roughness: (near-neutral atmosphere: h=50m)		143
4.25	$\sigma_z$ for varying surface roughness (near-neutral atmosphere: h=500m)		144
4.26	Velocity profiles for varying surface roughness conditions		145
4.27	Source for effective stack height and matching models		147
4.28	Comparison of numerical solutions with Pasquill/Gaussian plume model		152
D-1	Matrix for of equations		172

LIST OF TABLES

	Page	
2.1	Values of A and B in $\ln R_0 = A - \ln(U_*/V_g) + \left(\frac{K^2 V_g^2}{U_*^2} - B^2\right)^{1/2}$	30
2.2	Input data for numerical velocity profiles	36
2.3	Experimental and numerical values of A( $\mu$ ) and B( $\mu$ )	38
3.1	Effect of Boussinesq Approximation on plume growth	53
3.2	Comparison of visible plume length	57
3.3	Effect of drag coefficient on plume variables	64
3.4	Effect of solid particulate matter	67
3.5	Comparison of plume trajectory for three forms of energy equations	72
4.1	Summary of atmospheric diffusion coefficients	87
4.2	Comparison of maximum ground level concentration and its position using available $\sigma_y(x)$ and $\sigma_z(x)$ formulas	89
4.3	Input variables for $\sigma$ computations	109
4.4	Input variables for "total" numerical $\sigma$ -curves	134
4.5	Data for C-D equation solution using ADI scheme	153
D.1	Approximate Values of s in $\sigma_y \sim x^s$ for Cross-Wind Shear Dominated Region	165

## NOMENCLATURE

### Velocity Profiles:

A } B }	Constants as used in Rossby Number Similarity Theory (see eq. 2.1)
$C_g$	Geostrophic Drag Coefficient
c } D }	See equation (2.20)
f	Coriolis Parameter
h	Height of the Surface Layer
H	Height of PBL
k	Von-Karman's Constant
$K_o$	Eddy-viscosity at the Top of Surface Layer (see eq. 2.19)
K	Eddy-viscosity
$\ell$	Prandtl Mixing Length
L	Obukhov Length
N	Grid Point Corresponding to the Top of PBL
p	Exponent in Equation (2.13)
P	Pressure
$R_o$	Rossby Number ( $= V_g / z_o f$ )
u, v	Components of the Velocity Field in x and y Directions
$U_*$	Friction Velocity
$V_g$	Geostrophic Velocity
$\hat{z}$	Dimensionless $z (= fz / U_*)$
$z_o$	Surface Roughness

Greek Symbols:

$\alpha$	Cross-isobar Angle
$\Gamma$	Lapse Rate
$\tau_x, \tau_y$	Stress Components in x and y Directions ( $\rho\tau$ is true stress)
$\rho$	Density
$\nu$	Coefficient of Molecular Viscosity
$\nu + \delta$	Residual Stress at the Top of PBL
$\zeta$	See equation (2.22)

Plume Rise Theory:

$C_p$	Specific Heat at Constant Pressure (1.005 Joules/gm/ $o_k$ )
$C_d$	Drag Coefficient
$g$	Acceleration due to Gravity (9.8 m/sec <sup>2</sup> )
$G$	Atmospheric Moisture Gradient ( $G = \frac{\partial q_a}{\partial Z}$ )
$L$	Latent Heat (2500 Joules/gm)
$N$	Vaisala Frequency ( $N^2 = \frac{g}{T_a} \frac{\partial \theta_a}{\partial Z}$ )
$P$	Hydrostatic Pressure
$q$	Specific Humidity (gms/gm)
$R$	"Effective" Plume Radius
$t$	Time
$T$	Temperature ( $o_k$ )
$U$	Wind Speed
$V_p$	Centreline Plume Velocity ( $\vec{V}_p = u_x \vec{i} + w \vec{k}$ )
$v_e$	Entrainment Velocity
$u_x$	Horizontal Component of $V_p$
$w$	Vertical Component of $V_p$

$W_E$  Vertical Velocity of an Artificial Velocity Field  
 (see equation 3.4)  
 $x$  Horizontal Plume Coordinates Measured from the Top of Stack  
 $z$  Vertical Plume Coordinate Measured from Top of Stack

Greek Symbols:

$\alpha$  Entrainment Parameter  
 $\sigma$  Liquid Water Content (gms/gm)  
 $\psi$  Solid Matter Content (gms/gm)  
 $\rho$  Density

Subscripts:

$p$  Plume Property (exception  $C_p$ )  
 $a$  Atmospheric Property  
 $\nabla$  Excess of a Plume Variable over its Atmospheric Value

Superscripts:

$*$  Virtual Temperature

Atmospheric Diffusion:\*

$a$  }  
 $b$  } See equation (4.9)  
 $C_y$  }  
 $C_z$  } Virtual Diffusion Coefficients (equation 4.35)  
 $C$  Pollutant Concentration  
 $C^0$  }  
 $C^1$  } Zero, First and Second Moments of Concentration  
 $C^2$  }

c d	} See equation (4.9)
$h_s$	Source Height ("Effective Stack Height" = $h_t + \Delta h$ )
$h_t$	True Stack Height
$K_x, K_y, K_z$	Eddy Diffusivity Constants
L	Obukhov Length
n	Exponent of U (see equation 4.10)
$\bar{u}, U$	Mean Wind Speed
$U_{critical}$	Critical Wind Speed
$U_*$	Friction Velocity
$\vec{V}$	Wind Velocity Field ( $\vec{V} = \bar{u} \cdot \vec{i} + v \cdot \vec{j} + w \cdot \vec{k}$ )
$\vec{q}$	Turbulent Mass Flux
q	Pollutant Mass Emitted Per Unit Time
Q	Pollutant Source Strength (mass/unit time/unit volume)
$Q_a$	Pollutant Ground Absorption Rate
$R(\xi)$	Langrangian Auto Correlation
t	Time (secs)
$t_L$	Langrangian Time Scale
$x_{max}$	Point of Maximum Ground Level Concentration
$z_o$	Surface Roughness

Greek Symbols:

$\sigma_y$	Standard Deviation in y-direction (= $cx^d$ )
$\sigma_z$	Standard Deviation in z-direction (= $ax^b$ )
$\Delta h$	Plume Rise

\* Also See Symbols used in Velocity Profiles and Plume Rise Theory Section

## CHAPTER 1

### INTRODUCTION

#### 1.1 Scope:

The detailed investigation of atmospheric diffusion processes had its beginning during the First World War in the prediction of the spread of smoke and poison gas clouds. Predictive tools were devised based on known solutions of the diffusion equation. Since that time the limitations of these early approaches have led to the development of considerably more sophisticated methods.

With the continued mechanization and industrialization of our society, every year more and more pollutants are added to the environment. Although most air pollutants are removed from the atmosphere by natural cleaning processes, in many cases (e.g.  $\text{CO}_2$ , sulphur compounds) removal rates are less than input rates. For example, it has been estimated that for sulphur dioxide the residence time is about 43 days. Since this is a large value, the result is increased concentration of  $\text{SO}_2$  over a longer span of time in the atmosphere resulting in adverse effects on human health, plant life and animal life.

Severe pollution episodes occurring in the Meuse Valley of Belgium in 1930, Donora, Pa., in 1948, London (England) in 1952, 1957 and 1962, New York in 1953, 1963 and 1966, and in a number of other large cities around the world have drawn considerable public attention.

To prevent further severe pollution episodes, attempts are being made to monitor the pollutants which are likely to affect our society in one way or the other. As a result, a set of standards has been developed, by the appropriate government agencies, which are known as Emission

Standards (specified as rate of discharge or concentration of a pollutant) and Air Quality Standards (based on the effects of pollutants with an "exposure time").

A monitoring program, in general, involves prediction, measurement, control and eventually elimination of pollutants. This research work is concentrated on the prediction aspect. The study deals specifically with plume behaviour and the dispersion of atmospheric pollutants from elevated sources in the planetary boundary layer (PBL or "Ekman layer").

The practical importance of this analysis is becoming more and more evident in cases where "tougher" emission control regulations are met (by industries) by using the concept of high level releases (i.e. discharging pollutants high in the Ekman layer and thereby decreasing the ground level concentration of the gas discharged). The emissions from such elevated stacks diffuse within the PBL and require the modelling of physical processes which are different from those for low-level releases.

## 1.2 General Solution Methods:

Basically, the problem of dispersion of atmospheric pollutants has been treated in two ways -- either using an Eulerian description or a Lagrangian description of turbulent dispersion. In the Eulerian point of view, the diffusion equation is derived from a consideration of concentration and flux at fixed points in space. The specification of fluxes using a "K-theory" is a commonly used practice in Fluid Dynamics. In this way the turbulence is defined as a property of the fluid rather than as a property of the flow. Since turbulence is not a feature of fluids but of fluid flows, the idea of using a diffusion coefficient (K) to describe the effects of turbulence is rather misleading. However, the mathematical treatment

of the problem becomes easier.

In the Lagrangian viewpoint, attention is paid to the history of random movements of diffusing particles. The statistical properties of the motion of an ensemble of like particles are then used to derive practical dispersion results. This forms the basis for the widely-used "Gaussian Plume Model". A Gaussian plume model may also be derived from a constant 'K' solution to the diffusion equation. The major limitation of this model (as presently used) is the inherent assumption that the wind field and the statistical coefficients ( $\sigma$ 's) are independent of height above the ground. Thus, for example,  $\sigma$ 's used for computation of dispersion from elevated sources are strictly valid only for near ground level releases. Further, Gaussian Plume Models which have been used for years in making critical air quality decisions are inadequate for the large power plants that are now under construction (see for a discussion Carpenter et al (1971)).

An alternative approach is to use the three dimensional convective-diffusion (C - D) equation with an appropriate velocity field and empirical values of the turbulent diffusion coefficients ("K-theory"). In many ways the available K-theory approach is more general and flexible than Gaussian models that are presently used and allows one to study the pollutant distributions from different kinds of sources under arbitrary boundary conditions and environmental characteristics.

It is considered that a single diffusion model for prediction purposes is not adequate for each and every situation encountered in day to day use. Therefore, our approach includes the refinement of the existing models based on the inclusions of additional physics and recent experimental evidence. Also, whenever possible, approximate analytical solutions (in preference to completely numerical solutions) are given to

gain confidence in the new solutions.

### 1.3 Nature of this Investigation

An overview of the research problem is given in Figure 1.1. The significance of § in this figure is to inform the reader that solving atmospheric diffusion problems using the K-theory approach is much more expensive than solving it by the  $\sigma$ -theory route with appropriate approximations.

The aims of the study are:

- (i) to produce  $\sigma$  data for elevated sources, and to produce data which are more than just locally useful (a practical point)
- (ii) to improve our understanding of atmospheric dispersion especially the effects of: a) elevated releases and b) cross-wind shear effects and c) surface roughness,
- (iii) to examine some of the approximations used in plume rise theory: viz. the Boussinesq approximation (B.A.); the neglect of a drag coefficient; the effect of particulate mass loading and different forms of the energy equation.
- (iv) to evaluate the parameters A and B which arise in Rossby-number similarity theory (a by-product of the study).

As shown in figure 1.1, a modular approach is adopted for the solution of the problem. The basic nature of the problem and the method used in this report are briefly discussed here:

#### (a) Estimation of Atmospheric Dispersion Coefficients ( $\sigma$ s):

For practical use of  $\sigma$ s in dispersion calculations, one must determine their accurate numerical values. In the case of a future power plant such data are used to study the power plant's possible impact on air

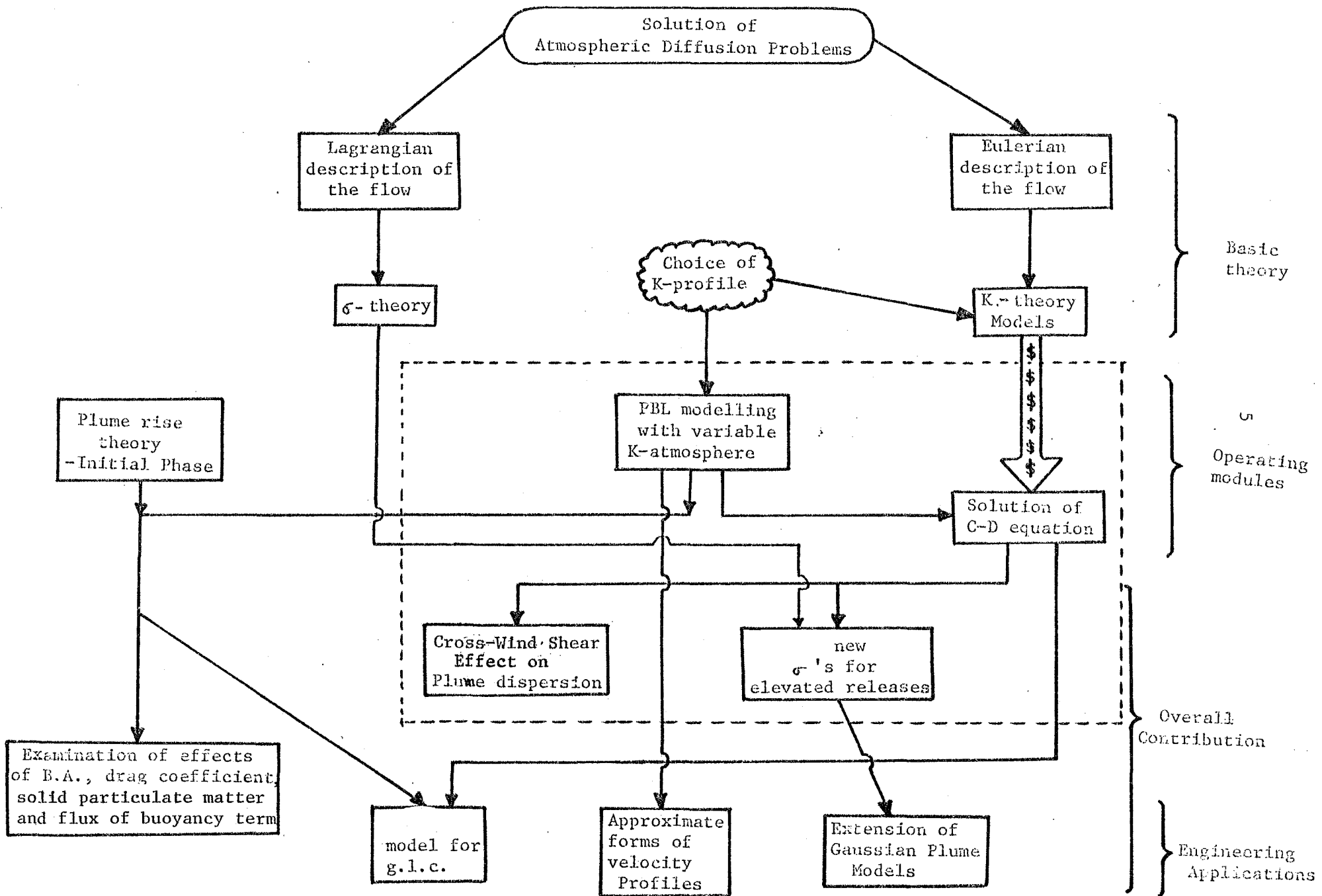


Figure 1.1: AN OVERVIEW OF THE RESEARCH PROBLEM

quality by considering factors such as; behaviour of effluents, maximum ground level concentration and concentration patterns.  $\sigma$ -information also forms the basis of many other management decisions - for example plant location - site selection, functioning of stacks, stack height, monitor locations, and the removal of radioactive material in the event of a loss in a nuclear plant.

Quite often, only one of many available  $\sigma$ -curves (obtained via field experiments using ground level release, or, at most, a single release height) is employed during the impact analysis process. The  $\sigma$ -curves for elevated releases obtained by TVA and Brookhaven National Laboratory are not widely used as these are usually considered to be of site-specific value.

An overestimation or an underestimation of sigmas directly affects the amount of ground level concentration and their inaccurate numerical value can therefore lead to pollutant concentrations greater than otherwise anticipated in a particular area. Further, decisions based on  $\sigma$ -data may force an industrial complex to build a new stack or to add new air pollution cleaning equipment to existing facilities thus increasing production cost (for example in Canada and U.S.A. steel industries and sulphur extraction plants).

From a practical point of view, it seems essential to have a general method to estimate diffusion coefficients from available meteorological data, or even from a general knowledge of a source area. This type of model may eventually eliminate the need for expensive field

experiments (once K-profiles are completely known and understood) except when a verification of theoretical results is required under new meteorological or topographical conditions.

As shown in Figure 1.1, one may obtain new sigmas for elevated releases (see Chapter - 4) by solving the C-D equation using an appropriate velocity field (obtained by PBL modelling), with a prespecified K-profile.

In this study, using the simplified equations of motion (Reynolds equations) and an appropriate model of turbulence, the velocity field is computed for various atmospheric conditions (using a finite-difference method). The flow is assumed to be steady and horizontal in nature. The C-D equation is solved by using the moment-concentration method to yield sigmas. By comparing the numerical results for ground level and high level releases with existing  $\sigma$ -curves, new sigmas are predicted for arbitrary release heights (Chapter - 4). Predicted sigmas also allow us to study cross-wind shear effects on plume dispersion.

(b) Examination of Effects of the Boussinesq Approximation, Horizontal Drag Coefficient and Solid Particulate Matter:

The equations of conservation of mass, momentum and energy are used to describe plume behaviour during its "initial phase" of growth when the plume's own turbulence dominates the mixing process. An existing model (see for example Wigley and Slawson (1975)) is extended to include the effects of density changes (Boussinesq Approximation), hydrostatic pressure field, solid matter content and solid-body drag effect.

The Boussinesq approximation is strictly valid only for that part of a plume which is weakly buoyant; i.e. where the density of the plume deviates very little from the density of the surrounding atmosphere. The pressure field is computed more accurately by solving the hydrostatic equation. The suspended solid matter may be important in the case of a plume from a cement plant or the cases where solid particle collectors (e.g. precipitators) are not used. Moreover, inclusion of this variable may be helpful in estimating the difference between field observations obtained by photographic techniques where solid particle collecting devices are shut down in order to obtain a good picture of the plume, and on actual plume trajectory. The drag term on the diffusing plume element may be important in the initial development of the plume trajectory.

In the energy (i.e. heat) conservation equation two different approximations to the flux of buoyancy have been used in the literature. These are referred to here as the Briggs, and Slawson and Csanady (S & C) forms. The relative accuracy of these two forms is examined by comparing numerical solutions of the equations using these forms with the solution obtained using the complete equations. The Briggs and S & C forms are alternative ways of expressing the equations which include the B.A. The complete equations are referred to as the N.B.A. case. Attempts are also made to draw qualitative conclusions from analytical solutions of the plume rise equations in the B.A. and N.B.A. cases (Chapter - 3), and in the case where solid particulate matter is included as a variable.

### 1.3.1 Comments on the Organization of the Report:

The problem under consideration really covers three distinct topics (wind profiles in the PBL, Plume rise theory, and Atmospheric diffusion) which could all be considered separately. Therefore, the need for Chapter - 2 (wind profiles in the PBL) and Chapter - 3 (Plume rise theory) is as an input into the diffusion model (Chapter - 4). One of the aims was to use the K-theory to predict wind profiles and diffusion: a self-consistent and self-contained model. At the same time the numerical diffusion model was designed to accept other wind profile input data. The plume rise part was needed in order to account for buoyancy effects without having to develop a diffusion model which did this - i.e. one which allowed the diffusion process to change from self-generated to atmospheric turbulence (Chapter - 4: section 4.3.8).

### 1.4 Summary

The original contributions of this study are the development of a general model to obtain sigmas for elevated releases (i.e. a synthesis and extension of Gaussian Plume models); the study of cross-wind shear effects on plume dispersion with arbitrary atmospheric stability, and the extension and analysis of plume rise models to examine various approximations commonly made (given in Chapters 2, 3 and 4). It is hoped that this work will be useful for ongoing environmental assessment and appraisal studies.

## CHAPTER 2

## WIND STRUCTURE IN THE PLANETARY BOUNDARY LAYER

2.1 Literature Survey:

The main characteristic of the PBL is that the eddy stress has approximately the same order of magnitude as the pressure and coriolis forces. There are three basic approaches to determine the velocity field of a Planetary Boundary layer each providing solutions of varying degrees of accuracy.

- (a) Analytical Solutions
- (b) Similarity Methods
- (c) Numerical Solutions

(a) Ekman, in 1905, solved the equation of motion for the steady state and constant diffusivity case eliminating nonlinear inertial terms. Ekman's work concerned the oceanic boundary layer. This classic work showed that the wind direction and speed changed according to the "Ekman spiral". Generalizations of Ekman's work to variable diffusivity cases are discussed by Brown (1974).

(b) In similarity methods concepts of dimensional analysis and similarity arguments are applied to the flow equations obtained without using any closure assumption (i.e. K-theory or a similar model of turbulence). The wall law and velocity defect law of fluid flow may then be used to obtain the results of practical interest. The expressions which are most commonly referred to in the literature are

$$\ell_n \frac{U_*}{V_g} = A - \ell_n \frac{V_g}{f z_0} + \left( \frac{k^2 V_g^2}{U_*^2} - B^2 \right)^{\frac{1}{2}} \quad (2.1)$$

(known as the Geostrophic Drag Law)

and

$$\sin \alpha = \frac{B}{k} \frac{U_*}{Vg} \quad (2.2)$$

where  $U_*$  and  $Vg$  are the friction velocity and geostrophic (i.e. free field) velocity;  $k$  is Von-Karman's constant;  $z_0$  is the surface roughness;  $f$  is the coriolis parameter;  $\frac{Vg}{fz_0}$  is the surface Rossby number  $\alpha$  is the cross-isobar angle; and  $A$  and  $B$  are constants and functions of atmospheric stability.

These equations have been derived using various theories and physical arguments by a number of researchers (Blackadar and Tennekes (1968), Gill (1967), Csanady (1967), Kazanskii and Monin (1960)). Csanady (1972) has extended the analysis to the diabatic layer (i.e.  $\Gamma_{ad} \neq \Gamma$  where,  $\Gamma = \text{lapse rate} = -\frac{dT}{dz}$  and  $\Gamma_{ad} = g/c_{p_d}$  is the dry adiabatic lapse rate). Wide variations are reported in the observed values of  $A$  and  $B$  even for a neutral case ( $\Gamma = \Gamma_{ad}$ ). Clarke (1970) has calculated these constants from experimental data and added a thermal stratification factor and found considerable variation in the neighbourhood of near-neutral conditions. There is still no agreement for the values of  $A$  and  $B$ , and further studies (experimental as well as numerical) are required to resolve this issue.

(c) A variety of numerical solutions are available in the literature based on different models of turbulence. In most of these solutions, attempts are made to compute space-time variations of the various variables (wind, temperature, moisture) which provide a description of the PBL.

The solution has been attempted in two ways using K-theory. One obvious way is the specification of K-profiles: this is basically the method used by early works in attempting to obtain analytical solutions.

Another way is to specify K through some other variables (such as Prandtl mixing length ( $\ell$ ) and/or the turbulent kinetic energy density) and numerically solving the new set of equations. It has been argued that the second approach is easier and more realistic than the direct specification of K so that the second route is better than the first one. However, with the available information (experimental, numerical and theoretical), the uncertainty in the direct specification of K is, at least, of the same order as the uncertainty in the specification of any other turbulence parameter.

Blackadar (1962), Blackadar and Ching (1965), Estoque and Bhumralkar (1970), Taylor (1969), Taylor and Delage (1971), Huang (1975) and others have obtained a steady state solution (numerical) for the horizontal PBL using Prandtl's mixing length concept (1932) to specify the K-profile.

$$K = \ell^2 \left[ \left( \frac{\partial u}{\partial z} \right)^2 + \left( \frac{\partial v}{\partial z} \right)^2 \right]^{1/2} \quad (2.3)$$

Several expressions for the variation of  $\ell$  with height have been used.

Examples are:

Blackdar (1962):

$$\ell = \frac{\kappa z}{1 + \frac{\kappa z}{\lambda}} \quad \text{where,} \quad \lambda = \frac{27 V_g \times 10^{-5}}{f}$$

Ohmstede and Appleby (1964):

$$\ell = \lambda \left[ 1 - \exp \left( - \frac{\kappa z}{\lambda} \right) \right] \quad \text{where,} \quad \lambda \text{ is as above}$$

Lettau (1962):

$$\ell = \frac{\kappa z}{1 + \left(\frac{z}{z_m}\right)^{5/4}} \quad \text{where, } z_m = \frac{736 U_*^* \cdot 10^{-4}}{f}$$

To include the effects of buoyancy (i.e. buoyancy generated turbulence as opposed to mechanically generated turbulence), Blackadar and Ching (1965) have suggested the following

$$K_{\text{new}} = \left( \kappa \left| \frac{\partial \vec{v}}{\partial z} \right|^2 + \frac{\gamma g H}{\rho c_p T} \right)^{1/3} \ell^{4/3}$$

$$\ell = \frac{\kappa(z + z_0)}{1 + \frac{1480 f z}{Vg}}$$

where,  $\gamma$  is a constant lying between 7 and 15 and  $H$  is turbulent heat flux (assumed constant with height).

Numerical solutions for the horizontal time dependent PBL with varying surface temperature have been obtained by Estoque (1963), Krishna (1968), Sasamori (1970) and others. 2-D unsteady-state solutions have been reported by Estoque and Bhumralkar (1970), Wagner (1966), Taylor (1969) and others. Deardorff (1970, 1972, 1973) has obtained the solutions for the three dimensional case by using an energy equation for  $K$ -specification. Higher order closure models for turbulent flows are also used by Donaldson (1973), Wyngaard and Coté (1974) and Lumley and Khajeh-Nouri (1975). Here, conservation equations for the turbulent fluxes are used along with the mean field equations with the hope of obtaining better field predictions and more detailed information about the turbulent structure of the PBL.

## 2.2 Numerical Model for Wind Structure:

The model presented in this section is based on a simplified form of Reynolds equations. It should be kept in mind that the PBL is a

turbulent boundary layer, and with the present knowledge a rigorous mathematical theory for the wind structure is not "yet" possible. This type of model is not suitable for weather forecasting or large scale meteorological work since it incorporates a number of assumptions which are not valid under these circumstances (see Holton, 1972 and Haltiner and Martin, 1957).

The basic difference between this model and the existing models is that a complete solution of PBL for a baroclinic atmosphere (inner as well as outer layer) is presented based on direct specification of K-profiles (see literature survey for further discussion). The profiles are consistent with the diffusion model ( $\sigma$ -generator) in that the same K-profiles are used for both. To the author's knowledge no other model has this internal consistency.

The steady-state boundary layer equations for the PBL may be written as

$$\frac{\partial \tau_x}{\partial z} + fv = \frac{1}{\rho} \frac{\partial P}{\partial x} \quad (2.4)$$

$$\frac{\partial \tau_y}{\partial z} - fu = \frac{1}{\rho} \frac{\partial P}{\partial y} \quad (2.5)$$

where, the components of the "stress"  $\tau$  are expressed as

$$\tau_x = K \frac{\partial u}{\partial z} \quad (2.6)$$

$$\tau_y = K \frac{\partial v}{\partial z} \quad (2.7)$$

(The true stress is  $\rho\tau$ . An extensive theoretical analysis of the Boussinesq approximation shows that it can be applied safely to the atmosphere (Spiegel and Veronis (1960) i.e.  $\frac{\partial \rho}{\partial z}$  terms can be neglected).  $\frac{\partial P}{\partial x}$  and  $\frac{\partial P}{\partial y}$ , the pressure gradients in the X and Y directions, can be related to the

geostrophic wind  $V_g$  by the expressions

$$-f V_g = -\frac{1}{\rho} \frac{\partial P}{\partial x} \quad (2.8)$$

$$f U_g = -\frac{1}{\rho} \frac{\partial P}{\partial y} \quad (2.9)$$

combining the above equations, one obtains

$$\frac{\partial \tau_x}{\partial z} = -f (v - V_g) \quad (2.10)$$

$$\frac{\partial \tau_y}{\partial z} = f (u - U_g) \quad (2.11)$$

The appropriate boundary conditions\* are as follows:

$$\begin{aligned} z = z_0 & \quad u = 0, \quad v = 0 \\ z = H \# & \quad u = U_g, \quad v = V_g \end{aligned} \quad (2.12)$$

$z_0$  and  $H$  are the roughness length and the height of the PBL measured from the ground.

In order to solve equation (2.6), (2.7), (2.10), and (2.11) the  $K$ -profiles (i.e.  $K = K(z)$ ) must be specified\*\*. In this report the following profile will be used (see Figure 2.1 and the following discussion):

\* Note that sometimes it is not possible to satisfy the condition at the upper boundary because of the choice of  $K$ -profile or the definition of  $K$  itself. An alternative boundary condition must then be used (e.g.  $\tau = 0$  at  $z = H$  : used by Misra (1975) for an analytical solution.)

\*\* A summary of  $K$ -profiles appearing in the literature during 1905 to 1972 is given by Wipperman (1973). He classifies the profiles into two categories: the first contains a list of 23 profiles which are expressed in terms of  $z$  and the second tabulates 13 models based on a hypothesis of the mixing length (indirect use of  $K$ -profiles).

# The difficulties in satisfying this boundary condition during a numerical solution are: (i) sudden change of velocity in adjacent layers and (ii) to obtain exact values of velocity at  $z = H$ . The numerical scheme used in this thesis overcome these difficulties.

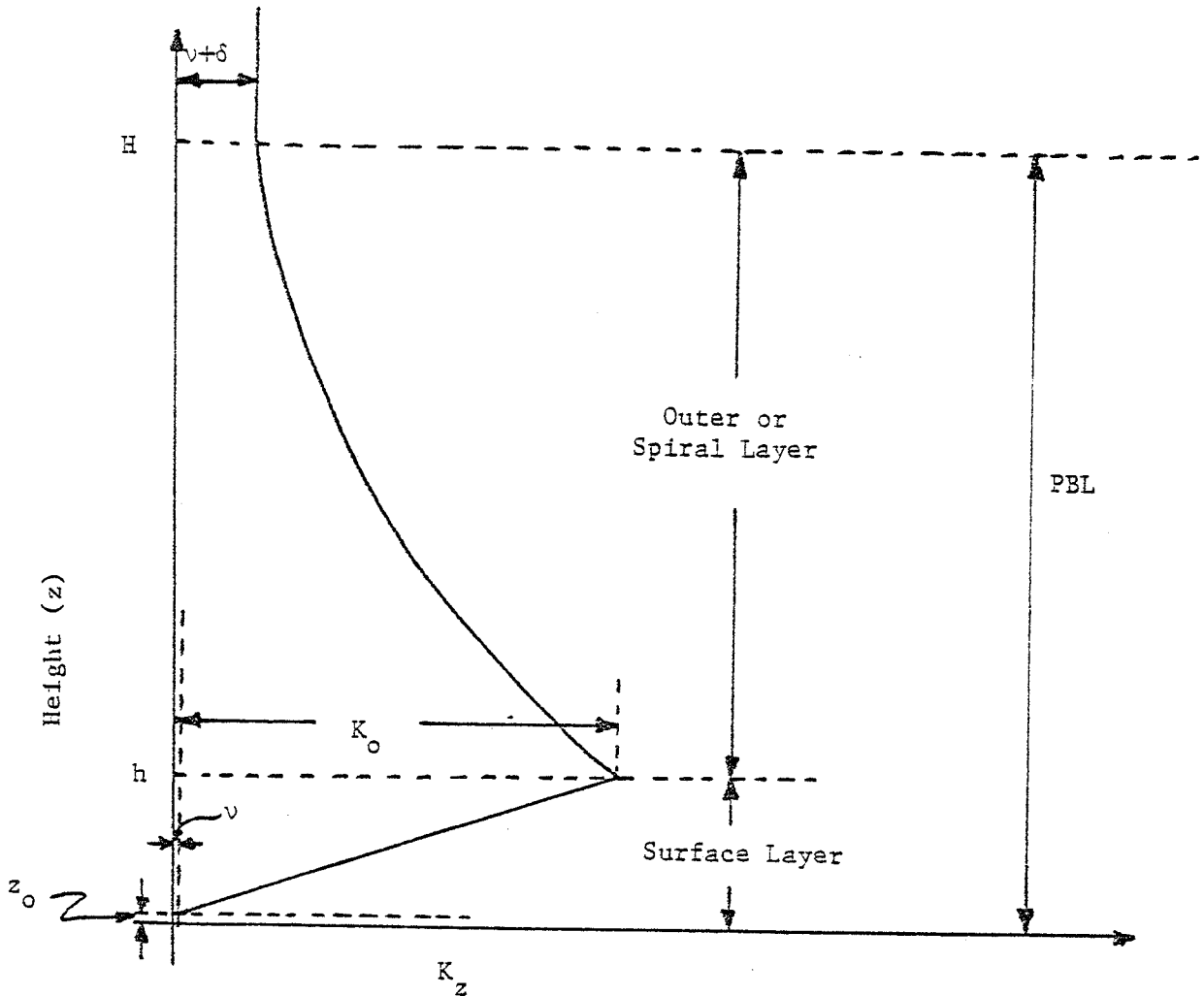


Figure 2.1: EDDY VISCOSITY PROFILES USED FOR THE SOLUTION

(Note: The values of  $h$  and  $H$  used in this thesis are subjective estimates. Further, Constant  $K$  model may not be applicable to small cloud sizes i.e. cloud sizes compared to the turbulence scale. Batchelor (1950) pointed out that for diffusing clouds of a size less than the large energy containing eddy sizes, the scale length should refer to the cloud size rather than the eddy size.)

$$\begin{aligned}
K &= \nu & 0 \leq z \leq z_0 \\
K &= \nu + K_0 (z/h) & z_0 \leq z \leq h \\
K &= \nu + \delta + (K_0 - \delta) \left(1 - \frac{z-h}{H-h}\right)^p & h \leq z \leq H \\
K &= \nu + \delta & z \geq H
\end{aligned}
\tag{2.13}$$

$K_0$ ,  $p$  and  $\delta$  are assumed to be functions of atmospheric stability.  $\nu$  is the coefficient of molecular viscosity for air and  $h$  is the height of the surface layer.

This is a realistic and fairly flexible profile. It agrees well with limited observations in the atmosphere (see Moore, 1975 and Clarke, 1970) and with wind tunnel data of Howroyd and Slawson (1975). This profile is also consistent with the following known facts:

- (i)  $K$  varies approximately linearly near the surface and attains a small constant value at the top of the PBL.
- (ii)  $K$  is composed of molecular and turbulent components, the latter dominating over most of the PBL.

The parameters  $p$ ,  $\delta$  and  $K_0$  can be estimated using the following:

- (1)  $p$  lies between 1 and 2:  $p \geq 1.5$  for a stable atmosphere and  $p \leq 1.5$  for an unstable atmosphere (see Misra (1975)).
- (2)  $\delta$  corresponds to a residual value of  $K$  found in the flow above the PBL. (Priestley (1954), Lettau and Davidson (1957), Howroyd and Slawson (1975)). (The PBL height,  $H$ , is thus defined as the height above which a zone of constant stress is encountered; see for other definitions, Hanna (1969)). Moore (1975) also indicates  $K$  does not fall to zero at the top of the boundary layer if there is any change of wind velocity with height

due to 'thermal wind' effects (i.e. the geostrophic wind is a function of height).

- (3)  $K_o \sim \kappa U_* h$  where,  $\kappa$  is the Von-Karman constant ( $\approx 0.4$ ) and  $U_*$  is the friction velocity. The specific expressions for various atmospheric stability conditions are:

$$K_o = \kappa U_* h \quad \text{Neutral Case}$$

$$K_o = \kappa U_* h (1 + 4.7h/L)^{-1} \quad \text{Stable Case}$$

(See Businger, 1973)

$$K_o = \kappa U_* h (1 - 16 h/L)^{0.25} \quad \text{Unstable Case}$$

(See Dyer and Hicks, 1970)  
(2.14)

(During the solution of the convective-diffusion equation under unstable conditions we use  $K_{o_m} = \kappa U_* h (1 - 16 h/L)^{0.5}$ ;  $K_{o_m}$  = eddy diffusivity for mass transfer. This is based on the results of Dyer and Hicks, 1970. A detailed discussion on flux-profile relationships is given by Dyer, 1974.)

$L$  is the Monin-Obukhov length.

$U_*$  can be computed by using a geostrophic drag coefficient  $C_g$  and geostrophic wind  $V_g$  as

$$U_* = C_g V_{g_o} \quad (2.15)$$

Lettau (1959) suggested the following empirical relationship for  $C_g$  in the case of a neutral atmosphere

$$C_g = 0.16 / (\log_{10} R_o - 1.8) \quad (2.16)$$

where,  $R_o$  is surface Rossby number ( $R_o = V_g / z_o f$ ). For unstable and stable

atmospheric conditions, the above  $C_g$  is adjusted using

$$\begin{array}{ll} C_g = 1.2 C_g \text{ (neutral Case)} & \text{Unstable Case} \\ \text{and} & \\ C_g = 0.7 C_g \text{ (neutral Case)} & \text{Stable Case} \end{array}$$

for this study. (2.17)

In order to account for possible vertical variations of pressure gradient the following relationship will be used

$$\underline{V}_g = \underline{V}_{g_0} + \underline{A} z \quad (2.18)$$

where,  $\underline{V}_{g_0}$  is the surface value of geostrophic wind and  $\underline{A}$  is the vector rate of increase with height. For computations  $\frac{A}{f} = 42$  is assumed. (In fact the values for  $\frac{A}{f}$  should change with atmospheric stability conditions. However, typical values are not available.) See Estoque, 1973.

The magnitude of the surface stress can be computed in terms of  $U_*$  using  $U_* = (\tau_x^2 + \tau_y^2)^{1/4}$  (where,  $\tau = \text{shear stress}/\rho$ ) and the cross-isobar angle  $\alpha$  is deduced from  $u$  and  $v$  using

$$\tan \alpha = \frac{v}{u} \quad (2.19)$$

by choosing the X-axis parallel to  $\underline{V}_{g_0}$ .

### 2.2.1 Finite-difference Scheme:

The PBL equations (2.6), (2.7), (2.10) and (2.11) are solved using a finite difference scheme. In order to obtain accurate results, a log-linear type of grid spacing and a wall layer is essential (Taylor and Delage, 1971). The log-linear type of spacing is desirable to overcome extremely strong gradients of velocity near the ground and relatively weak gradients in the upper levels of PBL. The wall layer is used to avoid the computational difficulties arising from the singular point at  $z = 0$ . In this constant thickness layer, a known solution for velocity is

used; for example a Log profile. The log profile in the wall layer is only an approximate solution for stable and unstable atmospheric conditions, but this approximation is used only for the (small) wall layer (thickness  $\sim 10 z_0$ )

Using the co-ordinate transformation

$$\zeta = c \ln \frac{z + z_0}{z_0} + D z \quad (2.20)$$

(where,  $c = A_1 / k$ ;  $D = A_1 / 4 k V g_0$  and  $A_1$  is a constant (to be chosen)) the equations (2.6), (2.7), (2.10) and (2.11) may be written as

$$K \frac{d^2 u}{dz^2} + \frac{dK}{dz} \cdot \frac{du}{dz} + f v = f V g$$

and

$$K \frac{d^2 v}{dz^2} + \frac{dK}{dz} \cdot \frac{dv}{dz} - f u = -f U g \quad (2.21)$$

or,

$$K F'^2 \frac{d^2 u}{d\zeta^2} + (K F'' + F'^2 \frac{dK}{d\zeta}) \frac{du}{d\zeta} + f v = f V g$$

and

$$K F'^2 \frac{d^2 v}{d\zeta^2} + (K F'' + F'^2 \frac{dK}{d\zeta}) \frac{dv}{d\zeta} - f u = -f U g$$

Here,

$$\zeta = F(z) \quad \text{and} \quad F' = \frac{d\zeta}{dz} \quad (2.22)$$

A finite difference form of these equations can be obtained by using central difference formulae at point  $n$  as

$$a_n \frac{u_{n+1} - 2u_n + u_{n-1}}{(\Delta\zeta)^2} + b_n \frac{u_{n+1} - u_{n-1}}{2\Delta\zeta} + f v_n = f V g_n$$

$$a_n \frac{v_{n+1} - 2v_n + v_{n-1}}{(\Delta\zeta)^2} + b_n \frac{v_{n+1} - v_{n-1}}{2\Delta\zeta} - f u_n = -f U_{g_n}$$

$$a = K F'^2$$

$$b = K F'' + F'^2 \frac{dK}{d\zeta}$$

(2.23)

Rearranging the terms, one obtains

$$AA \cdot u_{n+1} + BB \cdot u_n + CC \cdot u_{n-1} + f v_n = f V_{g_n}$$

$$AA \cdot v_{n+1} + BB \cdot v_n + CC \cdot v_{n-1} - f u_n = -f U_{g_n}$$

$$AA = \frac{a_n}{(\Delta\zeta)^2} + \frac{b_n}{2(\Delta\zeta)}$$

$$BB = -2.0 \frac{a_n}{(\Delta\zeta)^2}$$

$$CC = \frac{a_n}{(\Delta\zeta)^2} - \frac{b_n}{2(\Delta\zeta)}$$

(2.24)

Application of these equations to grid points 2,3,----, N-1 (Grid point 1 corresponds to the top of the wall layer where u and v are known: similarly grid point N is the top of the boundary layer where conditions are also known) result in 2(N-2) simultaneous nonlinear algebraic equations with a coefficient matrix of band structure (see Figure 2.2). The system is solved by Gaussian elimination. Several iterations are required using trial values of  $\alpha$ . The advantage of this method over existing methods is that a considerably smaller number of iterations are required to obtain the solution.

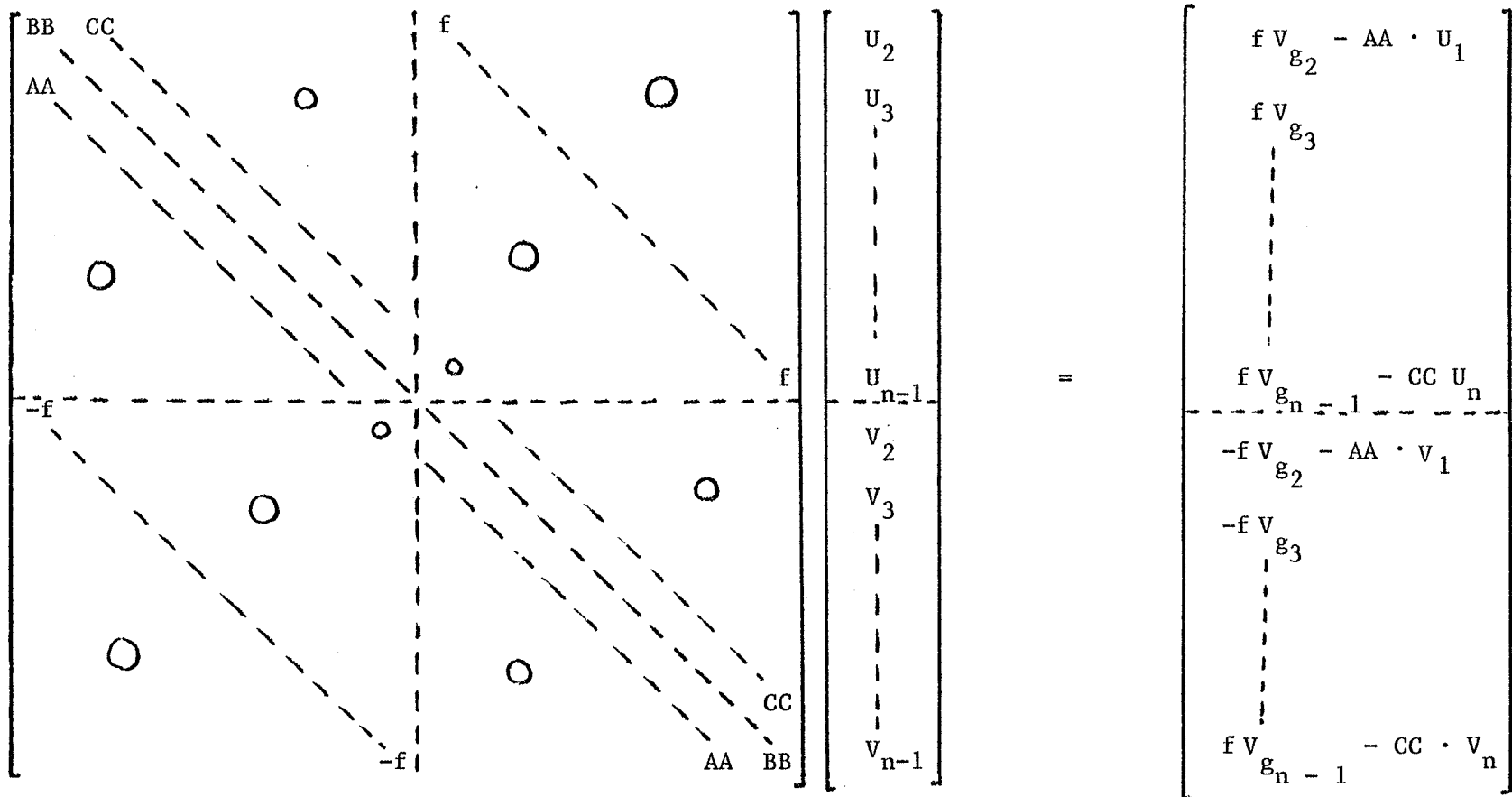


Figure 2.2: BAND STRUCTURE MATRIX

### 2.3 Numerically Computed Velocity Field:

In this section numerical solutions of the PBL equations are obtained using various K-profiles. The results are compared with the Wangara data (Clarke and Hess, 1974 and Clarke, 1970), a data set which is generally accepted as the best and most extensive available. We will make a detailed comparison with observations only for the near-neutral case, mainly because of the difficulties in assigning parameter values (see the following section). In a later section, however, profiles for various stabilities will be examined for realism by comparing A and B values with various observations.

#### 2.3.1 Comparison with Observations:

Profiles of wind departures ( $(u_{.15} - u)/U_*$  and  $(v - v_{.15})/U_*$ ) are given for three stability cases. The corresponding  $U_*$  values chosen were: (from Wangara data: see Clarke and Hess, 1974) for very unstable case  $U_* = 15.9$  cm/sec; for the near-neutral case  $U_* = 30.2$  cm/sec and for the very stable case  $U_* = 13.9$  cm/sec. The mean surface roughness for the Wangara experiments is reported as 3.5 m.m. The value of the corolis parameter  $f$  is  $8.275 \times 10^{-5} \text{ sec}^{-1}$  for the Wangara site.

There are several difficulties associated with the experimental data (e.g. rapid changes of temperature gradients occurring during frontal conditions) which arise whenever one tries to compare numerical results with such data. Even the best available data pose very serious problems in choosing input variables (such as geostrophic velocity and PBL height) for calculating numerical velocity profiles

The difficulty is further accentuated by the comments given by Clarke and Hess (1974): "...it is recognized that the drag-coefficient method for estimating  $U_*$  has its defects... The wind at  $\hat{z}$  ( $= fz/U_*$ ) = 0.15 is

on average nearly geostrophic in neutral conditions, but is systematically subgeostrophic in highly unstable conditions, and supergeostrophic in highly stable. . . . these values are tentative because of measurement difficulties and the effects of unsteadiness in the atmosphere. . . "

It is difficult to obtain the information on the variation of geostrophic velocity with height and on the PBL height. Furthermore, complete details on K-profiles are not available. Therefore, the discussion is limited to a near-neutral case with  $V_g = 10$  m/sec,  $p = 1.5$  and  $\delta = 0.1 \text{ m}^2/\text{sec}$ .

For the near-neutral case, the height of PBL is calculated using  $H = 0.15 U_* / f$  (from Figures 13 and 14 of Clarke and Hess, 1974) = 550 m. The value of the Obukhov length  $L$  is chosen as  $\infty$ , so that the stability indicator  $\mu (kU_* / fL) = 0$ .

Using the above data, numerical results are obtained which are then transformed to the co-ordinate system used in the experimental data (axes along and perpendicular to the surface winds). The results are plotted in Figures 2.3 and 2.4. The correlation between the experimental and numerical data is good considering the difficulties with the input data.

No detailed comparison has been made for unstable or stable atmospheres, primarily because of difficulties in choosing input data. Misra (1976), using a similar model for the outer layer (i.e. excluding surface layer), has compared analytical results for extremely stable and unstable cases with the Wangara data. He has found a good agreement between these results and the data (see Figure 2.5). Misra's work provides good support for our model for non-neutral conditions.

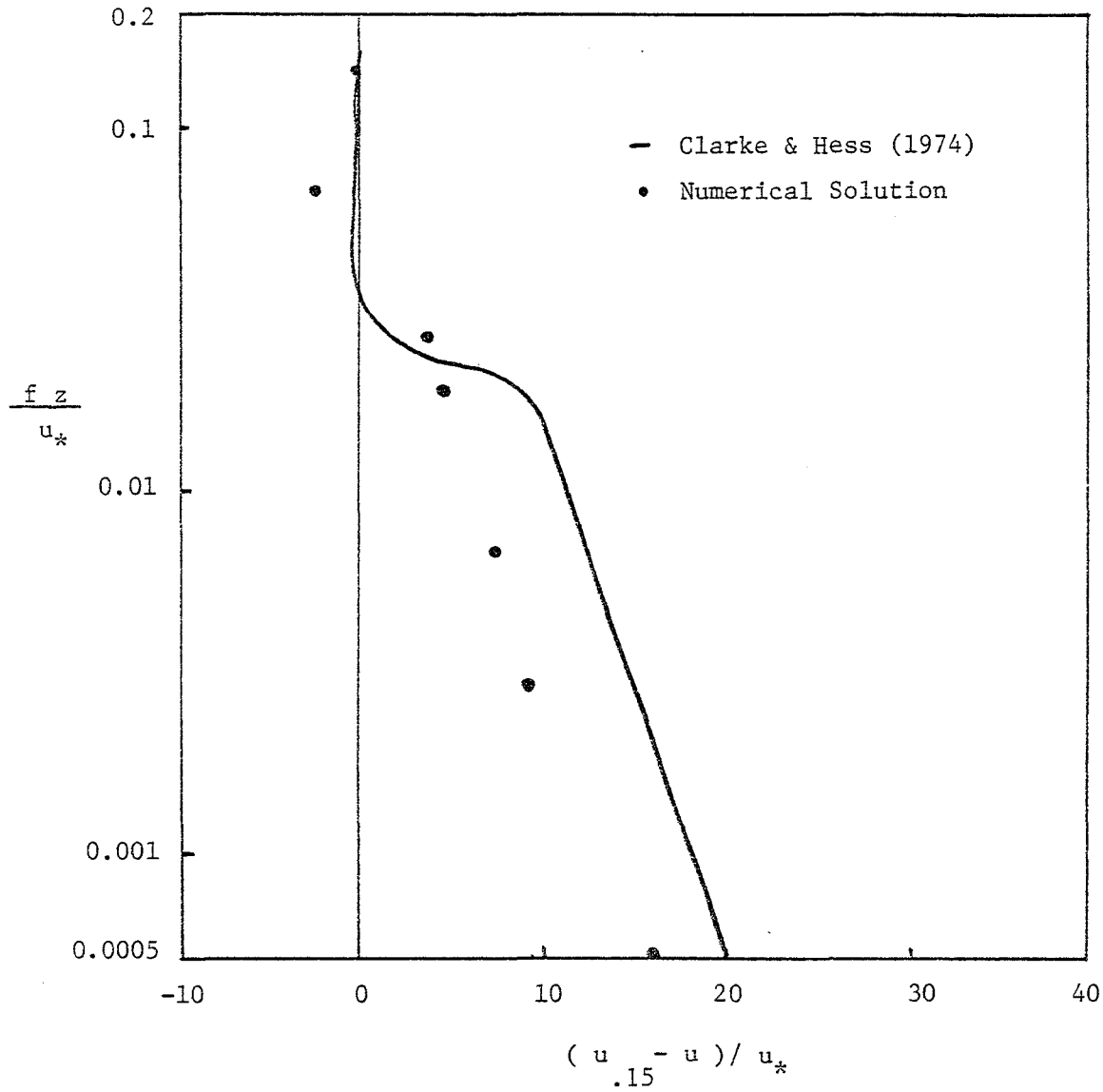


Figure 2.3: COMPARISON OF WANGARA DATA AND NUMERICAL SOLUTION FOR A NEAR-NEUTRAL ATMOSPHERE

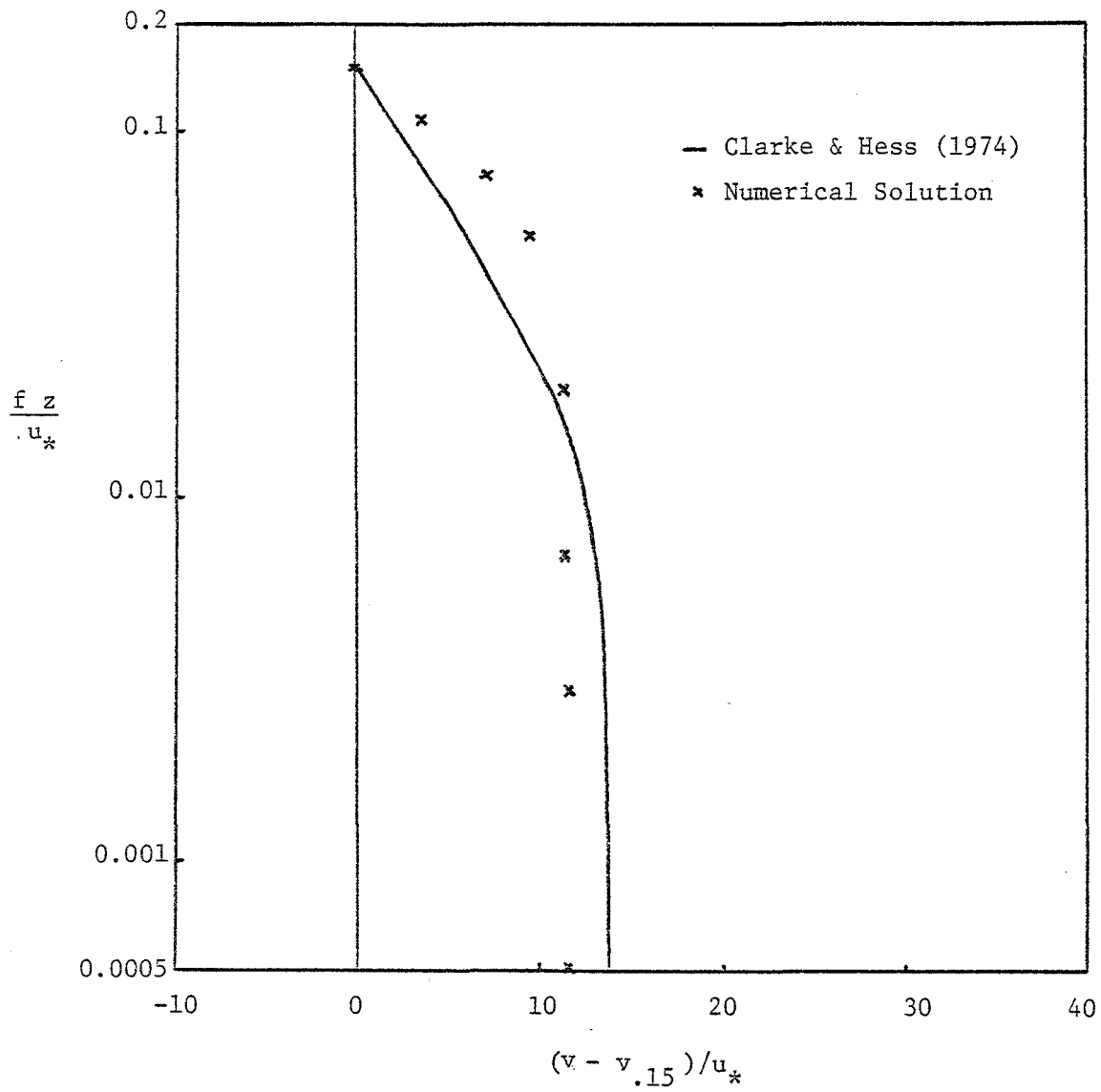


Figure 2.4: COMPARISON OF WANGARA DATA AND NUMERICAL SOLUTION  
FOR A NEAR-NEUTRAL ATMOSPHERE

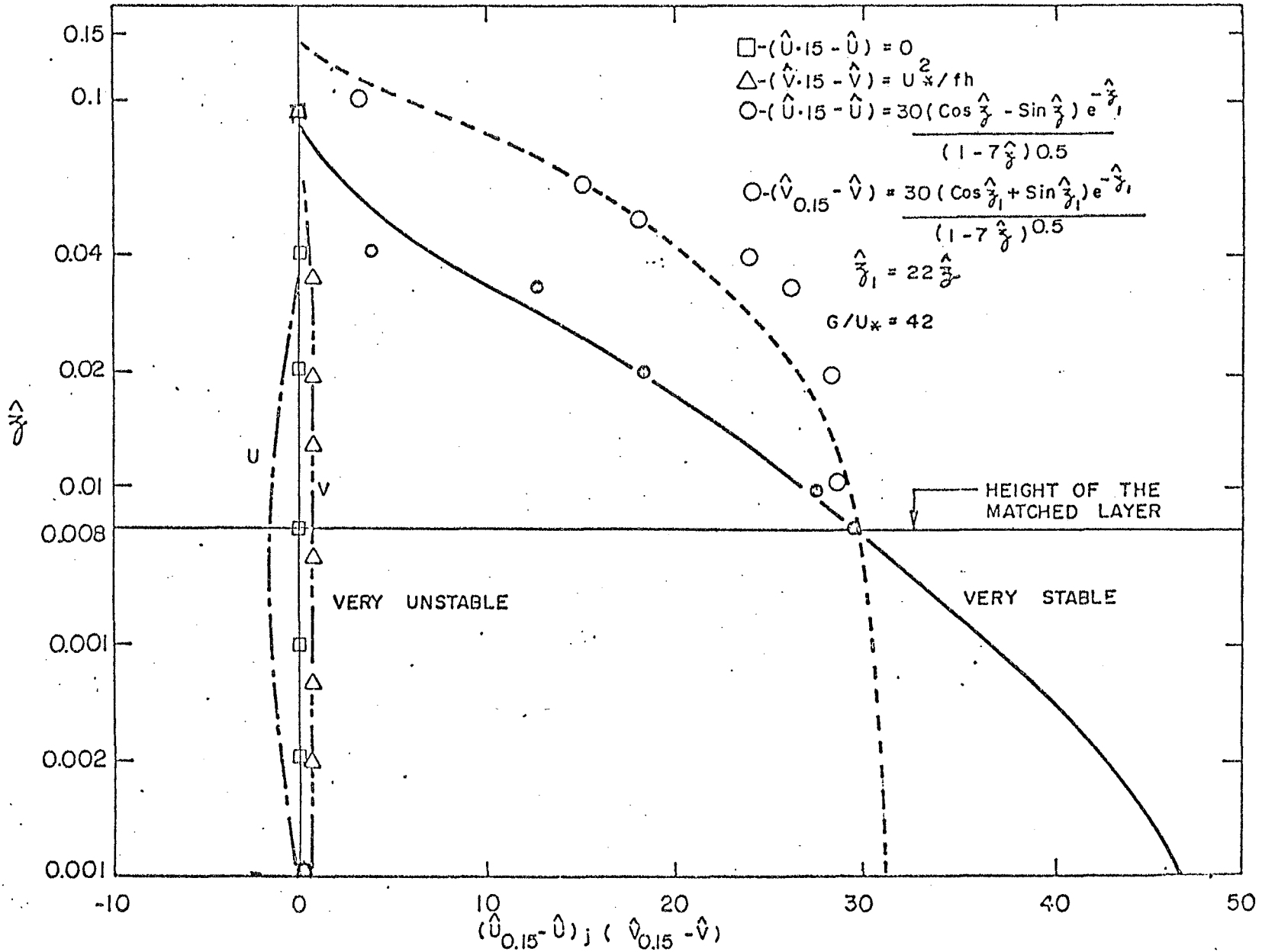


Figure 2.5: COMPARISON OF WANGARA DATA AND ANALYTICAL SOLUTIONS (FROM MISRA, 1976)

As a further test on the velocity profile model, values of the geostrophic drag law parameters are calculated and compared with other estimates.

### 2.3.2 Analysis of A and B in Rossby-Number Similarity Theory:

The geostrophic drag law as discussed earlier (section 2.1) may be written as

$$\ln R_o = A - \ln \frac{U_*}{|V_{g_o}|} + \left\{ \frac{k^2 |V_{g_o}|^2}{U_*^2} - B^2 \right\}^{1/2}$$

and

$$\sin \alpha = \frac{B U_*}{k |V_{g_o}|}$$

From the similarity theory arguments (see Brown, 1974), A and B are given by

$$A = \ln \frac{U_*}{fz_o} - \frac{U_g}{U_*} \cdot k$$

$$B = - \frac{k V_g}{U_*}$$

where,  $U_g$  and  $V_g$  are components of the geostrophic wind along and perpendicular to the surface wind. These expressions are used later for the calculation of A and B.

One has several options to obtain the values of A and B:

- a) laboratory experiments in wind tunnels
- b) field observations in the real atmosphere
- c) numerical simulation of the PBL.

In the last decade, a number of attempts have been made to resolve the values of A and B. The main conclusions of these researchers are:

- (i) A and B are almost universal constants for a neutral, barotropic atmosphere
- (ii) A and B vary with atmospheric stability, baroclinicity and the time of day
- (iii) A and B are very sensitive in the neighbourhood of near-neutral conditions
- (iv) A and B also depend on surface roughness.

The results so far are more qualitative in nature rather than quantitative for (ii), (iii) and (iv). Even for (i), there is no general agreement for numerical values of A and B (see Table 2.1). Further, regarding the effect of baroclinicity, the experimental results reported by Clarke and Hess (1974) do not match the theoretical work of Wipperman (1972).

It should be emphasized that the field data analysis of these functions are very few due to the need of very accurate determination of  $U_*$ , heat flux (for calculating L), geostrophic wind, thermal wind, etc., in order to achieve good quality results. Comparison between field data and theory is always subject to difficulty because hourly atmospheric fluctuations (the time scale for the problem  $\sim 1/|f|$ ) are unavoidable, and the atmosphere is never in a steady state.

Table 2.1 shows the values of A and B obtained by various investigators in the past for a near-neutral atmosphere. It is clear from the table that there is no general agreement for the values of A and B. One possible explanation for wide variations (in the case of A, -1.52 to 2.99; and in case of B, 1.57 to 5.0) may be given based on the observations of Clarke (1970). His figures 9 and 10 clearly indicate that the values are very sensitive to the stability parameter in near neutral conditions.

Table 2.1 VALUES OF A AND B IN  $\ln R_o = A - \ln \frac{U_*}{V_g} + \left( \frac{k^2 V_g^2}{U_*^2} - B^2 \right)^{1/2}$

	<u>Investigator</u>	<u>A</u>	<u>B</u>
1.	Blinova and Kibel (1937)	2.99	1.57
2.	Kazanski and Monin (1961)	1.7	1.81
3.	Gill (1967)	1.7	4.7
4.	Csanady (1967)		
	Scilly I	-1.52	4.29
	Leipzig II	0.0	4.29
5.	Blackadar and Tennekes (1968)	0.0	4.5
6.	Hanna (1969)	0.0	4.8
7.	Deardorff (1970)	1.3	3.0
	Twice the grid points	-0.2	3.2
8.	Wipperman (1970)	0.9	4.5
9.	Huang (1975)	1.2 - 0.8	3.58 - 3.63
10.	Clarke and Hess (1974)	1.1 ± 0.5	4.2 ± 0.7
11.	Present Study (using comparable data of Clark and Hess, 1974)		
	V = Vg at PBL height = 550m	1.49	4.75
	V = Vg at 550m, PBL height = 1000m	1.19	3.88

From 52 hourly observations Clarke and Hess (1974), using the Wangara data, reported the values of A and B as  $1.1 \pm 0.5$  and  $4.3 \pm 0.7$  respectively for a neutral, barotropic atmosphere. These estimates are qualified as tentative due to disturbing effects of (mainly high frequency) unsteadiness and baroclinicity. Using similar input data, the values obtained from the present model are:

- (i) A = 1.49 and B = 4.75 using wind as geostrophic  
at PBL height = 550m
- (ii) A = 1.19 and B = 3.88 using PBL height as 1000m  
and wind is geostrophic at 550m

Thus, the numerical results are in line with the observations.

From his 3-D numerical simulation Deardroff (1970) proposed A = 1.3 and B = 3.0 and, later on, revised these estimates as A = -0.2 and B = 3.2 by using a finer grid spacing. Huang (1975) studied the effect of surface roughness on these quantities and found that A varies from 1.2 to 0.8 for non-dimensional surface roughness ( $fz/kU_*$ ) of  $10^{-3}$  to  $10^{-7}$ , while the change in value of B is negligible. Wipperman (1973) has also listed various sources of A and B, and, from his theoretical arguments, recommends A = 0.9 and B = 4.5 for a neutral case.

One final reason for the difference between the A and B values obtained in this model and in other studies is due to the type of K-profiles used. (Although it should be noted that the present results for A and B fall well inside the range of values given in the literature.) The proposed profiles are different from those used in other studies. They have been justified earlier (section 2.2), and the A and B comparisons made above provide further justification. Nevertheless a consensus on choice of K profiles has yet to be established.

### 2.3.3 Numerically Generated Profiles:

In Figures 2.6 to 2.8, the wind profiles obtained numerically for different atmospheric conditions are shown. Here,  $u$  and  $v$  components of the velocity field are plotted and the geostrophic wind is assumed to have constant direction and linearly varying magnitude. Other parameters used are indicated on the figures or are listed in Table 2.2. The  $x$ -axis is assumed to be aligned with the geostrophic wind. Wind hodographs for a near-neutral case for surface roughnesses  $z_0 = 0.01$  m and  $0.11$  m are given in Figure 2.9.

The computer program is quite effective in generating the profiles. One iteration takes only 0.01 minute of computing time (for execution) on a IBM 360/65 computer and usually 6 or 7 iterations are required for the solution. If the surface cross-isobar angle is known, the profiles may be obtained in one iteration.

The numerical results agree with the observed fact that greater instability leads to a decrease in the cross-isobar inflow angle of the surface wind. The effects of increasing surface roughness are larger cross-isobaric angle and slower increase in the wind with height for the rougher surface.

### 2.3.4 Comparison of Variation of A and B with Stability to Wangara data:

Numerical values of A and B along with values from the Wangara data of Clarke (1970) for the stabilities considered are given Table 2.3 Keeping in mind the problems of comparing theory and experiments outlined in 2.3.1, the comparison between theory and field data is quite good. The present results confirm the observations of Clarke (1970) and Clarke and Hess (1974) that B is dependent on stability and are in disagreement with the theoretical prediction of Csanady (1972) that B should be constant.

Near - neutral case

$$K_o = 12.4 \text{ m}^2/\text{sec}$$

$$f = 10^{-4}$$

$$p = 1.5$$

$$u_g = 10 + 42 \cdot f \cdot z$$

$$z_o = 0.01 \text{ m}$$

$$v_g = 0$$

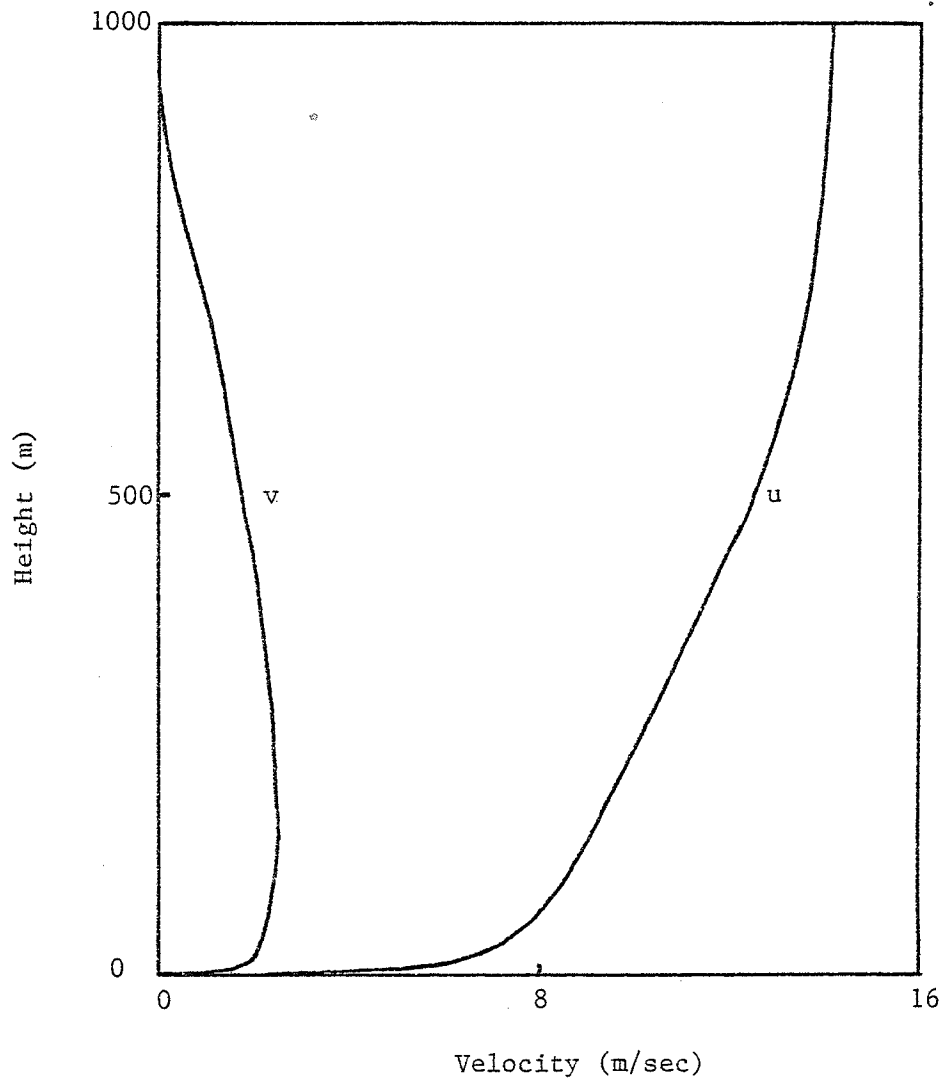


Figure 2.6: VELOCITY PROFILES FOR A BAROCLINIC BOUNDARY LAYER

## Unstable Case

$$K_o = 27.6 \text{ m}^2/\text{sec} \quad \Delta = 4.0 \text{ m}^2/\text{sec}$$

$$p = 1.1 \quad Vg = 5 + 42 \cdot f \cdot z$$

$$z_o = 0.01 \text{ m} \quad U_g = 0.0$$

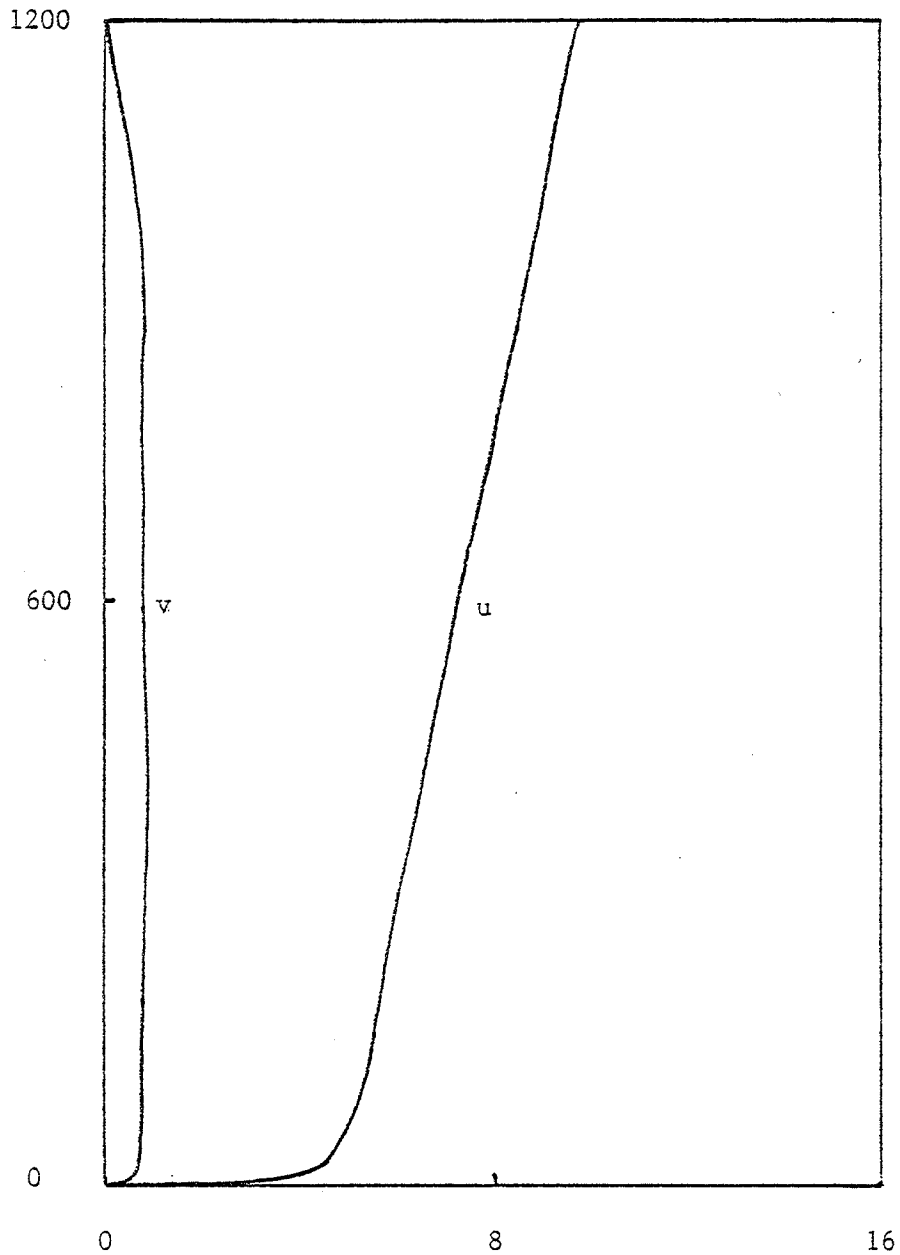


Figure 2.7: VELOCITY PROFILES FOR AN UNSTABLE BAROCLINIC ATMOSPHERE

## STABLE CASE

$$K_o = 2.28 \text{ m}^2/\text{sec} \quad U_g = 15 + 42 f z$$

$$Z_o = 0.01 \text{ m} \quad H = 450.0 \text{ m}$$

$$p_i = 1.9$$

$$f = 10^{-4}/\text{sec}$$

$$V_g = 0$$

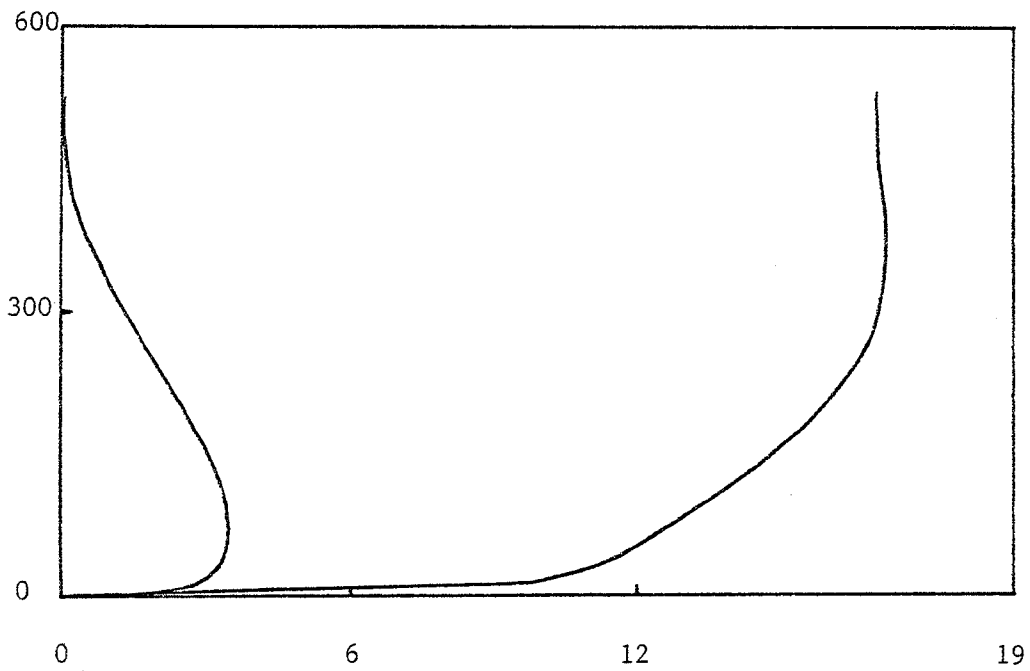
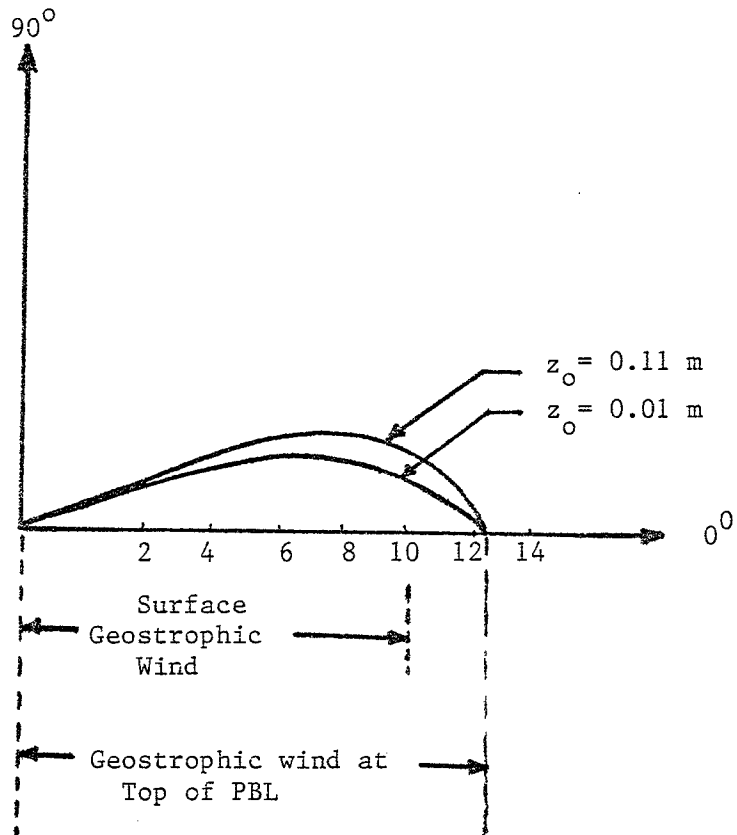


Figure 2.8: VELOCITY PROFILES FOR A STABLE BAROCLINIC ATMOSPHERE

Table 2.2 INPUT DATA FOR NUMERICAL VELOCITY PROFILES

Height of PBL	1200m Unstable Case
	1000m Neutral Case
	450m Stable Case
$\frac{h}{H}$	0.1 (Maximum h = 100m)
Surface Roughness	0.01m
	0.11m
Geostrophic Velocity at Surface	15m/sec Stable Case
	10m/sec Neutral Case
	5m/sec Unstable Case
$\frac{\partial \vec{V}_g}{\partial z}$	42.0 f (See, for example Estoque, 1973)
$\delta$ (m <sup>2</sup> /sec)	4.0 Unstable Case
	0.1 Neutral Case
	0.6 Stable Case
$U_*$	Using equations of section 2.2
$p$	1.1 Unstable Case
	1.5 Near-Neutral Case
	1.9 Stable Case
$L$	-10.0 Unstable Case
	$\infty$ Near-Neutral Case
	134.0 Stable Case
$f$	$1.03 \times 10^{-4}$ /sec



$$V_g = V_{g_0} + A z$$

$$V_{g_0} = 10 \text{ m/sec}$$

$$A = 42.f$$

$$H_{\text{PBL}} = 1000 \text{ m}$$

Figure 2.9: WIND HODOGRAPH FOR VARYING SURFACE ROUGHNESS

Table 2.3 EXPERIMENTAL AND NUMERICAL VALUES OF  $A(\mu)$  AND  $B(\mu)$ 

STABILITY CLASS	TYPE	$A(\mu)$	$B(\mu)$	
Unstable Case	Numerical*	2.1	1.6	
	Experimental**	6.0	2.0	Best fit
		5.0	1.5	Subjective estimate
Neutral*** Case	Numerical	0.2	3.8	
	Experimental	0.1	5.0	
Stable Case	Numerical	-5.5	6.3	
	Experimental	-7.5	10.5	Best fit
		-4.9	7.5	Subjective estimate

\* for a baroclinic atmosphere using the data of this report.

\*\* Clarke (1970) figures 9 and 10.

\*\*\* These values do not agree with Table 2.1 because this table is for a baroclinic atmosphere while the values given in Table 2.1 are for a barotropic atmosphere.

This implies Csanady's theory was oversimplified. Further, the numerical values are in line with the qualitative arguments of Swinbank (1974) that the geostrophic drag coefficients are dependent on thermal stratification.

#### 2.3.5 Closure:

One advantage of this numerical model is that it produces realistic objective estimates of the wind profiles. This is particularly gratifying, because the main purpose was to develop a model which used the same K-profiles as in the  $\sigma$ -model. Note here that it was not possible to obtain from the existing literature velocity profiles which were based on the same model of atmospheric turbulence as the  $\sigma$ -model, and, therefore, it was important for us to develop a consistent PBL velocity field model.

## CHAPTER 3

## PLUME RISE THEORY

3.1 Literature Review:

Four types of models have been used to describe plume behaviour.

(i) Statistical Models - for example Westlin et.al. (1972); used for cooling tower plumes (valid locally only).

(ii) Self-similar Models - valid only in a uniform environment (see Schmidt (1941)).

(iii) Quasi-similar Models - based on flux conservation of mass, momentum and heat (see Morton, Taylor and Turner (MTT) (1956)).

(iv) Quasi-similar Models - based on conservation of momentum, heat and kinetic energy (see Priestley and Ball (1955)).

Morton (1971) showed that the closure of the plume equations through the continuity equation is not equivalent to closure through the kinetic energy equation. Further, models based on conservation of mass, momentum and heat show increased rates of spread with large upper radius, whereas models based on conservation of momentum, K.E., and heat show large negative buoyancies and reversed entrainment with loss of plume fluid across the boundary. He states that the former class of models provide a more realistic model of the motion.

A summary of plume rise theories from 1926 to 1969 is given by Briggs (1969). For the sake of completeness, we will mention the main developments.

The buoyant plume problem was considered by Moore (1966), Bringfelt (1969) and others. Slawson and Csanady (1967, 1971) proposed a 3-phase theory and extended the theory to a non-neutral environment.

Methods for predicting plume rise covering a variety of situations have been suggested by Briggs (1975).

The entrainment theory was further extended to condensing plumes by Morton (1957), Csanady (1971), Wigley and Slawson (1971, 1972, 1975) Richards (1973), Weil (1974), Wigley (1975) and Hanna (1972, 1976).

The errors resulting from approximations used in plume rise theories such as the Boussinesq approximation (effects of density changes), exclusion of a drag term, solid particulate matter effects and the form of the energy equation flux term have not been examined in detail in the published literature.

### 3.2 Flow Regimes of a Plume:

A plume motion may be divided into various flow regimes. For the purposes of our discussion, we will consider the following (see Figure 3.1):

#### 1. Initial Phase:

##### (a) Vertical Jet Section:

The effluents are not deflected immediately upon entering the crossflow if the ratio of effluent velocity to the wind speed is greater than 4 (see Pratte and Baines (1967)). This region close to the stack is called the vertical jet.

##### (b) Bent-over Jet Section:

The entrainment of the crossflow in this region is rapid because by this time appreciable growth of vortices has taken place. This causes the jet to bend over.

##### (c) Thermal Section:

Self generated turbulence causes mixing and determines the growth of the plume.

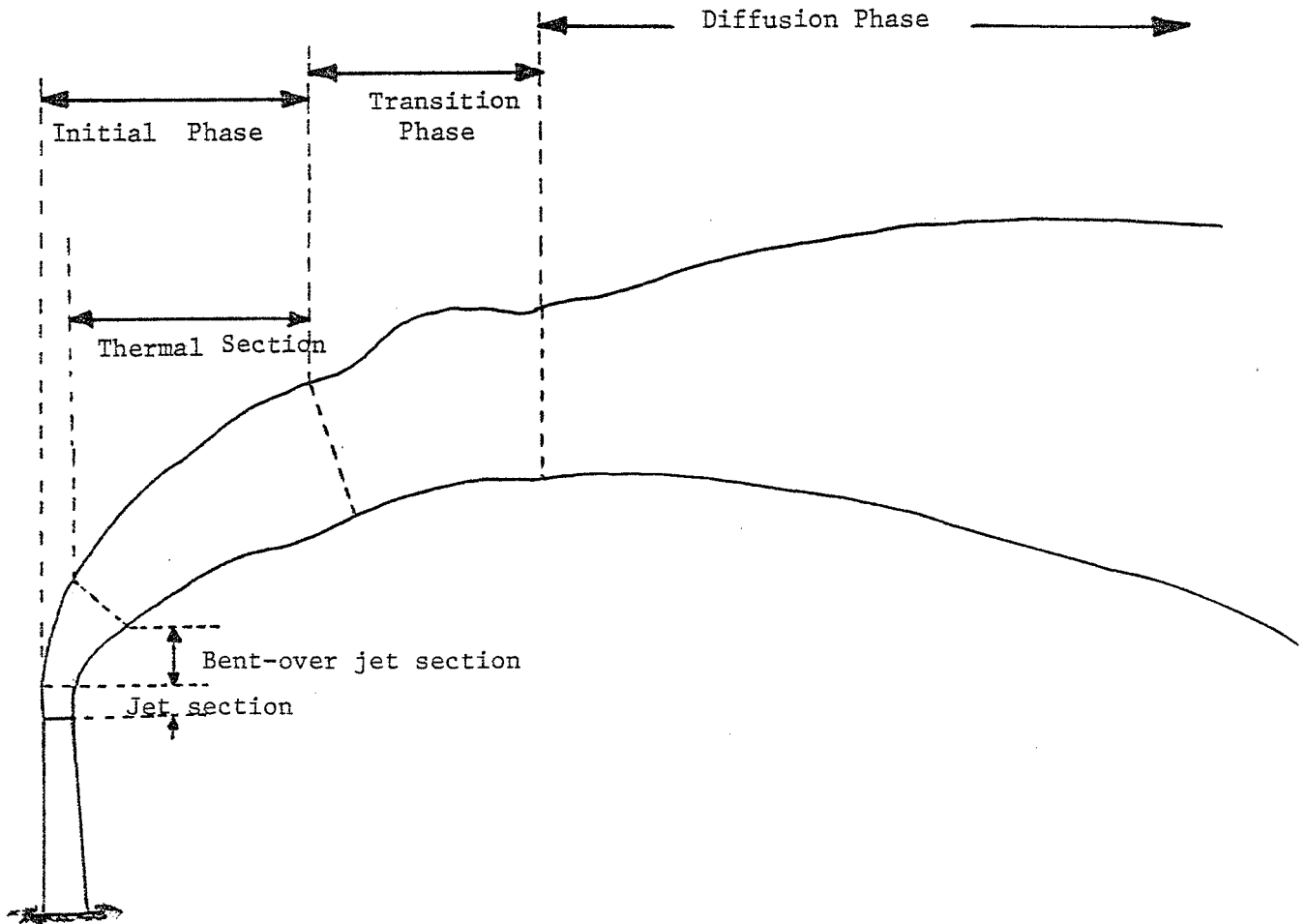


Figure 3.1: FLOW REGIMES OF A PLUME

## 2. Transition Phase:

In the initial phase it has been assumed that atmospheric turbulence is such that it merely moves the plume bodily contributing little to plume diffusion. However, at a sufficient distance downwind (i.e., where plume's internal turbulence levels have dropped enough) the atmospheric eddies in the inertial subrange determine the plume's growth.

## 3. Diffusion Phase:

In this region, the plume's own turbulence has dropped to such a level that the energy-containing eddies of atmospheric turbulence determine the growth of the plume.

Depending upon the flow situation not all of the above regimes may exist. For example, if the exit velocity ratio is small ( $< 3$ ) there may be no vertical jet section and the plume will bend over almost immediately. If atmospheric turbulence conditions are appropriate the transition phase may not exist. (see Slawson and Csanady (1971)).

### 3.3 Entrainment Theory with no Boussinesq Approximation (BA):

The B.A. is one of the most common assumptions used in plume rise theories. However, an investigation into its use is important on the following grounds:

- (a) the approximation is no good in the natural environment for height change  $\sim$  scale height ( $= R_d T_a / g \approx 8 \text{ km}$ ;  $T_a \approx \text{constant}$ ); see Spiegel and Veronis (1960)  
(also read page 51)

---

\* The net result of the Boussinesq approximation is that the flow may be treated as incompressible. The changes in B.A. are treated as small and are caused by thermal effects rather than pressure effects.

- (b) the change in the plume rise (between B.A. and no B.A. calculations) may be significant in the case of large heat sources (such as for proposed power plants in U.S.A.)
- (c) the ground level concentration (glc) is dependent on plume rise and as this study predicts a lower plume rise in the no B.A. case it will lead to higher glc in actual practice: this fact may help power plant designers and planners to evaluate large heat sources vrs. higher stack height.

The basic equations describing the dynamics and growth of a plume containing both liquid and solid particulate material ( $\psi$  is assumed to consist of very small particles with negligible free fall velocity) from an elevated source may be expressed as (for the no B.A. case):

Conservation of Mass:

$$\frac{d}{dt} (v_p R^2 \rho_p) = \frac{2v_e}{R} \cdot v_p R^2 \rho_a \quad (3.1)$$

Conservation of Moisture:

$$\frac{d}{dt} (v_p R^2 \rho_p (\Delta q + \sigma)) = -G v_p R^2 \rho_p w \quad (3.2)$$

Conservation of Energy (Heat):

$$\frac{d}{dt} (v_p R^2 \rho_p (\Delta T^* - \frac{L\sigma}{c_p})) = v_p R^2 \rho_p w (\Gamma - \Gamma_d) \quad (3.3)$$

Conservation of Vertical Momentum:

$$\frac{d}{dt} (v_p R^2 \rho_p w) = v_p R^2 \rho_p g \left( \frac{\Delta T^*}{T_a^*} - \sigma - \psi \right) + W_E \frac{d}{dt} (v_p \rho_p R^2) \quad (3.4)$$

Conservation of Horizontal Momentum:

$$\frac{d}{dt} (v_p R^2 \rho_p (v_x - u)) = c_d (u - v_x)^2 R |\sin \theta| \rho_a v_p \quad (3.5)$$

Conservation of Solid Particles:

$$\frac{d}{dt} (v_p R^2 \rho_p \psi) = 0 \quad (3.6)$$

Even though this is a steady-state formulation it is convenient to use a time coordinate as independent variable,  $t$  is a time variable measured along the centreline plume path and related to distance along this,  $s$ , by  $v dt = ds$ . The plume rise  $z$  and downwind distance  $x$  are related to time  $t$  by the following equations:

$$\begin{aligned} \frac{dz}{dt} &= w \\ \frac{dx}{dt} &= v_x \end{aligned} \quad (3.7)$$

Further, a hydrostatic environment is assumed containing no liquid or solid particulate matter and it is assumed that pressure equalizes instantaneously between plume and environment.

$$\frac{dP}{dt} = -\rho_a g w \quad (3.8)$$

Notice here that in formulating the above set of equations the Boussinesq Approximation has not been used and that solid-body drag effects (in the horizontal only) are included. These two approximations are usually made in plume theory (even in numerical work, see Wigley and Slawson (1975)).

As a subsidiary aim in this thesis, the validity of these approximations will be examined.

The vertical drag term in equation (3.4) is neglected because no information is available in the open literature for the plumes under consideration.

Downwash is neglected during computations i.e.  $W_E = 0$ . Here,  $W_E$  is the vertical velocity of an artificial environment wind field acting down in the region downwind of the source (see Slawson and Wigley (1975)). At present, we do not have sufficient, reliable or accurate analytical expressions for  $W_E$  in the published literature.

The entrainment velocity of  $v_e$  is calculated by using  $v_e = \alpha |w|$ ;  $\alpha$  is assumed constant (i.e. independent of position along the plume).

The equations can be closed by using the equilibrium assumption that  $q_p = q_{sp}$  if  $\sigma > 0$ ; non-equilibrium effects including supersaturation are discussed by Wigley (1975) and are invariably unimportant in the determination of plume trajectory. The saturated specific humidity is computed by an extremely accurate formula given by Richards (1971, see also Wigley, (1974)).

The equations are solved numerically using a fifth order Runge-Kutta method incorporating a variable step size.

### 3.4 Approximate Forms of the Energy Equations:

Two different forms of the energy equation have appeared in the literature ( using the Boussinesq Approximation):

(a) Briggs (1969) form:

$$\frac{d}{dt} \left( R^2 v_p \frac{\Delta T}{T_p} \right) = v_p \frac{R^2 w}{T_a} (\Gamma - \Gamma_d) \quad (3.9)$$

with the vertical momentum equation as

$$\frac{d}{dt} (R^2 v_p w) = R^2 v_p \frac{\Delta T}{T_p}$$

(in order to have the same flux terms).

(b) Slawson and Csanady (1971) form:

$$\frac{d}{dt} (R^2 v_p \frac{\Delta T}{T_a}) = v_p \frac{R^2 w}{T_a} (\Gamma - \Gamma_d) \quad (3.10)$$

Csanady (1973) noted these two different forms of flux term and favored the use of Briggs form for the plume rise work. He further noted that the difference in plume rise data is only of the order of 15%.

Still one is not sure which form is closer to the N.B.A. case. Therefore, we have compared the results for a typical case using the three equations in order to assess their "relative accuracy".

### 3.5 A Simple Analytical Solution for the N.B.A. Case:

Following is a simple analysis of plume rise theory by assuming a linear variation of temperature change between the source exit and the point where  $T_{\text{environment}} = T_{\text{plume}}$ . The purpose of this rather "crude" analysis is to help us in explaining a lower rise in the N.B.A. case for a dry plume.

The conservation of mass equation may be written as

$$\frac{d}{dz} (v_p R^2 \rho_p) = 2 \alpha v_p R \rho_a \quad (3.11)$$

using the bent-over assumption,  $v_p \approx u = \text{constant}$ , this becomes

$$\frac{d}{dz} (R^2_{\rho_p}) = 2\alpha R \rho_a \quad (3.12)$$

If  $\rho_p = \rho_a - \Delta\rho$  then

$$\frac{d}{dz} (R^2_{\rho_a}) - \frac{d}{dz} (R^2_{\Delta\rho}) \approx 2R\rho_a\alpha \quad (3.13)$$

Comparing the above equation with that for the BA case (i.e.  $\frac{d}{dz} (R^2_{\rho_a}) = 2\alpha R \rho_a$ ), we can say that mathematically, the omission of  $\frac{d}{dz} (R^2_{\Delta\rho})$  is the main effect of the BA.

Now turning back to equation (3.12), we have

$$\frac{dR}{dz} + \frac{1}{2\rho_p} \frac{d\rho_p}{dz} R = \alpha \frac{\rho_a}{\rho_p}$$

$$\therefore R = \frac{\alpha}{\rho_p^{1/2}} \int \frac{\rho_a}{\rho_p^{1/2}} dz + \frac{\text{Const.}}{\rho_p^{1/2}} \quad (3.14)$$

(This result can easily be checked by back substitution.)

Using  $z = 0$  and  $R = R_0$ , one obtains

$$R = R_0 \sqrt{\frac{\rho_p}{\rho_{p_0}}} + \frac{\alpha}{\sqrt{\rho_p}} \int_0^z \frac{\rho_a}{\rho_p} dz$$

or,

$$R = R_0 \sqrt{\frac{T_p}{T_{p_0}}} + \alpha \sqrt{T_p} \int_0^z \sqrt{\frac{T_p}{T_a}} dz \quad (3.15)$$

In order to simulate the decrease of  $\Delta T$  as plume rises, we assume

$$\frac{\Delta T}{T_a} = \frac{\Delta T_0}{T_{a_0}} - az \quad (a > 0) \quad (3.16)$$

$$\therefore \frac{T_p}{T_a} = \frac{T_{p_0}}{T_{a_0}} (1 - bz) \quad \text{where, } b = \frac{T_{a_0}}{T_{p_0}} a \quad (3.17)$$

To give a rough idea of the magnitude of  $b$ , let us consider the point where  $\Delta T = 0$  and  $z = z_s$ . This implies that  $b \sim \frac{1}{z_s} \frac{\Delta T_0}{T_{p_0}}$  so that for a typical industrial stack  $b \sim \frac{1}{100} \cdot \frac{30}{300} \sim 10^{-3} \text{ m}^{-1}$ .

$$\begin{aligned} \therefore R &= R_0 \sqrt{\frac{T_p}{T_{p_0}}} + \alpha \sqrt{\bar{T}_p} \int_0^z \frac{1}{\sqrt{\bar{T}_a}} \cdot \sqrt{\frac{T_{p_0}}{T_{a_0}}} \sqrt{1 - bz} \, dz \\ R &\approx R_0 \sqrt{\frac{T_p}{T_{p_0}}} + \alpha \sqrt{\frac{T_p}{T_a}} \sqrt{\frac{T_{p_0}}{T_{a_0}}} \left[ -\frac{(1 - bz)^{3/2}}{3/2 b} \right]_0^z \end{aligned} \quad (3.18)$$

where,  $\bar{T}_a$  is the mean value of  $T_a$  over the range 0 to  $z$ .

Expanding in powers of  $bz$  (since  $bz \ll 1$ )

$$\begin{aligned} R &\approx R_0 \sqrt{\frac{T_p}{T_{p_0}}} + \alpha \sqrt{\frac{T_p}{T_a}} \sqrt{\frac{T_{p_0}}{T_{a_0}}} \frac{2}{3} b \left[ -\left(1 - \frac{3}{2} bz + \frac{3}{8} b^2 z^2 - \dots\right) + 1 \right] \\ R &\approx R_0 \sqrt{\frac{T_p}{T_{p_0}}} + \alpha \sqrt{\frac{T_p}{T_a}} \sqrt{\frac{T_{p_0}}{T_{a_0}}} z \left[ 1 - \frac{1}{4} bz + \frac{1}{8} b^2 z^2 - \dots \right] \end{aligned} \quad (3.19)$$

For small  $z$ ,  $T_p = T_{p_0}$ ,  $\bar{T}_a \approx T_{a_0}$  and  $bz \ll 1$ , so we have

$$R \approx R_0 + \alpha \frac{T_{p_0}}{T_{a_0}} z = R_0 + \alpha^* z \quad \text{where, } \alpha^* > \alpha \quad (3.20)$$

Thus, in the NBA case there is, effectively, enhanced entrainment (i.e. greater  $\alpha$ ) for "small"  $z$ .

This will lead to reduced plume rise. The reduction is greater for greater  $T_{p_0}/T_{a_0}$  as one would expect. For "normal" industrial plumes and/or cooling tower plumes the enhancement factor is ~ 5 to 15%, a noticeable effect, but still within the uncertainty in estimating the entrainment parameter,  $\alpha$ .

In practice this means that empirical  $\alpha$  determined using the B.A. theory are over estimates of  $\alpha$  - values which would be determined by fitting data to a NBA theory. Deficiencies in the BA theory are thus compensated for by the empirical determination of  $\alpha$ . As  $\alpha$  values have been determined largely from industrial plants with moderate  $\Delta T_0$ , one might expect

- (a) application directly to cooling tower plumes (lower  $\Delta T_0$ ) would consistently under-estimate plume rise by ~ 5%: i.e. C.T. plumes would rise a little higher than predicted by simple B.A. theory results. Thus B.A. theory is conservative, though by an amount which would be difficult to observe.
- (b) application to very high temperature sources (e.g. a volcano) would considerably over estimate plume rise: i.e. something like a volcano plume (very large  $\Delta T_0$ ) would rise much less than predicted by B.A. theory results which used an industrial-source empirical  $\alpha$ .

The magnitudes of this effect given above are only approximate because of the approximations made in the solution. However, the qualitative conclusions may be accepted with some confidence. They will be confirmed later by a more detailed numerical solution of the equations. Note finally that the effect is generally small, but is more pronounced

for large  $T_{p_0}$ . This result is completely in accord with the expectation that the B.A. effect should be significant only when plume rise is significant in comparison with the scale height, and should be greater for greater rise.

One physical reason for an under-estimate of plume rise in the NBA case as compared to the BA case may be given on the basis of flux (terms involving  $\rho_p$ ). In the NBA case actual plume density is used while in the BA case plume density is calculated using atmospheric temperature because of the BA assumption. Since  $T_p > T_a$ ,  $\rho_p$  (or flux) in the NBA case is less than the density (or flux) in the BA case. Note here that density affects vertical momentum of plume which is dominant in the critical stages of plume rise.

### 3.6 Numerical Results:

Three specific examples corresponding to a typical scrubbed industrial stack ( $R_0 = 3\text{m}$ ,  $W_0 = 20\text{m/sec}$ ,  $T_{p_0} = 55^\circ\text{C}$ ), a natural-draught Cooling Tower ( $R_0 = 20\text{m}$ ,  $W_0 = 2\text{m/sec}$ ,  $T_{p_0} = 25^\circ\text{C}$ ) and a plume (cloud) from a volcano\* ( $R_0 = 10\text{m}$ ,  $W_0 = 10\text{m/sec}$ ,  $T_{p_0} = 1100^\circ\text{C}$ ) are considered (the later case is considered as an extreme mainly for examining the validity of the Boussinesq Approximation). The atmospheric conditions (unless and otherwise stated in the text) are: Wind speed 7m/sec (constant), Relative humidity 0 to 100% (constant for a particular case) and constant lapse rate varying from  $-0.01$  to  $0.01^\circ\text{C/m}$ . The atmospheric temperature and pressure were taken as  $0^\circ\text{C}$  and 1000 mb at the plume exit point.

---

\* Technically, a volcano is a vent connecting a reservoir of molten matter in the crust of the earth to the surface of the earth. The ejected material consists of liquid lava, broken fragments and volcanic gases. The chief constituent of the gases is water (70% to 95% by volume), and the lava temperature varies from  $800^\circ\text{C}$  to  $1200^\circ\text{C}$  depending upon the type of lava (based on my general reading on this topic).

A number of computer runs were made to study the sensitivity of plume variables to various parameters and are discussed in the following sections.

### 3.6.1 Effects of B.A. on Plume Growth and on Visible Plume Length:

The numerical results shown in Table 3.1 and Figures 3.2 and 3.3 are in line with the theoretical predictions i.e. use of the B.A. leads to an overestimate\* of the plume path and the plume rise, and underestimates the plume radius. Since the plume radius is increased for a given plume rise (z) in the N.B.A. case, more air is entrained causing downward displacement of the plume as compared to the B.A. case.

From a practical point of view, for present-day industrial stacks and cooling towers, the effects of the B.A. on plume growth are not important. For very large heat sources (as may happen with the new power plants) the effects may become significant for large plume rise ( $\geq 2000\text{m}$ ): but conditions leading to large plume rise also give low ground level pollutant concentrations and so use of the B.A. is still "acceptable". For the volcano plume, the B.A. effect is most noticeable. In such a case, all the plume variables (e.g. plume rise, condensation level etc.) are drastically affected. The differences can be explained by large temperature differences (i.e. density) between the plume and the environment.

Numerical results for the example of a volcano show cloud formation at 105m above the source and a maximum plume rise of 996 m. This rather surprising and interesting result agrees with the estimates of Cadle (1975): ". . . emissions of volcanoes of the Hawaiian type . . . seldom directly penetrate the tropopause . . . The estimate that on the average about 3.7% of erupted volcanic gases reaches the

---

\* In real life the empiricle constant  $\alpha$  takes into account errors due to the B.A.

Table 3.1: EFFECT OF BOUSSINESQ APPROXIMATION ON PLUME GROWTH

Source: Volcano

$$(\Gamma = 0.008^{\circ}\text{C/m})$$

Downwind Distance  x (m)	B.A.		N.B.A.	
	z (m)	R (m)	z (m)	R (m)
0.0	0.0	10.0	0.0	10.0
50.0	134.4	52.4	68.2	31.4
101.6	224.2	83.5	118.6	48.0
200.7	368.9	132.4	200.6	74.9
504.4	729.7	254.2	397.7	139.9
1007.9	1197.1	413.4	645.2	221.2
2001.5	1885.1	649.5	930.5	318.5
2748.1	2265.2	748.5	995.6	341.7*
3016.2	2378.8	825.2		
4870.9	2750.6	968.7*		

\* Corresponds to the point of maximum rise.

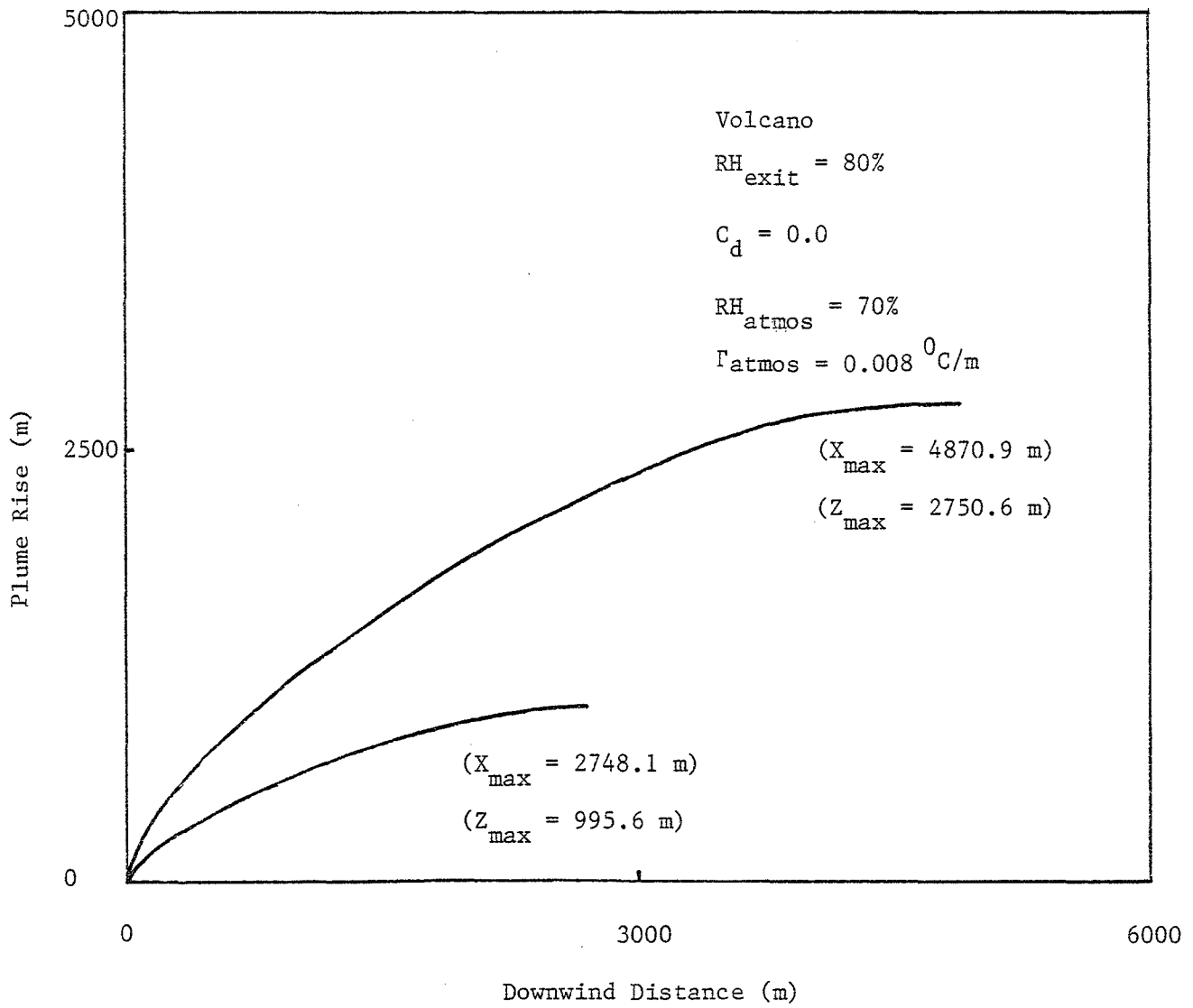


Figure 3.2: COMPARISON OF PLUME TRAJECTORIES IN BA AND NBA CASES

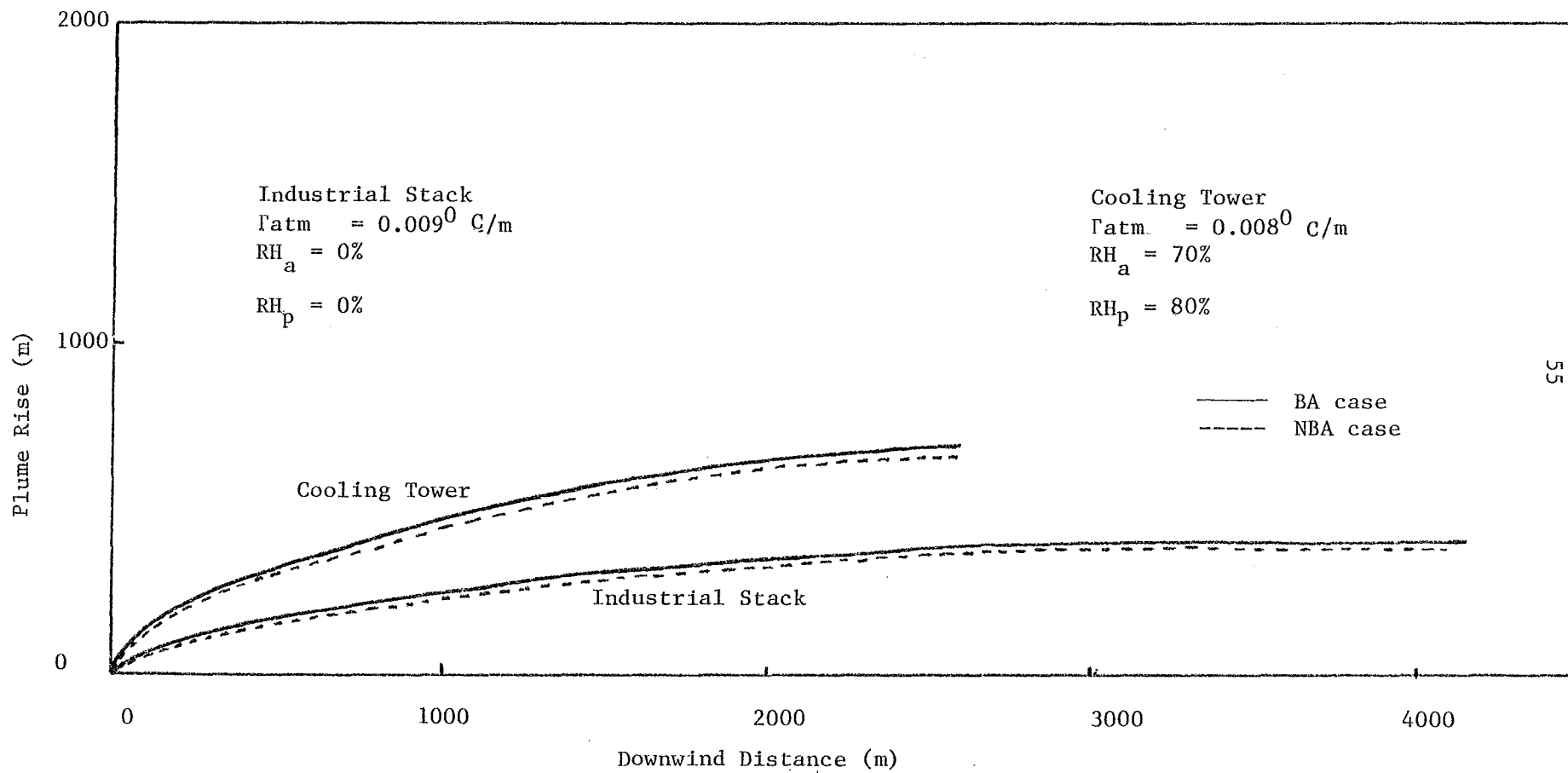


Figure 3.3: COMPARISON OF PLUME TRAJECTORIES IN BA AND NBA CASES

stratosphere seems rather large but is not entirely unreasonable in view of the many assumptions that had to be made to obtain that figure . . . ". Such a comparison indicates the potential of this model for future volcanic research. Note that the estimates given by Cadle are for passive or non-explosive (i.e. plumes) type of volcanos.

The results on visible plume path ( $L_p$ ) are compared with the work of Wigley and Slawson (1975) (uses BA case) and are shown in Table 3.2.

The following conclusions are drawn:

- (a) no significant changes are observed in  $L_p$  at low relative humidities.
- (b) the effect on  $L_p$  is largest under least stable atmospheric conditions. This can be explained using the fact that  $L_p$  is very sensitive to relative humidity and so is very sensitive to plume temperature and/or density.

The values of  $L_p$  in the Table 3.2 for warm and least stable atmospheric conditions are several magnitudes higher than that of Wigley and Slawson (1975). The reason is that their solution contains a well-defined evaporated (invisible) portion of the plume before the plume reappears. In the present solution this section (where the plume is actually still condensing) shows only as a section of reduced condensate contents which does not pass the assumed "cut-off" limit of visibility (i.e. remains visible);  $\sigma = 1.0 \times 10^{-5}$  gm/gm.

### 3.6.2 Effects of B.A. on the Maximum Plume Rise Due to Condensation:

Wigley (1975) presented the results of a numerical solution of moist plume equations and compared the results with Wigley and Slawson

Table 3.2: COMPARISON OF VISIBLE PLUME LENGTH\*

T <sub>a</sub> <sub>o</sub>	RH(%)	GRAPHICAL METHOD (m)	METHOD TYPE	LAPSE RATE				
				- 0.01	- 0.005	0	0.005	0.01
				(°C/m)				
0°C	40	20	Present Study	50	60	60	60	60
			W & S (1975)	60	60	60	60	70
	65	60	Present Study	110	110	120	120	130
			W & S (1975)	110	120	120	130	140
	90	300	Present Study	990 <sup>+</sup>	1180 <sup>+</sup>	1540 <sup>+</sup>	2650 <sup>+</sup>	> 7000
			W & S (1975)	950 <sup>+</sup>	1120 <sup>+</sup>	1440 <sup>+</sup>	2370 <sup>+</sup>	> 5000
10°C	40	N.C.**	Present Study	< 10	< 10	< 10	< 10	< 10
			W & S (1975)	< 10	< 10	< 10	< 10	< 10
	65	N.C.	Present Study	20	20	20	20	20
			W & S (1975)	20	20	20	20	20
	90	60	Present Study	190	220	270	2090	> 7000
			W & S (1975)	160	190	220	260	340

\*

+ extends beyond the point of maximum rise

\*\* no condensation

(1972), Hanna (1972) and Weil (1974). He found that Weil's (1974) predictions are not any better than that of Wigley and Slawson (1972). Hanna's (1972) results are closer to the numerical solution and are based on modification to initial flux of buoyancy. The solutions of Wigley are obtained from a set of equations which employed the B.A.

The ratio of wet plume maximum rise ( $z_{mw}$ ) to dry plume maximum rise ( $z_{md}$ ) is proportional to the radii at the point of maximum rise, i.e.

$$\frac{z_{mw}}{z_{md}} \propto \frac{R_{mw}}{R_{md}}$$

Earlier it has been shown that under NBA condition, plume radius is more in magnitude than the corresponding BA case. Also, the plume rise for a wet plume will generally be greater than the plume rise of a dry plume for the same stack and environmental conditions. Thus the increment (magnitude) in  $R$  (from its BA case value) for a wet plume is more than the increment in  $R$  for a dry plume at the point of maximum rise. Therefore, using the above relationship, one can conclude that the ratio of  $z_{mw}/z_{md}$  will be greater in NBA case than the BA case.

The numerical results are shown in Figures 3.4 and 3.5. These figures are an extension of the Figures 2 and 3 of Wigley (1975). Here wet and dry plumes are characterized by extreme conditions of relative humidities ( $RH_{p_0} = RH_{a_0} = 100\%$  for wet plume and  $RH_{a_0} = RH_{p_0} = 0\%$  for dry plume). As can be seen from these graphs, the ratio  $z_{mw}/z_{md}$  for a given stability class is higher in the NBA case than in the BA case. These results agree with the above qualitative deductions. The solution is still

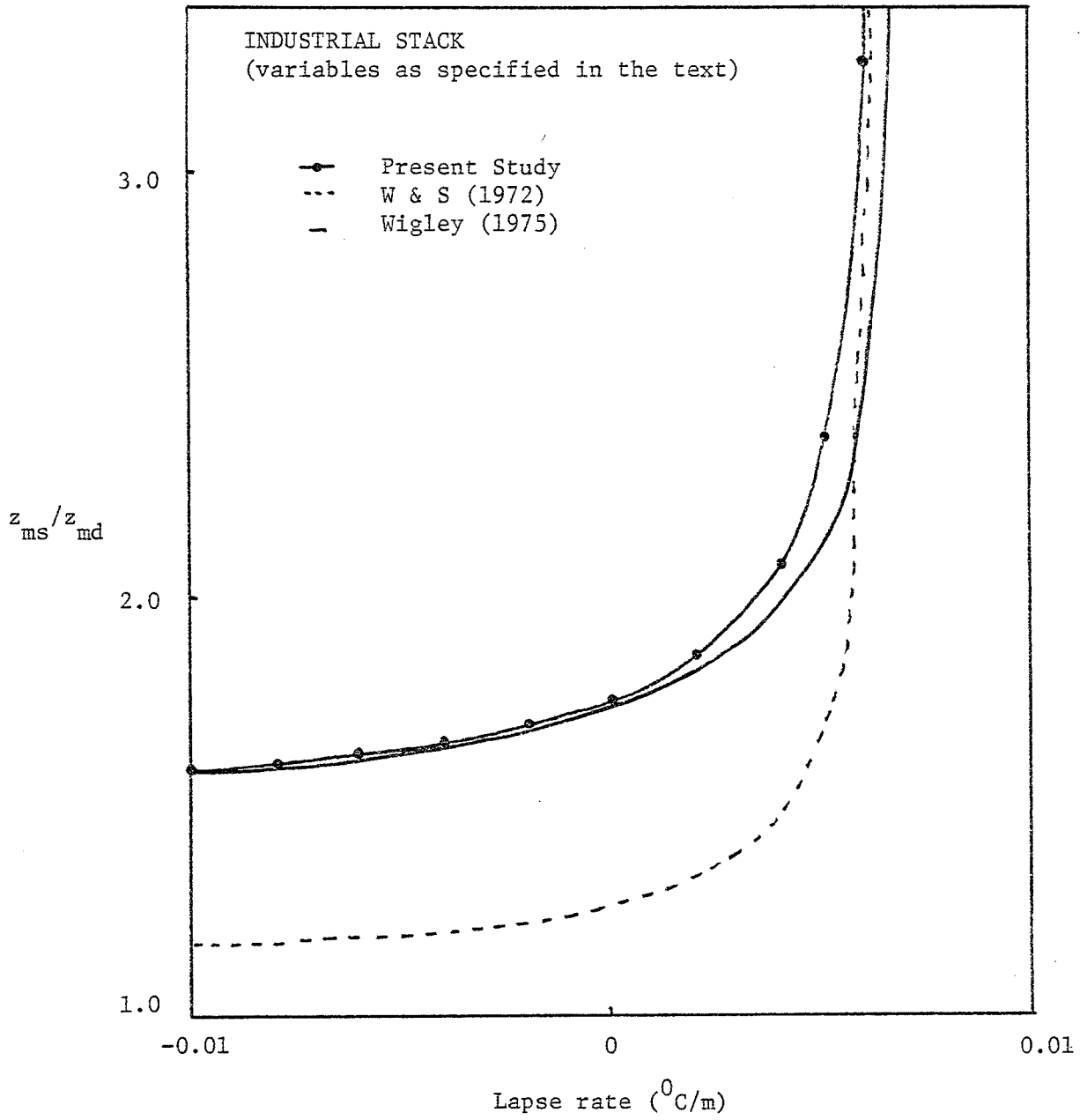


Figure 3.4: RATIO OF MAXIMUM PLUME RISE FOR WET AND DRY PLUMES  
FOR VARYING ATMOSPHERIC STABILITY

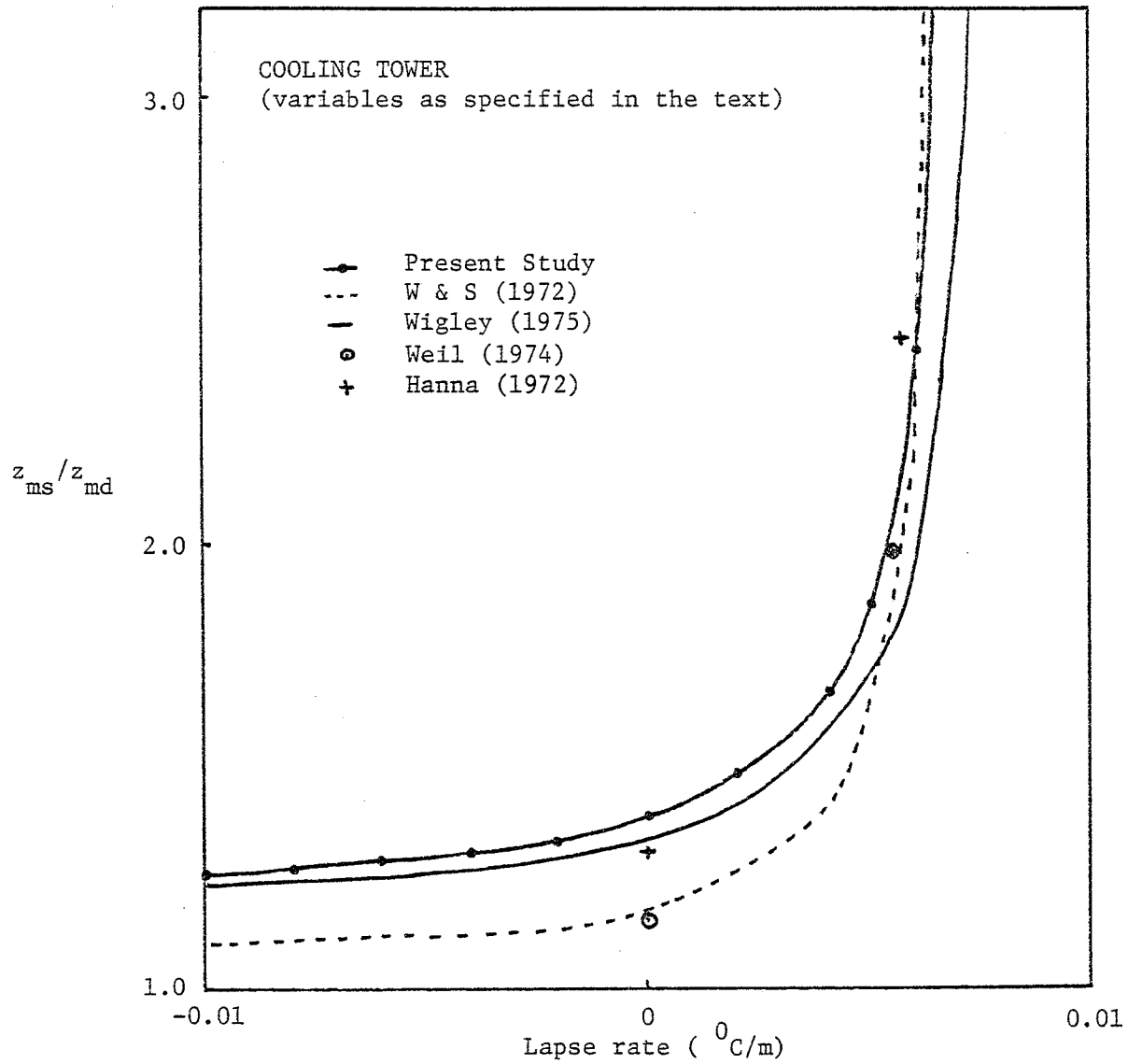


Figure 3.5: RATIO OF MAXIMUM PLUME RISE FOR WET AND DRY PLUMES FOR VARYING ATMOSPHERIC STABILITY

finite ( $z_{mw}/z_{md} = 7.5$  at  $\Gamma = 0.009^\circ\text{C}/\text{m}$  for the Cooling Tower and  $z_{mw}/z_{md} = 14.24$  for an Industrial Stack plume at same  $\Gamma$ ) and does not rise asymptotically to infinity as the lapse rate approaches to the saturated adiabatic lapse rate (assumed constant =  $0.0065^\circ\text{C}/\text{m}$ ) as proposed by Wigley and Slawson (1972). This has been explained by Wigley (1975) as due to the change in saturated adiabatic lapse rate with height.

Variation of downwind distance corresponding to the maximum rise point of wet and dry plume is given in Figure 3.6. Use of the B.A. consistently underestimates this ratio. As far as approximate solutions are concerned Wigley and Slawson (1972) predictions are closer to the actual solution (NBA case) than Weil's (1974) solution.

### 3.6.3 Effects of Horizontal Drag Coefficient $C_d$ :

The horizontal drag coefficient plays two roles in plume dynamics:

- (1) it will change the plume path, and since the drag force acts on the plume along the wind direction, the tendency will be to lower the plume trajectory
- (2) to increase the visible plume length.

As there are no field data available for  $C_d$  on plumes, four values ranging from 0.0 (no drag force) to 0.30 are used. The value  $C_d = 0.3$  has been used by Ooms (1972) and corresponds to a rigid cylinder.

Figure 3.7 and Table 3.3 illustrate the effect of  $C_d$  in the case of a Cooling Tower obtained via numerical solution. The results show a reduced plume rise and increased  $L_p$  (visible plume length) with increasing values of  $C_d$ .

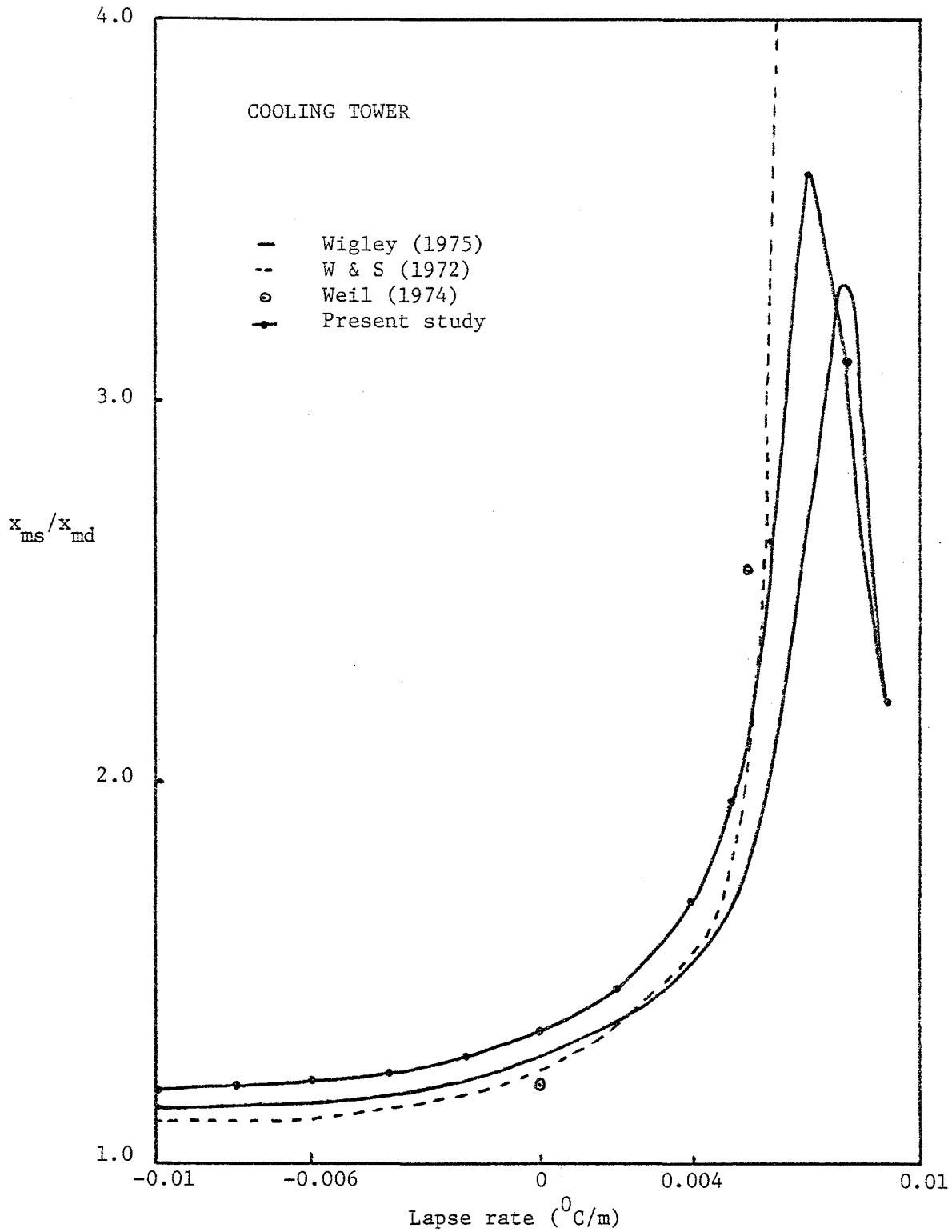


Figure 3.6: VARIATION OF RATIO OF THE DOWNWIND DISTANCES TO THE MAXIMUM RISE OF WET PLUME ( $x_{ms}$ ) AND A CORRESPONDING DRY PLUME ( $x_{md}$ ) WITH ATMOSPHERIC STABILITY

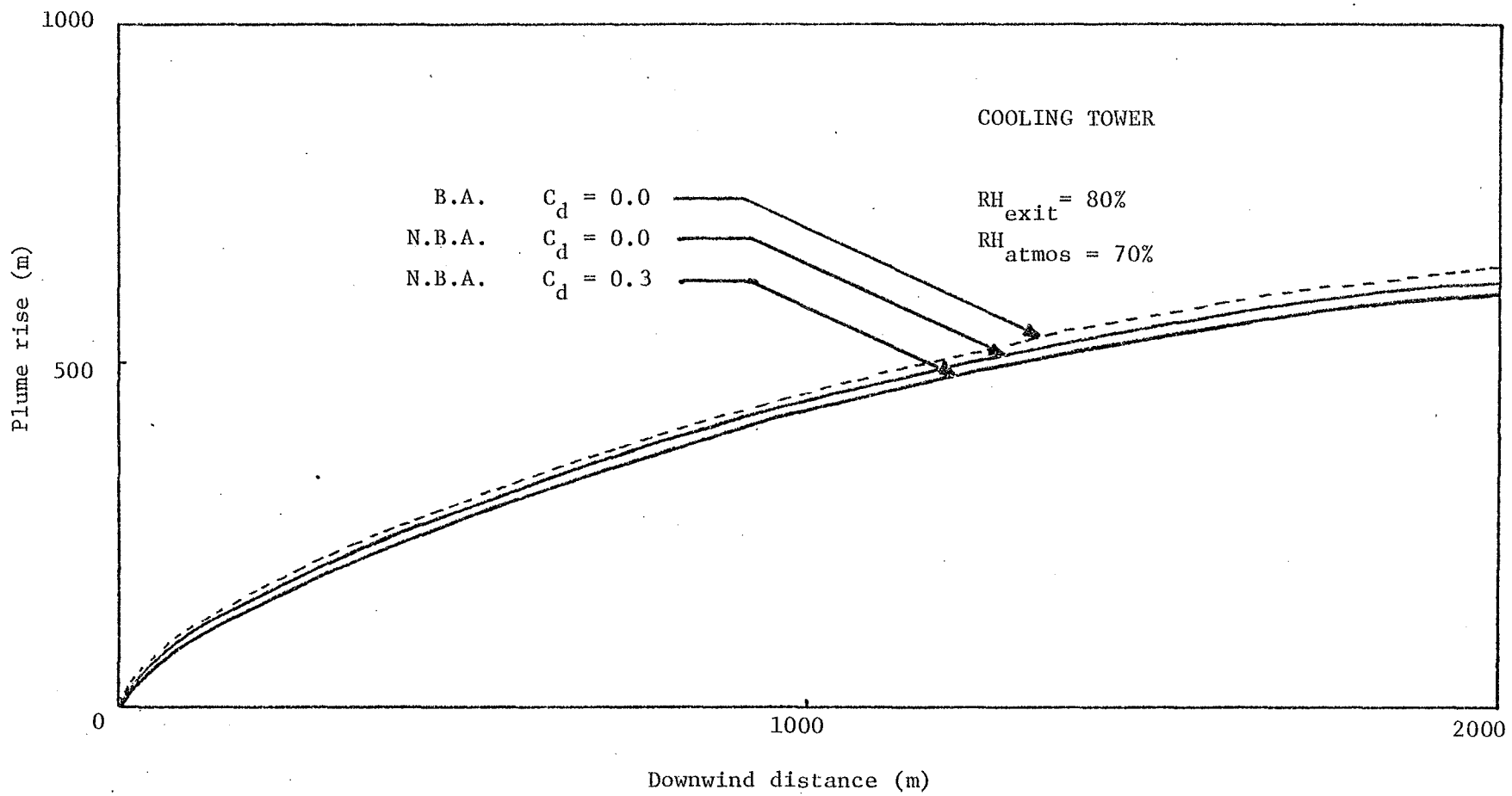


Figure 3.7: VARIATION OF  $C_d$  ON PLUME TRAJECTORY

Table 3.3: EFFECT OF DRAG COEFFICIENT ON PLUME VARIABLES

Source: Cooling Tower

	$C_d$	PLUME RISE $z_{\max}$	POINT FOR $z_{\max}$ $x$ (max)	VISIBLE PLUME LENGTH $L_p$ (m)
B.A.	0.00	673.6	2644.2	78.8
NBA	0.00	656.8	2645.6	73.2
	0.10	654.7	2661.0	78.9
	0.20	653.0	2672.2	83.3
	0.30	651.6	2682.1	84.4

Source: Industrial Stack

	$C_d$	VISIBLE PLUME LENGTH $L_p$ (m)
B.A.	0.00	212.1
NBA	0.00	196.1
	0.10	197.2
	0.20	198.0
	0.30	198.9

From Table 3.3 one can see that  $C_d$  has no appreciable effect on  $L_p$  for an industrial stack while in the case of a Cooling Tower  $L_p$  is increased noticeably by the introduction of a drag coefficient. For example, if  $C_d = 0.30$  is used, the value of  $L_p$  is increased by 15% as compared to the no-drag case. These effects are in the opposite direction to the BA effects discussed above and so tend to compensate partly for the BA. Table 3.3 shows that the BA case is a compromise between the NBA case with  $C_d = 0.0$  and  $C_d = 0.30$ . Overall, the effects are noticeable, but of little practical significance.

#### 3.6.4 Effects of Solid Particulate Matter:

To study this effect, we have included a solid particulate matter flux term in the vertical momentum equation and added a conservation equation for solid particulate matter to the plume rise equations. For a dry plume under neutral atmospheric conditions using BA and bent-over assumption ( $v_p = u = \text{constant}$ ) and assuming that at  $x = 0$  and  $z = 0$ ,  $R = 0$  (virtual origin approach), one may solve these equations analytically to find the plume trajectory as (using S & C form for energy equation):

$$z = \left[ \frac{3}{2} \frac{w_o R_o^2 g}{u^3 \alpha} \left( \frac{\Delta T_o}{T_{a_o}} - \psi_o \right) \right]^{1/3} x^{2/3} \quad (3.21)$$

Thus,

$$\frac{z_{\text{particulate}}}{z_{\text{no particulate}}} = \frac{\frac{\Delta T_o}{T_{a_o}} - \psi_o}{\frac{\Delta T_o}{T_{a_o}}} = 1 - \psi_o \cdot \frac{T_{a_o}}{\Delta T_o} \quad (3.22)$$

Some interesting results can be drawn using this relationship.

For  $T_{a_0} = 283^{\circ}\text{K}$ ,  $\Delta T_0 = 50.0$  and  $\psi_0 = 0.1, 0.01$  and  $0.001$  we obtain,

$$z_{\text{particulate}} = 0.434 \cdot z_{\text{no particulate}} \text{ for } \psi_0 = 0.1 \text{ gm/gm}$$

$$z_{\text{particulate}} = 0.94 \cdot z_{\text{no particulate}} \text{ for } \psi_0 = 0.001 \text{ gm/gm}$$

$$z_{\text{particulate}} = 0.995 \cdot z_{\text{no particulate}} \text{ for } \psi_0 = 0.0001 \text{ gm/gm.}$$

Thus we can see (as one would expect) that the more the particulate matter concentration, the lower is the plume rise and the greater would be the ground level concentration.

In practice, particulate emission standards are such that particulate concentrations in plumes are always quite low. The Los Angeles County Air Pollution Control District (L.A.C.A.P.C.D.) and the Bay Area (B.A.A.P.C.D.) the particulate emission is limited to  $0.3 \text{ grain/ft}^3$  ( $\approx 0.0001 \text{ gm/gm}$ ) (Strauss, 1966). Weir et al (1976), in their experimental study of the opacity of plumes from coal-fired generating stations, indicates mass concentrations of particulate matter ranging from  $0.004 - 0.4 \text{ grain/scf}$ . Particulates are therefore expected to lower plume rise by no more than 5%.

To verify the above results complete numerical solutions were obtained. These results, which are presented in Table 3.4 are in agreement with the earlier results.

In summary the plume rises higher for a lighter (low  $\psi$ ) plume than for a heavier (high  $\psi$ ) plume, and minor changes in the solid particulate matter content do not effect the plume rise very much for industrial stacks.

TABLE 3.4: EFFECT OF SOLID PARTICULATE MATTER

Source: Industrial Stack

(RH<sub>atmos</sub> = 0%,  $\Gamma_{\text{atmos}}$  = 0.009°c/m and RH<sub>exit</sub> = 0%)

	$\psi$ (gm/gm)	PLUME RISE $z_{\text{max}}$ (m)	POINT FOR $z_{\text{max}}$ $x$ (m)
B.A.	0.0	478.7	4171.8
NBA	0.0	452.3	4173.5
	0.001	451.6	4173.5
	0.01	444.6	4173.0
	0.1	358.3	4096.8

### 3.6.5 Calculation of Plume Variables Using Briggs and S & C Forms of the Flux of Buoyancy:

Different forms of the energy equations have been given in section 3.4. Expanding and rearranging these equations (3.9 and 3.10) one can see the differences between them and can compare them with the more precise equation (3.3) in which the BA is not made. We find:

S & C form:

$$\frac{d}{dz} (R_p^2 v_p \Delta T) - v_p R_p^2 (\Gamma - \Gamma_d) = -T_a R_p^2 v_p \Delta T \frac{d}{dz} \left( \frac{1}{T_a} \right)$$

or,

$$\begin{aligned} \frac{d}{dz} (\rho_p R_p^2 v_p \Delta T) - \rho_p v_p R_p^2 (\Gamma - \Gamma_d) &= -\rho_p T_a R_p^2 v_p \Delta T \frac{d}{dz} \left( \frac{1}{T_a} \right) \\ &+ R_p^2 v_p \Delta T \frac{d\rho_p}{dz} \end{aligned} \quad (3.23)$$

Briggs form:

$$\begin{aligned} \frac{d}{dz} (R_p^2 v_p \Delta T) - v_p R_p^2 (\Gamma - \Gamma_d) &= \frac{\Delta T}{T_a} v_p R_p^2 (\Gamma - \Gamma_d) \\ &- (T_p) v_p R_p^2 \Delta T \frac{d}{dz} \left( \frac{1}{T_p} \right) \end{aligned}$$

or,

$$\begin{aligned} \frac{d}{dz} (\rho_p R_p^2 v_p \Delta T) - \rho_p v_p R_p^2 (\Gamma - \Gamma_d) &= \frac{\Delta T}{T_a} \rho_p v_p R_p^2 (\Gamma - \Gamma_d) \\ &- \rho_p T_p R_p^2 v_p \Delta T \frac{d}{dz} \left( \frac{1}{T_p} \right) \\ &+ R_p^2 v_p \Delta T \frac{d\rho_p}{dz} \end{aligned} \quad (3.24)$$

NBA form:

$$\frac{d}{dz} (\rho_p R^2 v_p \Delta T) = \rho_p v_p R^2 (\Gamma - \Gamma_d) \quad (3.25)$$

To analyze the above forms further, the following are used to reconstruct the terms on R.H.S.

$$P = P_o e^{-\frac{g}{R_d \bar{T}} z}$$

and

$$P = \rho_a R_d T_a = \rho_p R_d T_p$$

where,  $\bar{T}$  is the mean atmospheric temperature.

$$- T_a R^2 v_p \Delta T \frac{d}{dz} \left( \frac{1}{T_a} \right) \approx - \frac{(R_o + \alpha z)^2 u \cdot \Delta T \rho_a g}{P_o e^{-\frac{g}{R_d \bar{T}} z}}$$

(using  $v_p \approx u$  and  $R = R_o + \alpha z$ ) (3.26)

and

$$- (T_a + \Delta T) v_p R^2 \Delta T \frac{d}{dz} \left( \frac{1}{T_p} \right) \approx - \frac{(R_o + \alpha z)^2 \Delta T \cdot u (\rho_a - \Delta \rho) g}{P_o e^{-\frac{g}{R_d \bar{T}} z}}$$

(3.27)

comparing the above equations, one may conclude:

- (a) the error decays exponentially in the S & C form as quickly as the temperature difference  $\Delta T$  tends to zero; beyond this point the error term is positive or negative depending upon

the nature of  $\Delta T$  (see Figure 3.8) while this is not true for Briggs form due to the term

$$\frac{\Delta T}{T_a} v_p R^2 (\Gamma - \Gamma_d)$$

- (b) for  $\Gamma < \Gamma_d$ , it is difficult to make a general statement
- (c) for  $\Gamma > \Gamma_d$ , the Briggs form is closer to the NBA case than the S & C form
- (d) for  $\Gamma = \Gamma_d$ , the Briggs form is closer to the NBA case than the S & C form
- (e) for  $T_a = \text{Constant}$ , (a), (b), (c), and (d) do not apply and the Briggs form is much better over the S & C form.

Numerical results for two cases ( $\Gamma = 0$  and  $\Gamma = 0.009^\circ\text{C/m}$ ) are shown in Table 3.5 for the S & C form, the Briggs form and for the complete (NBA) equations. For the example shown  $u = 10$  m/sec,  $T_{p_0} = 100^\circ\text{C}$ , and  $RH_a = 0\%$  is used.

Therefore, one may conclude the following:

- (i) Briggs form is closer to the NBA case than the S & C form under most atmospheric conditions. This agrees with the work of Csanady (1973).
- (ii) However, since both forms are in practice fitted to observations by determining  $\alpha$  empirically, the result will be that a person using the Briggs equation fitted to trajectory would get different  $\alpha$  from the S & C form. Note that this is not so if one gets  $\alpha$  from  $R = R_0 + \alpha z$ .

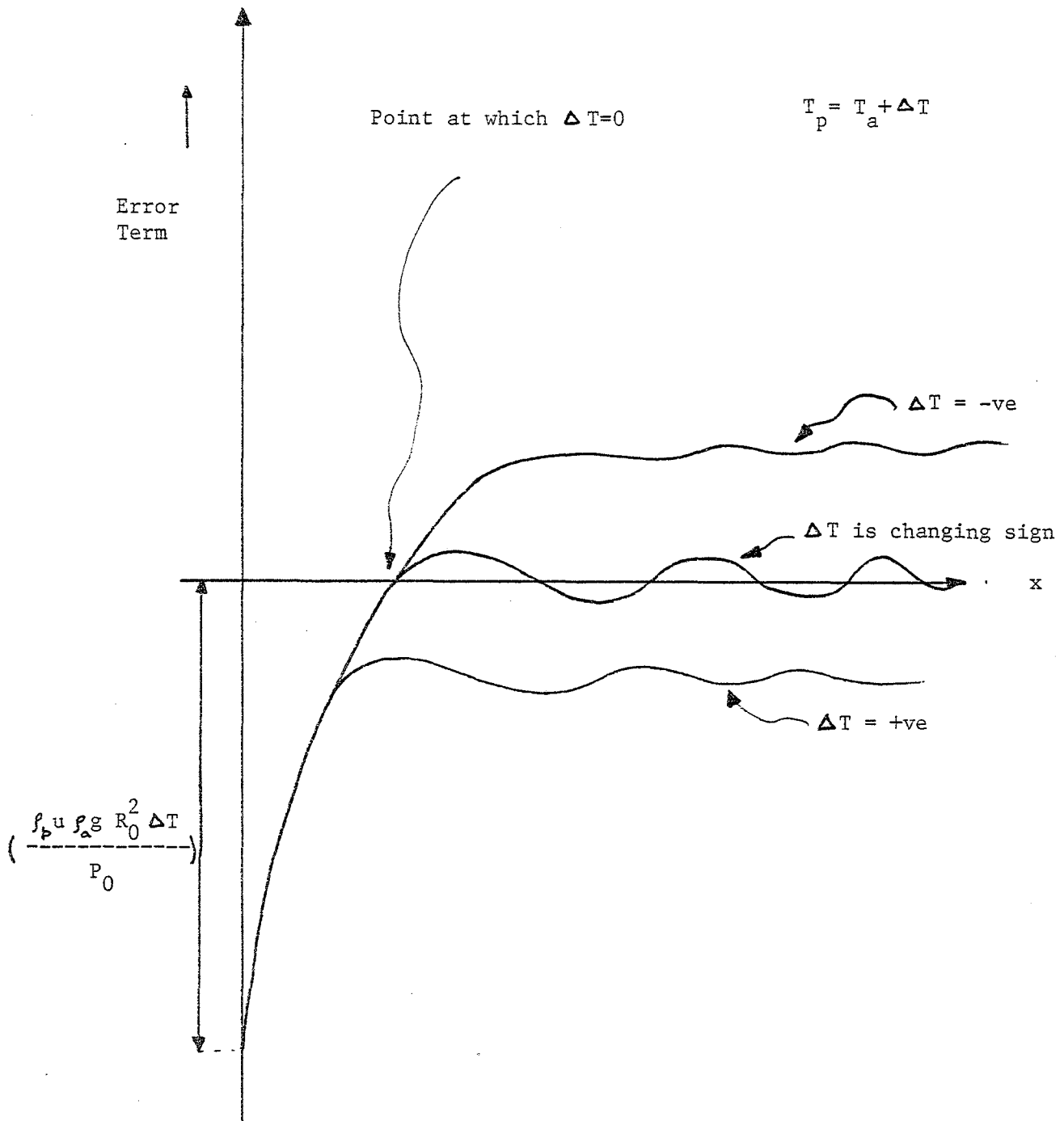


Figure 3.8: NATURE OF ERROR TERM IN S & C FORM

Table 3.5: COMPARISON OF PLUME TRAJECTORY FOR THREE FORMS OF ENERGY EQUATION<sup>1</sup>

x (m)	PLUME RISE Z(m)					
	$\Gamma = 0.0 \text{ } ^\circ\text{C/m}$			$\Gamma = 0.009 \text{ } ^\circ\text{C/m}$		
	NBA	BRIGGS	S & C	NBA	BRIGGS	S & C
0	0.0	0.0	0.0	0.0	0.0	0.0
100	45.1	48.1	50.8	45.1	48.1	51.0
200	68.2	71.3	76.7	68.8	71.8	77.3
500	119.4	121.9	133.3	123.1	126.2	137.6
800	155.3	157.2	173.0	167.6	170.1	186.5
1000	172.7	173.7	192.2	193.6	195.9	215.2
1200	184.9	185.6	205.5	217.9	219.8	242.3
1500	194.1	193.7	215.6	251.8	253.2	279.1
1600	194.7*	194.0*	216.1*	261.8	263.5	290.7
2000				300.6	301.0	333.1
4000				434.3	432.3	479.2
5973.5				476.6*	472.7*	525.0*

<sup>1</sup> based on same value of  $\alpha$

\* near the point of maximum rise

CHAPTER 4  
ATMOSPHERIC DIFFUSION

4.1 Literature Survey:

Diffusion studies available in the literature may be grouped into the following categories from the point of view of this thesis.

1. Theoretical Approach:

- (a) Gaussian Plume Models
- (b) Analytical K-theory Solutions
- (c) Numerical K-theory Models

(Note: The statistical theory, the similarity theory and higher order closure models are not considered in detail. Any discussion is on as required basis).

2. Experimental Approach:

- (a) Wind/Water Tunnel Modelling
- (b) Field Studies

4.1.1 Theoretical Approach:

Most of the early work in this area is given in two prominent text books by Sutton (1952) and Pasquill (1962). The Gaussian Plume Models are based on the statistical theory of turbulence (by measuring the diffusive power in the form of the variance of an ensemble of air "particles" over a time period) and use of a Gaussian expression for pollutant distribution. (See Sutton (1952).) Also see Chapter-1.

Analytical solutions of the K-theory convective - diffusion (C-D) equation for steady-state conditions have been reported by several researchers (e.g.: Roberts (1923), Rounds (1955)) for different boundary conditions and different expressions for velocity

( $\vec{V}$ ) and eddy diffusivities ( $K$ ) as functions of the independent variables. These analytical solutions assume  $K$  and  $\vec{V}$  functions which are somewhat oversimplified. Direct application to atmospheric dispersion problems with arbitrary  $K$  and  $V$  distributions is therefore not possible; or is, at the best, only semi-quantitative.

To circumvent this, the equation has been solved using numerical techniques by Hino (1968), Shir (1970), Randerson (1970), Berlyand (1972), Lantz (1972), Egan and Mahoney (1972), Roffman and Grimble (1974), Runca and Sardij (1975), Lebedeff and Hameed (1975), Ragland and Dennis (1975) and others. This added complexity is believed by some people to be unnecessary because of the other deficiencies in the formulation of the diffusion equation and because of the usual lack of precise meteorological information. On the other hand, it is only numerical solutions which allow us to study economically the sensitivity of various variables (i.e. their relative importance); the effects of a variety of meteorological and topographical conditions; the effects of using assumptions which are not physically justified (extending the range of validity of the solutions); and the "what if" questions arising during air quality management planning and decision-making process. In a sense, numerical simulation allows one to perform controlled "experiments" which may be impossible in the natural environment.

Hino (1968) has used a forward finite-difference scheme to solve the steady-state 3-D C-D equation over a complicated topography. He computes velocity from the simplified Navier-Stokes equations using potential theory. The eddy diffusivity,  $K_z$ , is assumed to be proportional to the wind speed and to a power of the height from the ground. Randerson (1970) has calculated the concentration field of  $SO_2$  over Nashville, Tennessee using an explicit-finite difference scheme.

Shir (1970) has obtained air pollution distributions downwind from a line source (2D-case) by using equations for heat, momentum and mass conservation which are solved by an iterative finite difference scheme. Constant diffusion coefficients are used for his computations. Danard (1972) has solved the 2-D C-D equation to calculate the carbon monoxide concentration near highways using the Dufort and Frankel explicit finite difference technique.

Lantz (1972) presented a numerical model which calculated 3-D boundary layer winds considering flow obstacles, along with 3-D C-D equation (solved by the Alternating Direction Implicit finite difference scheme) using a power-law K-profile. A numerical, grid-element 3-D model has been developed for the study of air pollution transport from urban area sources by Egan and Mahoney (1972). In their paper the "pseudo-diffusive" errors (i.e. "false" or "numerical" diffusion) associated with conventional finite-difference approximations to the advective term are eliminated by a material-conserving computation procedure involving first and second moments of the concentration distribution within each grid element.

Roffman and Grimble (1974) use a successive orthogonal coordinate transformation (to avoid false diffusion) in which one of the axes is parallel to the flow at each segment of the flow path. This transformation coupled with the wind and diffusivity profiles from similarity theory, is used in the integration of the diffusion equation. Runca and Sardei (1975) have developed a mixed Lagrangian-Eulerian finite difference scheme for calculating 2-D convection diffusion from a point source. In this scheme concentration is obtained by separating the contribution due to the advection and diffusion terms.

Ragland and Dennis (1975) have obtained a solution to the steady-state diffusion equation using a finite difference scheme. They consider

only one-component of velocity by using similarity theory. Lebedeff and Hameed (1975) use an integral method for the solution of 2-D C-D equation but the z-dependence of K is ignored.

Gillani and Husar (1975) have solved the 3-D C-D equation using separation of variables and integral transform methods. K is considered a function of downwind distance and the velocity field is assumed constant. Their model includes the effect of pollutant absorption (or desorption) by considering a first order rate process. Attempts are also made to study particle settling and washout.

Russian work in this field is summarized in the book by Beryland (ed.) (1973). In the case of an industrial stack, solutions of the steady state (elliptic) C-D equation are obtained by using

$$U = U_1 \frac{\ln(z/z_0)}{\ln(z_1/z_0)}$$

and

$$K_z = \begin{cases} v + k_1 z/z_1 & z \leq h \\ v + k_1 h/z_1 & z > h \end{cases}$$

where  $U_1$  and  $k_1$  ( $\gg v$ ) are the values of  $u$  and  $K_z$  respectively for  $z = z_1$  ( $z_1 = 1m$ ). This K-profile is quite unrealistic\*. In his review paper, Beryland (1972) indicates that the solutions to pollutant dispersion problems are also obtained by combining the equations of turbulent diffusion with the equations of motion and heat transfer. However, no details are given regarding the numerical scheme employed for this task.

Thus, the following problems are encountered in the solution of the C-D equation:

\*This is due to the use of  $z_1 = 1m$ . A realistic value of  $z_1$  will be of the order of 50m.

1. Deficiencies in the theoretical basis of the equation.
2. Choice of K-profile.
3. Choice of velocity profile.
4. Problems arising from the solution method. i.e.
  - (a) Results of limited applicability for the analytical solution case.
  - (b) Numerical problems in the numerical solution case.

The form of eddy diffusivity  $K(z)$  under various stability conditions is only known approximately. In addition, the velocity profile depends on the K-profile. As a further complication in plume dispersion problems, most plumes have an initial self-generated turbulence phase in which their dispersion is independent of the K-profile. All of the above mentioned solutions have ignored this point.

#### 4.1.2 Current Methods for Determination of Sigmas:

The numerical values of sigmas used in Gaussian models are usually based upon one of these methods:

- (a) Experimental data
- (b) Modification of experimental sigmas using intensity of turbulence
- (c) Modification of no wind shear  $\sigma_y$  by a rough estimate of the centroid of each plume segment displacement
- (d) Use of the Lagrangian auto correlation function
- (e) Moment concentration method

## (a) Experimental Data\*:

Most popular  $\sigma$ -curves currently in use are based on experiments performed in open fields (e.g. Pasquill (1961), Sutton (1947), TVA (see Carpenter et. al., 1971) and BNL (see Smith and Singer, 1965)). The main advantages of these curves are that they are easy to use and widely accepted by government agencies for environmental assessment work. A summary of experimental field diffusion data is given by Draxler (1976) and Gifford (1976). Other papers of general interest are: Hosker (1974), MacCready et. al. (1974), Whaley (1972) and Turner (1970).

## (b) Modification of Experimental Sigmas Using Intensity of Turbulence:

Csanady (1973), in his book, suggested the use of intensity of turbulence measurements to modify the Pasquill curves for elevated releases. The main problem with this approach is that reliable data are not available for intensity of turbulence. A different method for stably stratified conditions has been discussed by Sethu Raman et. al. (1974).

(c) Modification of No-Wind-Shear  $\sigma_y$  by a Rough Estimate of the Centroid of Each Plume Segment Displacement:

Weil (1974) proposes to modify  $\sigma_y$  by estimating the displacement of the centroid of each plume segment in the vertical direction assuming that the crosswind component of each plume segment is proportional to the wind component in that direction at that height.

$$\sigma_{y_s}^2 = \sigma_y^2 + \frac{\lambda^2}{12} \left( \frac{d\phi}{dz} \cdot x \right)^2 H_m^2$$

(Note: Just about the same as given by Pasquill(1976)

where,

$$\text{R.H.S.} = \sigma_y^2 + \frac{1}{10} (\Delta\phi)^2 x^2$$

$\sigma_{y_s}$  is the standard deviation for the entire cross-section in the y-direction in the presence of cross-wind shear

\* A number of other authors have reported  $\sigma$ -curves having novel features. However, in this survey it was not possible to include everyone.

$\phi$  is the wind direction (Assumption  $\phi = 0$  at  $z = 0$ )

$z$  is the distance from the midpoint of the mixing layer

$H_m$  is the mixing depth of the layer

$\lambda$  is a proportionality constant ( $\lambda \approx 0.9$ : from experimental data of Weil)

and  $\Delta\phi$  is the total change of mean wind direction

(d) Use of the Lagrangian Auto Correlation Function:

Draxler (1976) applied the theory of diffusion developed by Taylor to collected data of documented diffusion studies in the following way.

By Definition,

$$\sigma_y^2 = \overline{v^2} \int_0^T \int_0^t R(\xi) d\xi dt$$

where

$R(\xi)$  Langrangian auto correlation (varies from 1 (at start) to 0 (for large diffusion times))

$\overline{v^2}$  variance of lateral component of wind velocity

and  $T$  diffusion time

Using Pasquill (1971)

$$\sigma_y = \sigma_v T f_1(T/t_L)$$

and

$$\sigma_z = \sigma_w T f_2(T/t_L)$$

where,  $t_L$ , the Lagrangian time scale is defined as

$$t_L = \int_0^\infty R(\xi) d\xi$$

and  $\sigma_v$ ,  $\sigma_w$  are S.D. of the horizontal and vertical wind components.

Now, using  $\sigma_{yT} \approx \sigma_{\theta} x$ ,  $\sigma_{zT} \approx \sigma_{\phi} x$  (where,  $\sigma_{\theta}$  and  $\sigma_{\phi}$  are the S.D. of the azimuth and elevation angles) and suitable expressions for  $R(\xi)$  from theoretical considerations, attempts are made to define  $f_1$ ,  $f_2$  and  $t_L$ . Once these quantities are known  $\sigma_y$  and  $\sigma_z$  may be computed.

This method does not work for the cases such as vertical diffusion from ground sources during unstable stratification and vertical diffusion from elevated sources, presumably because of lack of vertical homogeneity.

(e) Moment Concentration Method:

This method due to Aries (1956) has been used in theoretical investigations to study cross-wind shear effects by Saffman (1962), Smith (1965), Csanady (1968) and Tyldesley and Wallington (1965) (for numerical work) for ground level releases. No attempt was made in the above work to relate the computed  $\sigma_y$ 's with the available experimental  $\sigma$ -curves. Furthermore, the results of the above authors do not include atmospheric stability as an explicit variable. Smith(1972) presented the results for  $\sigma_z$  for ground level releases.

4.1.3. Windshear Effects:

Several investigators (Saffman (1962), Smith (1965), Tyldesley and Wallington (1965), Csanady (1968)) have shown theoretically that the effect of wind shear on the dispersion of air pollutant is considerable. Experimental results reported by Pasquill (1962, 1969), Hogstrom (1964), Csanady (1972) and Brown and Michael (1974) are also in line with the theoretical findings.

Saffman (1962) considered the spread of an instantaneous cloud released from ground level in a turbulent wind using variable  $K$  within a bounded layer (comparable to a pipe) and an unbounded layer (comparable to a semi-infinite atmosphere). He found theoretically that the horizontal

spread cannot be described by a constant diffusivity and that horizontal mean-square dispersion does not increase linearly with time as constant K theory would suggest. These results have been verified experimentally by Hogstrom (1964) and theoretically by Smith (1965).

Tyldesley and Wallington (1965) solved the diffusion equation on an Analog computer using an Ekman spiral wind structure (constant K) to study the effect of wind shear and vertical diffusion. They also considered the case of  $K_z$  decreasing linearly with height to zero and  $K_y = 0$  but u and v constant with height.

Csanady (1968) obtained analytical solutions of the C-D equation using constant diffusivity and the Ekman layer velocity profile (constant eddy viscosity) for estimating the ground level trajectory of an instantaneously released cloud. Use of constant K make this model unrealistic. It overestimates the cloud growth and the angle between the surface wind and geostrophic wind.

Pasquill (1962, 1969), based on his experimental results, indicates that at distances as far as 130 Km downwind over a rural terrain very little wind effect is observed during the daytime when good mixing occurs in the boundary layer; however, during inversion conditions, significant shearing effects occur beyond 2 to 3 Km downwind from a source. At great distances the shear contribution to the crosswind standard deviation becomes dominant. Brown and Michael (1974) experimentally found that the crosswind standard deviations are greater during stable conditions than during neutral conditions. This is due to large wind shears associated with increased stability; without wind shear one would expect lower crosswind dispersion under stable conditions.

#### 4.1.4 Experimental Studies:

A number of experiments are carried out every year which are unique in relation to the type and location of source and instrumentation used. Experimental studies have been made in the open atmosphere (field studies), in wind tunnels, in water channels and in tanks.

Wind tunnel modelling has two advantages over open atmosphere experiments. Firstly, data extraction is much easier, and, secondly, one has control over the experimental conditions. The atmosphere rarely behaves the way one wishes. However, wind-tunnel modelling has a severe restriction in dynamical scaling. Scaling problems have aroused much controversy in these studies because it is not possible to satisfy all the similarity conditions. Usually some of these laws lead to conflicting requirements.

The current state of field experimental data available for comparison purposes can be best summarized as:

- (a)  $\sigma_y$  from continuous releases in the first few hundred meters above the earth's surface has been the prime target of various investigators. Three basic features of the results are:  $\sigma_y \propto x^{0.7}$  to  $x^{0.9}$ , a relationship between  $\sigma_y$  and the horizontal component of turbulence; and a dependence on the sampling time over which the average concentration distribution is measured. Limited results from elevated sources indicate the varying effect of cross-wind shear with atmospheric stability.
- (b) Relatively little attention has been paid to measuring  $\sigma_z$  mainly because of the larger cost of making such

measurements. The common approach is to derive this variable indirectly from ground level concentration measurements and  $\sigma_y$ . Thus, at least, two areas of errors are introduced: effects of deposition and errors in measuring g.l.c.

- (c) Concentration measurements are usually limited to ground level. These results include the effects of deposition and therefore, the "true" (i.e. in the absence of deposition) concentration with distance may be quite different.

Finally, experimentalists are unable to come to an agreement on a uniform approach for collecting and presenting all atmospheric diffusion data.

#### 4.1.5 Conclusions from Literature Survey:

General results for dispersion of pollutants in PBL are not available. No theoretical work has been done, at least for elevated releases, to study statistical coefficients (sigmas) under varying atmospheric conditions. (Usually  $\sigma$ -curves are obtained for ground level releases or at the most, for a particular stack height; the TVA and BNL/ASME elevated release experimental curves are most probably only of local validity.) Ground level release simulation work is limited to a constant K-case or to a linear variation of K (ground to the top of PBL). No wind variation with realistic K-profile is taken into consideration in these studies.

#### 4.2 General Background:

For the transport of a given pollutant, the principle of conservation of diffusing material may be written, in the form of the convective - diffusion equation, as

$$\frac{\partial C}{\partial t} + \nabla \cdot (C\vec{V}) = \nabla \cdot \vec{q} + Q + Q_r - Q_a \quad (4.1)$$

where,

- C Pollutant concentration ( $\text{Kg/m}^3$ )
- $\vec{q}$  Turbulent Mass flux ( $\text{Kg/m}^2/\text{sec}$ )
- Q Pollutant source strength ( $\text{Kg/m}^3/\text{sec}$ )
- $Q_r$  Rate of loss or gain (e.g.  $\text{H}_2\text{SO}_4$  aerosol by  $\text{H}_2\text{O} + \text{SO}_3$ ) of pollutant due to reaction ( $\text{Kg/m}^3/\text{sec}$ )
- $Q_a$  Pollutant Ground Absorption rate ( $\text{Kg/m}^3/\text{sec}$ )
- t Time (secs)
- $\vec{V}$  Wind Velocity Field (m/sec)
- $\vec{V} = u \cdot \vec{i} + v \cdot \vec{j} + w \cdot \vec{k}$

The gradient transfer theory (or K theory) may be used for the computation of the turbulent mass flux  $\vec{q}$  i.e.

$$\vec{q} = -\left(K_x \frac{\partial C}{\partial x} \vec{i} + K_y \frac{\partial C}{\partial y} \vec{j} + K_z \frac{\partial C}{\partial z} \vec{k}\right) \quad (4.2)$$

where the K's are eddy diffusivity constants (units:  $\text{m}^2/\text{sec}$ )

It is further assumed that the eddy diffusivity constants for mass and momentum transfer are equal except where accurate expressions are available. These are discussed in the Wind Structure section.

##### 4.2.1 Analysis of Gaussian Dispersion Models:

The Gaussian dispersion models are applicable to the following

conditions:

1. Uniform atmosphere (wind velocity and lapse rate)
2. Flat terrain
3. No chemical reaction of pollutants
4. No absorption of the pollutant at the ground
5. Single source (uncertainty about multiple sources)
6. Diffusivity coefficients independent of  $z$ .

These models are strictly applicable to these conditions, but generally used for other situations (with some success too!).

A particular solution under the above conditions is (for a continuous point source):

$$C(x,y,z) = \frac{q}{2\pi\bar{u}\sigma_y\sigma_z} e^{-\frac{y^2}{2\sigma_y^2}} \left[ e^{-\frac{(z-h_s)^2}{2\sigma_z^2}} + e^{-\frac{(z+h_s)^2}{2\sigma_z^2}} \right] \quad (4.3)$$

where

- $q$  Pollutant mass emitted per unit time from a point source or effective point source
- $\bar{u}$  Mean wind speed
- $y$  Lateral distance from the centre line
- $h_s$  Source height
- $\sigma_y$  Standard deviation in  $y$ -direction (function of  $x$ )
- $\sigma_z$  Standard deviation in  $z$ -direction (function of  $x$ )

For  $z = 0$ , the above equation reduces to

$$C(x,y,0) = \frac{q}{\pi\bar{u}\sigma_y\sigma_z} e^{-\left[\frac{y^2}{2\sigma_y^2} + \frac{h_s^2}{2\sigma_z^2}\right]} \quad (4.4)$$

where,  $C(x,y,0)$  is the ground level concentration (g.l.c.)

In applying this result to dispersion of real plumes a point source is assumed to exist at some "effective stack height" above ground level. This height,  $h_s$ , can be found using one of a number of plume rise formulae (see Briggs (1969)):  $h_s$  is the sum of the true stack height and plume rise.

$$h_s = h_t + \Delta h \quad (4.5)$$

The centerline ( $y = 0$ ) ground level concentration is given by

$$C(x,0,0) = \frac{q}{\pi u \sigma_y \sigma_z} e^{-\frac{h_s^2}{2\sigma_z^2}} \quad (4.6)$$

$C(x,0,0)$  is a function of  $x$  which is small for large and small  $x$  and which has a maximum value given by

$$C_{\max} \approx \frac{2q}{\pi u h_s^2} \frac{\sigma_z}{\sigma_y} \quad (4.7)$$

occurring approximately at the distance where  $\sigma_z = h_s/\sqrt{2}$ . This expression is derived by assuming  $\sigma_z/\sigma_y \approx \text{constant}$ .

One can readily see that an error in  $\sigma_y$  or  $\sigma_z$  directly changes the value of  $C_{\max}$ . The sensitivity of  $C_{\max}$  (to dispersion coefficients) thus, directly depends on changes in the ratio of  $\sigma_z/\sigma_y$ . Also, there is considerable disagreement between various "standard" expressions for  $\sigma_y$  and  $\sigma_z$  as functions of  $x$  which lead to different values of  $C_{\max}$  (see Table 4.1).

Table 4.1 SUMMARY OF ATMOSPHERIC COEFFICIENTS

$$(\sigma_z = ax^b, \sigma_y = cx^d)^*$$

S. NO.	STABILITY CLASS	a	b	c	d
1.	Pasquill/Gifford				
	Unstable (class B)	0.05	1.07	0.40	0.87
	Neutral (class D)	0.45	0.62	0.17	0.88
	Stable (class E)	0.43	0.56	0.12	0.88
2.	BNL/ASME				
	Unstable	0.33	0.86	0.36	0.86
	Neutral	0.22	0.78	0.32	0.78
3.	TVA				
	Neutral	0.37	0.74	0.37	0.76
	Stable	2.94	0.34	0.78	0.63
4.	TURNER				
	Unstable	0.056	1.10	0.41	0.86
	Neutral	0.73	0.55	0.14	0.89
	Stable	0.63	0.45	0.075	0.89

\*  $\sigma_y$  and  $\sigma_z$  curves only match these expressions approximately in general.

A comparison of maximum ground level concentration and its position using various  $\sigma_z(x)$  and  $\sigma_y(x)$  formulae (Table 4.1) is given in Table 4.2. Significant differences can be observed for the same source and velocity field ( $Q$ ,  $h$  and  $\bar{u}$ ). For example, for a neutral atmosphere the peak concentration predicted by the TVA formulae is 87% higher than Turner's calculation, and the BNL/ASME concentration is 45% higher than Turner's concentration. The important conclusion to be drawn from Table 4.2 is that in applying various diffusion parameters care must be taken in the choice of  $\sigma$ -formulae and in interpreting the results.

#### 4.2.2 Calculations for Critical Concentration:

The following analysis is intended to provide general expressions for critical concentration under varying atmospheric stability conditions. Critical concentration is obtained by maximizing the ground level concentration both with respect to distance and wind speed. The wind speed at which the critical concentration occurs is usually known as the "critical" wind speed.

The centerline ground level concentration is given by

$$C = \frac{q}{\pi \bar{u} \sigma_y \sigma_z} e^{-\frac{h_s^2}{2 \sigma_z^2}} \quad (4.8)$$

Let us assume that the plume growth may be approximated by

$$\sigma_z = ax^b \quad \text{and} \quad \sigma_y = cx^d \quad (4.9)$$

where,  $a$ ,  $b$ ,  $c$ ,  $d$  are constants, and the plume rise is given by

$$\Delta h = \frac{B}{\bar{u}^n} \quad (4.10)$$

Table 4.2 COMPARISON OF MAXIMUM GROUND LEVEL CONCENTRATION  
AND ITS POSITION USING AVAILABLE  $\sigma_y(x)$  and  $\sigma_z(x)$  FORMULAS  
h = 50 m h = 100 m

STABILITY	$X_{\max}$ (m)	$\left(\frac{C_{\max} \cdot e \cdot \pi}{uh^2 \cdot 2q}\right)^*$	$X_{\max}$ (m)	$\frac{C_{\max} \cdot e \cdot \pi}{uh^2 \cdot 2q}$
Unstable				
1. BNL/ASME	229.3	0.917	513.4	0.917
2. Pasquill (class B)	460.3	0.426	879.8	0.485
3. TVA	—	—	—	—
4. Turner	351.3	0.558	659.7	0.649
Neutral				
1. BNL/ASME	673.4	0.688	1637.5	0.688
2. Pasquill	1139.8	0.425	3486.4	0.318
3. TVA	474.3	0.884	1210.1	0.868
4. Turner	1158.4	0.474	4085.1	0.309
Stable				
1. BNL/ASME	7976.1	0.194	21174.9	0.194
2. Pasquill (class E)	2627.9	0.288	9060.9	0.194
3. TVA	1502.4	0.452	11539.0	0.250
4. Turner	7707.6	0.164	35964.6	0.083

\* Note:  $C_{\max}$  has been nondimensionalized.

Here  $n$  is a parameter which will be left arbitrary because it varies with stability and  $\Delta h$  is assumed to be inversely proportional to  $\bar{u}^n$ .

Results for  $\sigma_z/\sigma_y = 1$  (i.e. equal growth) and  $n = 1$  are given by Pasquill (1962), for  $\sigma_z/\sigma_y = \text{constant}$  and  $n = 1$  are provided by Csanady (1973), and for  $\sigma_z/\sigma_y \neq \text{constant}$  and  $n = 1$  are discussed by Ragland (1976). From 4.8 and 4.9, the maximum ground level concentration occurs when

$$\frac{dC}{dx} = 0 \quad \text{i.e.}$$

$$X_{\max} = \left[ \frac{b h_s^2}{a^2 (b + d)} \right]^{\frac{1}{2b}} \quad (4.11)$$

and

$$C_{\max} = \frac{q \exp\left(-\frac{b+d}{2b}\right)}{\pi \bar{u} a c \left[ \frac{b \left(h_t + \frac{B}{\bar{u}^n}\right)^2}{a^2 (b+d)} \right]^{\frac{1}{2b}}} \quad (4.12)$$

Here, the effective stack height  $h_s$  is assumed constant.

Using (4.4) and (4.10) and differentiating (4.12) with respect to  $\bar{u}$ , one can obtain the critical wind speed as

$$U_{\text{critical}} = \left[ \frac{B}{h_t} \left\{ \frac{(b+d)n}{b} - 1 \right\} \right]^{\frac{1}{n}} \quad (4.13)$$

For wind speeds above or below the critical wind maximum glc will be less. In order to find the peak glc of air pollutants released from tall stacks, an expression for critical plume rise may be derived as

$$\Delta h_{\text{critical}} = \frac{h_t}{\left\{ \frac{(b+d)n}{b} - 1 \right\}} \quad (4.14)$$

To obtain the expressions for the corresponding critical concentrations and the point at which it occurs, a value for  $n$  may be estimated either from theory or experiments under different atmospheric conditions.

A more general discussion using an inclined model for a neutral atmosphere (similar to that of Csanady (1973)) for an unequal plume growth is given in Appendix A.

#### 4.3 Evaluation of sigmas for elevated continuous releases:

The following sections describe two different ways to obtain sigmas

1. based on the Moment-Concentration method for sigmas and using an empirical velocity field
2. based on the Moment-Concentration method for sigmas and using a numerical solution for the velocity field.

Method (2) requires more detailed information on meteorological parameters such as geostrophic velocity variation and PBL height. Method (1) is therefore more suitable for operational purposes while Method (2) may be used as a research tool and can serve for improvement in Method (1). Method (1) is cheaper than Method (2) from the computer operational point of view.

##### 4.3.1 Mathematical Formulation of the Problem:

The steady state diffusion equation for a continuous point source may be written as:

$$u \frac{\partial C}{\partial x} + v \frac{\partial C}{\partial y} = \frac{\partial}{\partial y} \left( K_y \frac{\partial C}{\partial y} \right) + \frac{\partial}{\partial z} \left( K_z \frac{\partial C}{\partial z} \right) + Q \quad (4.15)$$

(The x-axis is taken in the direction of mean wind.)

This equation is a simplified form of the original convective-diffusion equation (Equations 4.1 and 4.2) and uses a number of assumptions (e.g. the ground is assumed to be a perfect reflector and eddy diffusion in the x-direction is neglected).

The following development is based on the Moment-Concentration method and has the following features:

- (a) capability to include atmospheric stability and surface roughness,
- (b)  $\sigma_z$  is computed directly,
- (c) cross-wind shear effects due to varying atmospheric conditions can be computed.

The model can be used to generate  $\sigma$ -curves (i.e.  $\sigma = \sigma(x)$ ) for any release height.

In order to compute  $\sigma_y$  and  $\sigma_z$  as functions of downwind distance, x, we define zero, first and second moments of concentration in the y and z directions as follows:

- (i) y - direction:

$$\begin{aligned} C_y^0 &= \int_{-\infty}^{\infty} C dy \\ C_y^1 &= \int_{-\infty}^{\infty} y C dy \\ C_y^2 &= \int_{-\infty}^{\infty} y^2 C dy \end{aligned} \quad (4.16)$$

(ii) z - direction

$$\begin{aligned}
C_z^0 &= \int_0^{\infty} C dz \\
C_z^1 &= \int_0^{\infty} z C dz \\
C_z^2 &= \int_0^{\infty} z^2 C dz
\end{aligned} \tag{4.17}$$

Note that the zero, first and second moments are related to the total amount of pollutant, the position of the pollutant centre of mass and standard deviation (or spread) of pollutant respectively. The relationships for  $\sigma_y$  and  $\sigma_z$  in terms of these moments are:

$$\sigma_y^2 = \frac{C_y^2}{C_y^0} - \left( \frac{C_y^1}{C_y^0} \right)^2$$

and

$$\sigma_z^2 = \frac{C_z^2}{C_z^0} - \left( \frac{C_z^1}{C_z^0} \right)^2$$

(4.18)

Integrating equation (4.15) from  $-\infty$  to  $+\infty$  and applying the definitions given in (4.16) and (4.17), one obtains.

For the y-moments:

$$\begin{aligned}
u \frac{\partial C_y^0}{\partial x} &= \frac{\partial}{\partial z} \left( K_z \frac{\partial C_y^0}{\partial z} \right) \\
u \frac{\partial C_y^1}{\partial x} &= v C_y^0 + \frac{\partial}{\partial z} \left( K_z \frac{\partial C_y^1}{\partial z} \right) \\
u \frac{\partial C_y^2}{\partial x} &= 2v C_y^1 + \frac{\partial}{\partial z} \left( K_z \frac{\partial C_y^2}{\partial z} \right) + 2K_y C_y^0
\end{aligned} \tag{4.19}$$

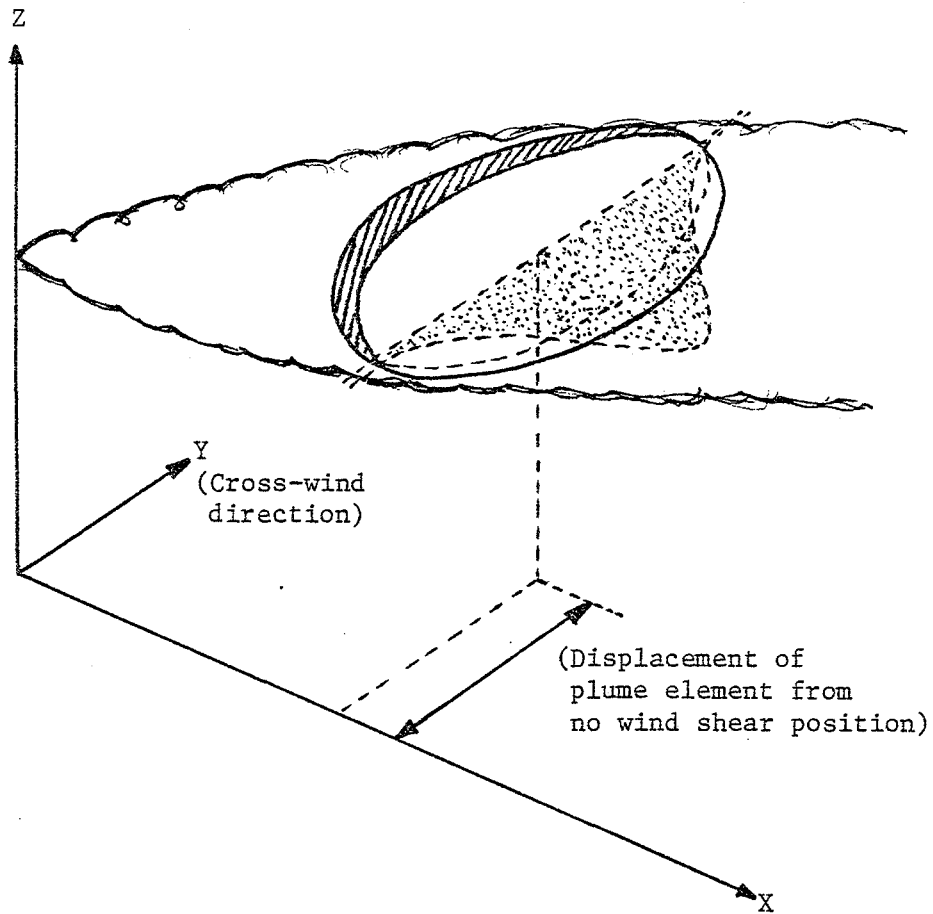


FIGURE 4.0: PLUME ELEMENT UNDER A TYPICAL CROSS-WIND SHEAR CONDITION

(Note: This diagram is schematic .  
The plume cross-section under  
cross-wind shear conditions  
will be skewed.)

For the z-moments:

$$u \frac{\partial C^0_z}{\partial x} + v \frac{\partial C^0_z}{\partial y} = \frac{\partial}{\partial y} \left( K_y \frac{\partial C^0_z}{\partial y} \right)$$

$$u \frac{\partial C^1_z}{\partial x} + v \frac{\partial C^1_z}{\partial y} = \frac{\partial}{\partial y} \left( K_y \frac{\partial C^1_z}{\partial y} \right) \quad (4.20)$$

and

$$u \frac{\partial C^2_z}{\partial x} + v \frac{\partial C^2_z}{\partial y} = \frac{\partial}{\partial y} \left( K_y \frac{\partial C^2_z}{\partial y} \right) + 2K_z C^0_z$$

The source term is treated as a boundary condition in each equation and will be discussed later on.

#### 4.3.2 Numerical Scheme:

The system of equations represented by (4.19) and (4.20) may be solved by finite-difference methods.

In the following the detailed finite difference form for the zero order moment equations (using an irregular grid) is given.

The zero order y-moment equation

$$u \frac{\partial C^0_y}{\partial x} = \frac{\partial}{\partial y} \left( K_z \frac{\partial C^0_y}{\partial z} \right)$$

becomes, in finite difference form

$$u_{i,k} \frac{C^0_{y_{i,k}} - C^0_{y_{i-1,k}}}{\Delta x^-} =$$

$$\frac{K_{z_{k+\frac{1}{2}}} C^0_{y_{k+1}} - \left( \frac{K_{z_{k+\frac{1}{2}}}}{\Delta z^+} + \frac{K_{z_{k-\frac{1}{2}}}}{\Delta z^-} \right) C^0_{y_k} + \frac{K_{z_{k-\frac{1}{2}}}}{\Delta z^-} C^0_{y_{k-1}}}{\frac{\Delta z^+ + \Delta z^-}{2}} \quad (4.21)$$

This may be written as

$$BB C^0_{y_{k+1}} + AA C^0_{y_k} + CC C^0_{y_{k-1}} = DD \quad (4.22)$$

where,

$$\Delta x^- = x_i - x_{i-1}$$

$$\Delta z^+ = z_{k+1} - z_k$$

$$\Delta z^- = z_k - z_{k-1}$$

$$AA = - \left( \frac{\frac{z_{k+\frac{1}{2}}^k}{\Delta z^+} + \frac{z_{k-\frac{1}{2}}^k}{\Delta z^-}}{\frac{\Delta z^+ + \Delta z^-}{2}} + \frac{u_{i,k}}{\Delta x^-} \right)$$

$$BB = \frac{z_{k+\frac{1}{2}}^k}{\Delta z^+ \left( \frac{\Delta z^+ + \Delta z^-}{2} \right)}$$

$$CC = \frac{z_{k-\frac{1}{2}}^k}{\Delta z^- \left( \frac{\Delta z^+ + \Delta z^-}{2} \right)}$$

$$DD = - u_{i,k} \frac{C^0_{y_{i-1,k}}}{\Delta x^-}$$

For the z-moment, the zero order equation is

$$u \frac{\partial C^0_z}{\partial x} + v \frac{\partial C^0_z}{\partial y} = \frac{\partial}{\partial y} \left( K_y \frac{\partial C^0_z}{\partial y} \right)$$

In finite-difference form this becomes

$$\begin{aligned}
 u_{i,k} & \frac{C^0_{z_{i,j}} - C^0_{z_{i-1,j}}}{\Delta x^-} + v_{i,j} \frac{C^0_{z_{i,j+1}} - C^0_{z_{i,j-1}}}{(\Delta y^+ + \Delta y^-)} \\
 & = \frac{K_{y_{j+\frac{1}{2}}} \left( \frac{C^0_{z_{j+1}} - C^0_{z_j}}{\Delta y^+} \right) - K_{y_{j-\frac{1}{2}}} \left( \frac{C^0_{z_j} - C^0_{z_{j-1}}}{\Delta y^-} \right)}{\frac{\Delta y^+ + \Delta y^-}{2}}
 \end{aligned} \tag{4.23}$$

or,

$$BB C^0_{z_{j+1}} + AA C^0_{z_j} + CC C^0_{z_{j-1}} = D \tag{4.24}$$

where,

$$\Delta y^- = y_j - y_{j-1}$$

$$\Delta y^+ = y_{j+1} - y_j$$

$$AA = - \left( \frac{2K_{y_{j+\frac{1}{2}}} + K_{y_{j-\frac{1}{2}}}}{\Delta y^+ (\Delta y^+ + \Delta y^-)} + \frac{u_{ij}}{\Delta x^-} \right)$$

$$BB = \frac{2K_{y_{j+\frac{1}{2}}}}{\Delta y^+ (\Delta y^+ + \Delta y^-)} - \frac{v_j}{\Delta y^+ + \Delta y^-}$$

$$CC = \frac{2K_{y_{j-\frac{1}{2}}}}{\Delta y^- (\Delta y^+ + \Delta y^-)} + \frac{v_j}{\Delta y^+ + \Delta y^-}$$

$$D = \frac{u_{ij}}{\Delta x^-} C^0_{z_{i-1,j}}$$

During computations  $K_y$  was set equal to  $K_z$  in order to be consistent with the velocity model.

#### 4.3.3 Source Term as a Boundary Condition:

If the source flux is  $q$  gm/sec. and is distributed over one grid rectangle  $(\Delta z, \Delta y)$  then the concentration at the corresponding grid point is

$$C = \frac{q}{u \cdot \Delta y \cdot \Delta z} \quad \text{gm/m}^3 \quad (4.25)$$

where,  $u$  is the wind velocity. This can be used as a boundary condition on  $C$ , replacing the need for the ad hoc procedure used by other authors of distributing a point source over a three dimensional grid element. The corresponding boundary conditions on the  $y$ -moments are:

$$C_y^0 = \int_{-\infty}^{\infty} C \, dy = \int_{-\infty}^{\infty} \frac{q}{u \cdot \Delta y \cdot \Delta z} \, dy = \frac{q}{u \cdot \Delta z} \quad (4.26)$$

$$C_y^1 = \int_{-\infty}^{\infty} y C \, dy = \int_{-\infty}^{\infty} y \frac{q}{u \cdot \Delta y \cdot \Delta z} \, dy = 0$$

$$C_y^2 = \int_{-\infty}^{\infty} y^2 C \, dy = 0$$

Similar expressions may be derived for  $C_z^0, C_z^1, C_z^2$ .

#### 4.3.4 Velocity Profiles:

Computation of  $\sigma$ 's requires the velocity field as an input. As indicated earlier, one may either use a numerically calculated velocity field or specify it based on experimental data and/or profiles obtained from other theories. In order to keep the model as simple as possible and physically realistic, we have kept both options open.

#### 4.3.4.1 Use of Empirical Relationships:

In this section we shall discuss the "empirical" formulae for the velocity field in the PBL. Here  $U$  is the mean velocity and  $u$  and  $v$  are its components in  $x$  and  $y$  directions.

(i) Surface Layer:

(a) Neutral Atmosphere:

$$U = \frac{U_*^*}{\kappa} \ln \left( \frac{z+z_0}{z_0} \right) \quad (4.27)$$

For surface layer (The Logarithmic profile).

(Note: From Businger (1973) - "There is considerable experimental evidence that verifies this profile,...")

(b) Stable Atmosphere:

$$U = \frac{U_*^*}{\kappa} \left[ \ln \left( \frac{z+z_0}{z_0} \right) + \frac{4.7}{L} z \right] \quad 0 < z \leq L$$

$$= \frac{U_*^*}{\kappa} \left[ \ln \left( \frac{z+z_0}{z_0} \right) + 4.7 \right] \quad L < z \leq h \quad (4.28)$$

For surface layer (Log-linear profile).

(c) Unstable Atmosphere:

$$U = \frac{U_*^*}{\kappa} \left[ 2(\tan^{-1} x - \tan^{-1} x_0) + \ln \left( \frac{x-1}{x_0-1} \right) - \ln \left( \frac{x+1}{x_0+1} \right) \right]$$

$$x = [1 - 15(z+z_0)/L]^{1/4} \quad (4.29)$$

$$x_0 = [1 - 15 z_0/L]^{1/4}$$

(see Ragland and Dennis, 1975 and Paulson, 1970)

## (ii) Ekman Layer:

A linear wind profile from  $h$  to  $H$  is used for the Ekman Layer for each stability class

$$U = (U_g - U_{sl}) \left( \frac{z - h}{H - h} \right) + U_{sl} \quad (4.30)$$

Calculation of  $u$  and  $v$  Components:

The following assumptions are made to derive the cross-wind component of velocity from the mean velocity:

- (a) The mean wind is approximately aligned with the surface wind throughout the surface layer i.e.  $v$ -component is zero.
- (b) The angle between the mean wind and the  $u$ -component at the top of PBL is equal to the surface cross-isobar angle. This is based on the assumption that the angle between the geostrophic wind and the mean wind is zero at the top of the PBL.
- (c) The rate of increase of angle between the mean wind and  $u$ -component is linear i.e. Rate =  $(\alpha_0)/(H - h)$  and  $\alpha = \text{Rate} * (z - h)$  for Ekman layer.
- (d) The wind direction is considered constant above the top of the PBL.

4.3.4.2 Numerical Profiles:

The profiles are discussed in Chapter 2.

#### 4.3.5 The Computer Model:

The physics involved in the solution of the problem and the numerical schemes used have been described in considerable detail in the preceeding sections. The softwares were developed using FORTRAN IV computing language. The program consists of a Main Program which calls for a number of built-in subroutines to calculate  $\sigma_y$  and  $\sigma_z$ . Velocity computations are carried out independently. The Thomas algorithm (see Appendix B) is used in the solution of tridiagonal system of equations. A number of runs were made to find a suitable range for the step size and then the appropriate size is chosen.

##### 4.3.5.1 Input Data Required for Running the Computer Program:

The data requirements are:

1. Grid network, source location and source strength
2. Topographical data: surface roughness and friction velocity
3. PBL data: Height of PBL and surface layer
4. Eddy viscosity/diffusivity data: User's specified profiles based on experiments or as indicated in theory (i.e. a value of  $p$  - see Chapter 2)
5. Velocity profiles:
  - a) Experimental data for  $u$  and  $v$  components of velocity specified at each grid point
  - or b) Numerical data: obtained via PBL modelling
  - or c) Empirical data: as indicated in theory (cross isobar angle and velocity at the top of PBL)

#### 4.3.6 Numerical Results for Sigmas Using Empirical Velocity Profiles:

Figures 4.1 to 4.6 show the  $\sigma_y$  and  $\sigma_z$  for a 100m release obtained from a numerical simulation using the empirical velocity profiles and eddy diffusivity profiles given by equations (4.27) to (4.30) and (2.13), and the input data as tabulated in Table 4.3. In Figures 4.1 and 4.2 horizontal and vertical standard deviations for a neutral atmosphere are plotted while sigmas for an unstable and stable atmosphere are predicted in 4.3 to 4.6. A comparison of sigmas for a constant K and a constant wind field (mean value = U) is given in Appendix C (numerical results vs. analytical results).  $\sigma$ -curves for other release heights are considered later. The results are compared with widely used experimental data, which are available in the open literature, of ASME/BNL, Pasquill\*, TVA and Sutton. Observations from some other sources are also included (Brown and Michael, 1974) in the comparison.

It is interesting to note that the results agree qualitatively with the theoretical work of Saffman (1962), Smith (1965), Csanady (1969) and Tyldesley and Wallington (1965), and are in agreement with the general conclusions drawn by Pasquill (1962, 1969) and Brown and Michael (1974) based on their experimental studies.

In strong instability (similar to clear warm days) the air is very turbulent and therefore the plume is diffused more rapidly in the vertical as well as in the horizontal plane. During stable atmospheric conditions (clear evenings and nights) the cloud does not disperse significantly until it has reached a considerable downwind distance. Sigmas are therefore much less than those obtained under unstable conditions due to reduced turbulence. Also,  $\sigma_z$  shows an explosive behaviour during unstable atmospheric conditions. These characteristics of vertical and

---

\* also, known as Pasquill-Gifford (P-G) curves.

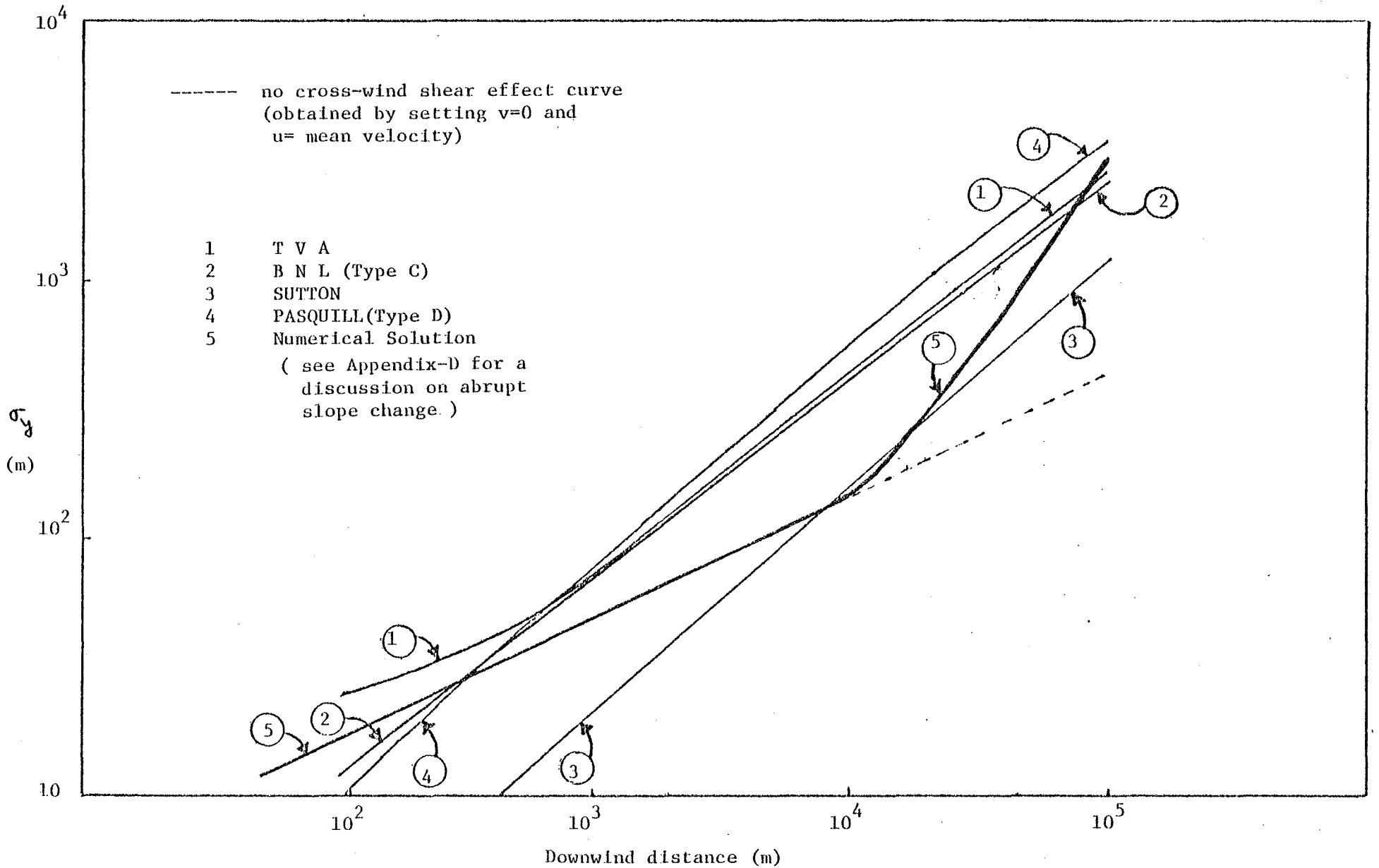


Figure 4.1: COMPARISON OF NUMERICAL AND EXPERIMENTAL  $\sigma_y$  CURVES FOR A NEAR-NEUTRAL ATMOSPHERE

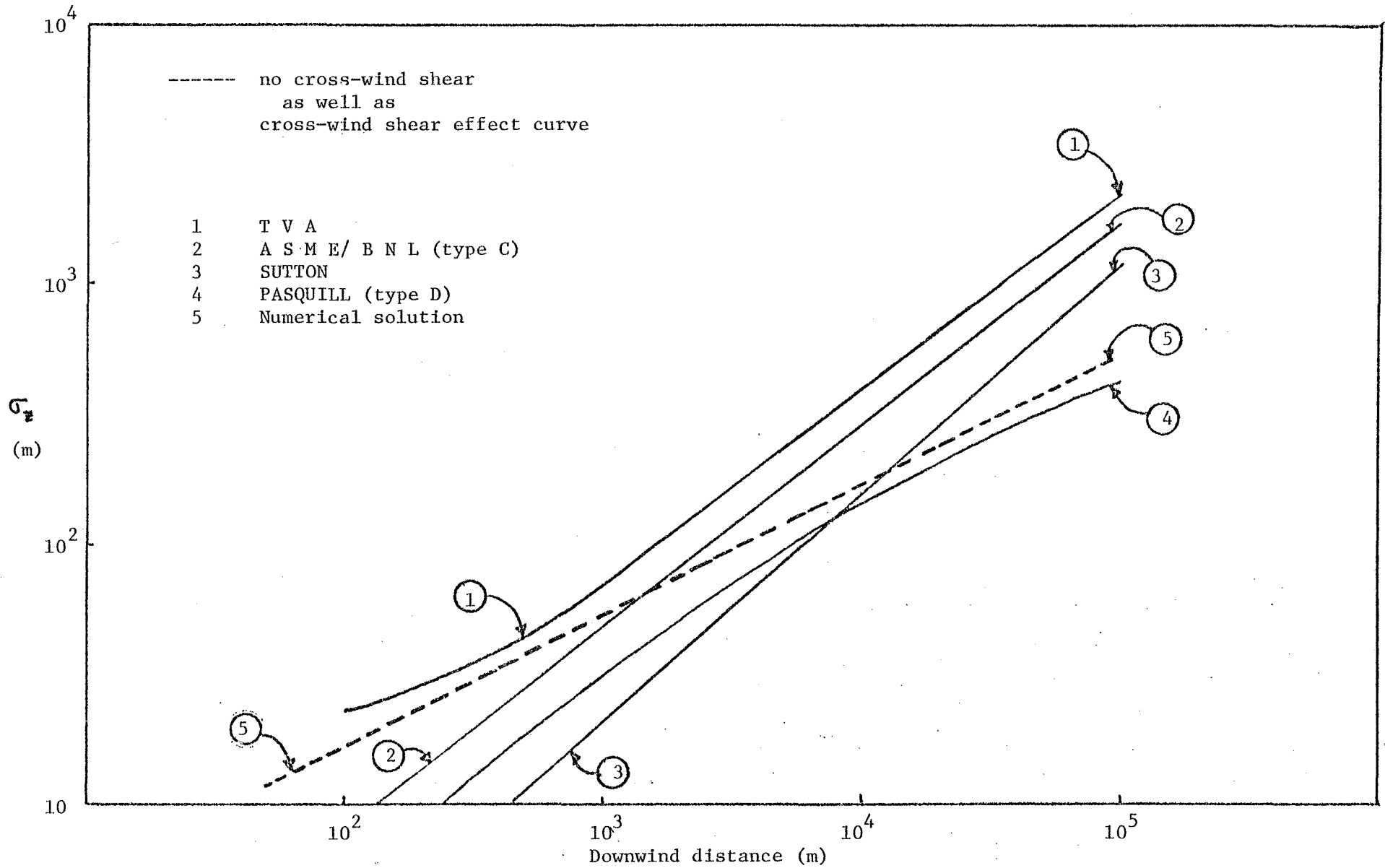


Figure 4.2: COMPARISON OF NUMERICAL AND EXPERIMENTAL  $\sigma_2$  CURVES FOR A NEAR-NEUTRAL ATMOSPHERE

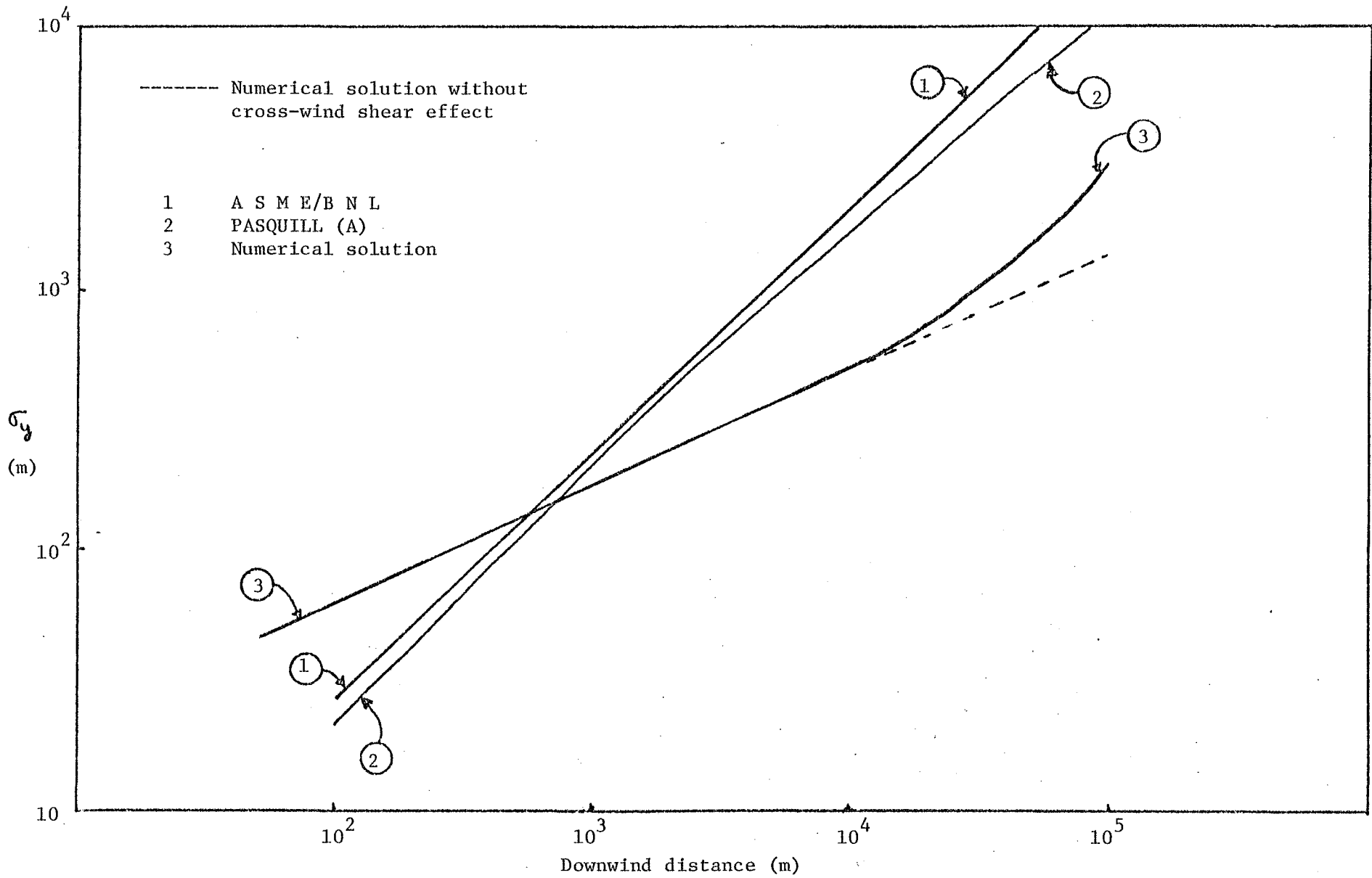


Figure 4.3: COMPARISON OF NUMERICAL AND EXPERIMENTAL  $\sigma_y$  CURVES FOR A UNSTABLE ATMOSPHERE

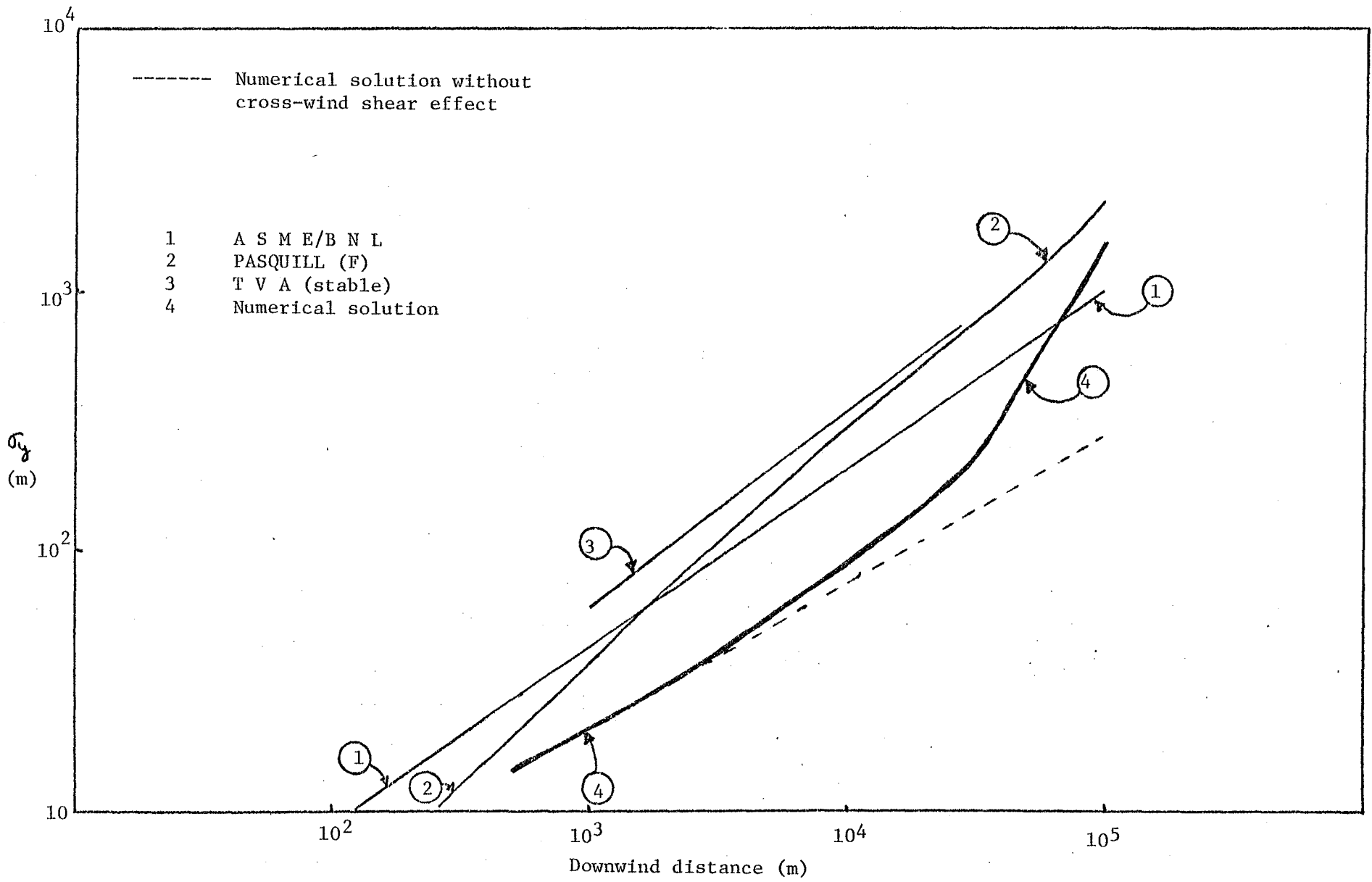


Figure 4.4: COMPARISON OF NUMERICAL AND EXPERIMENTAL  $\sigma_y$  CURVES FOR A STABLE ATMOSPHERE

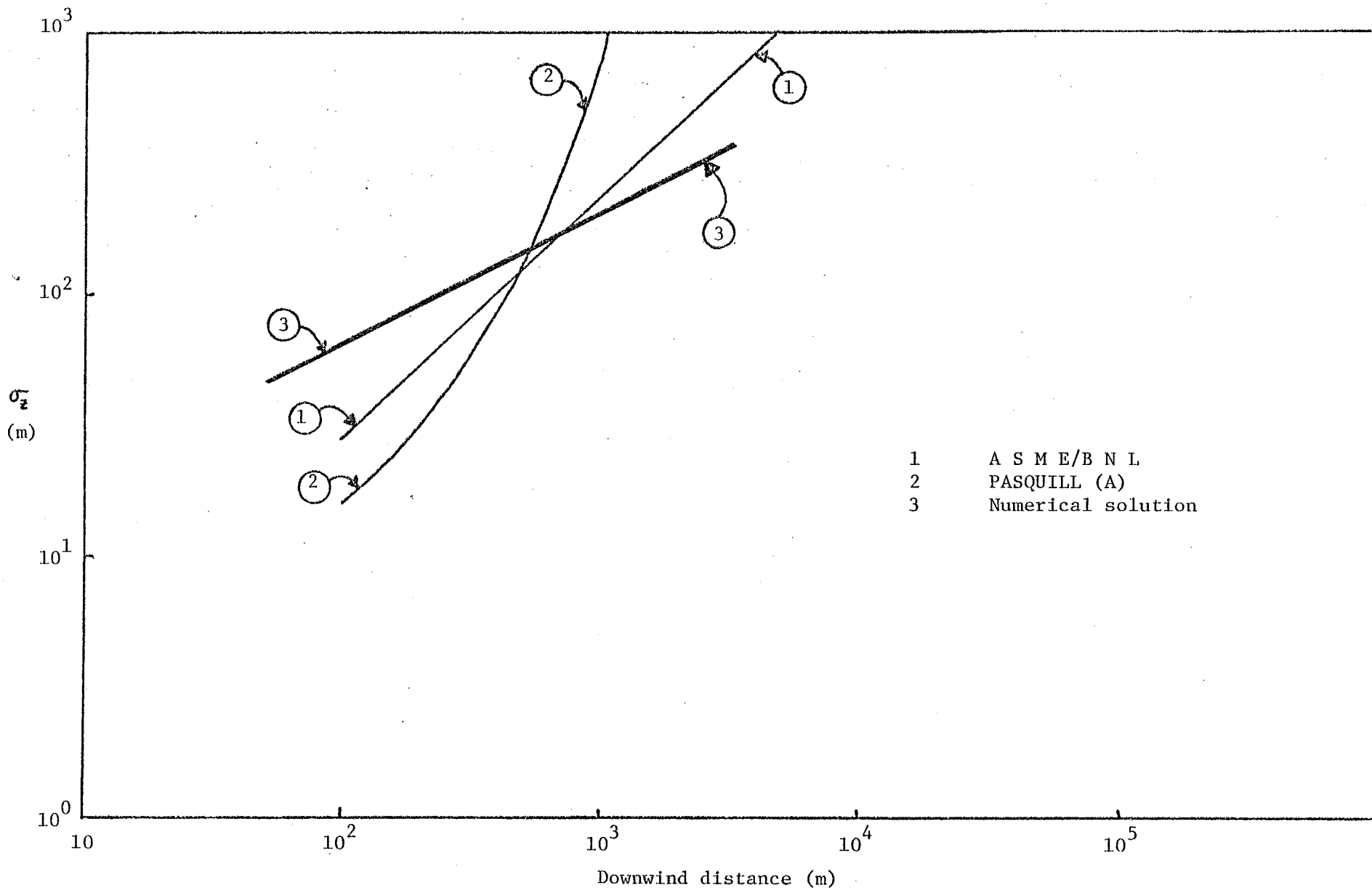


Figure 4.5: COMPARISON OF NUMERICAL AND EXPERIMENTAL  $\sigma_z$  CURVES FOR A UNSTABLE ATMOSPHERE

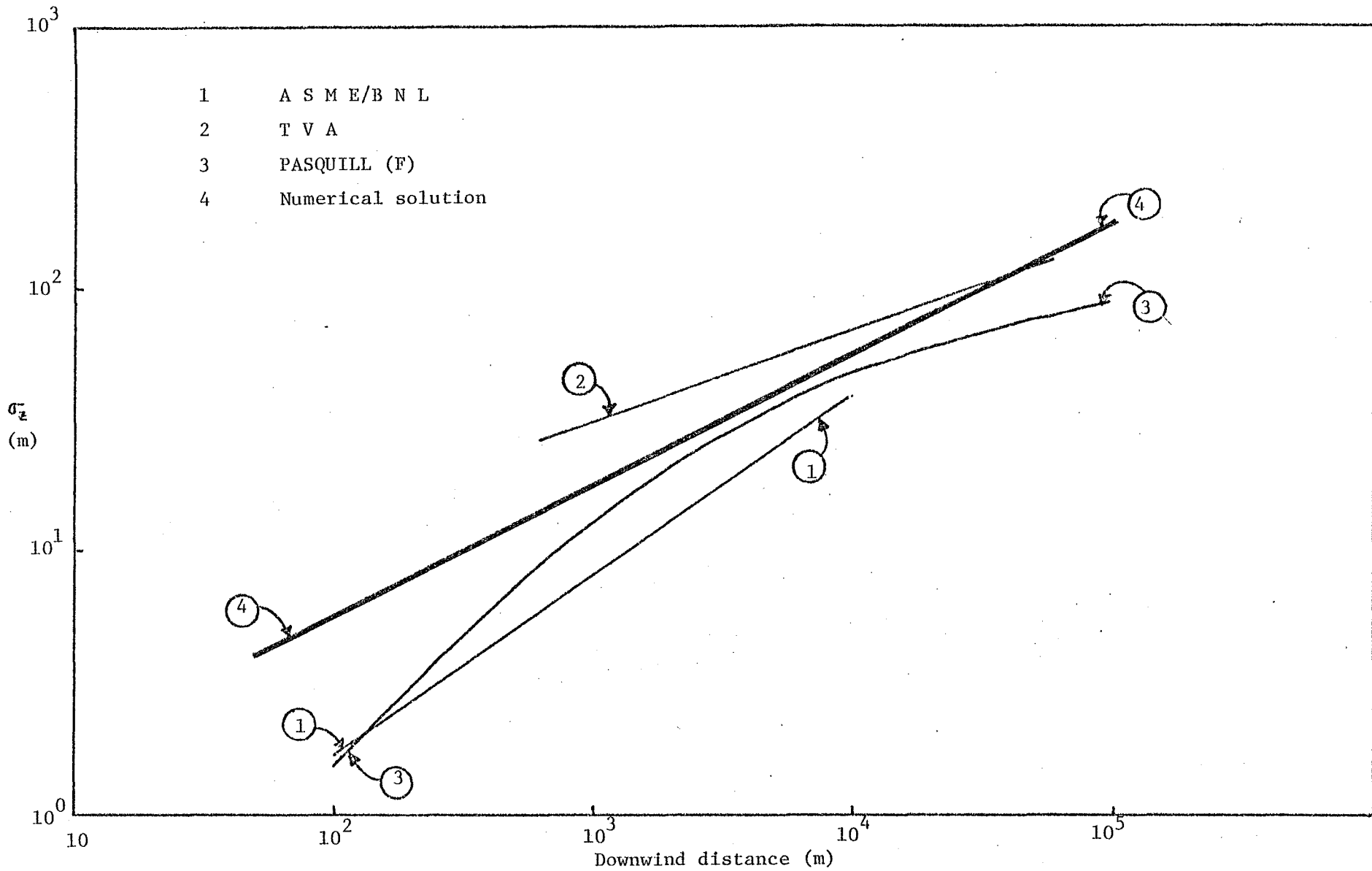


Figure 4.6: COMPARISON OF NUMERICAL AND EXPERIMENTAL  $\sigma_z$  CURVES FOR A STABLE ATMOSPHERE

Table 4.3: INPUT VARIABLES FOR  $\sigma$  COMPUTATIONS

Surface Roughness $z_0$	= 0.001 m
Height of PBL	= 1000 m
Ratio of Surface Layer Height/ PBL Height	= 0.1
K	= 0.4
Friction Velocity	= 0.2 m/sec
$\delta$	= 0.1
P	= 1.0 Unstable case
	= 1.5 Near-neutral case
	= 2.0 Stable case
h/L	= -10 Unstable case
	= 0 Near-neutral case
	= 1.5 Stable case
$\alpha_0$	= $10^\circ$ Unstable case
	= $30^\circ$ Near-neutral case
	= $45^\circ$ Stable case
$v_{g_{stop}}$	= 15 m/sec
Grid Size $\Delta x$	= 50 m for $x < 3000$ m
	= 100 m for $x > 3000$ m

horizontal standard deviations are evident from Figures 4.3 to 4.6.

Care must be taken in comparing these results with experimental work, and the following points may be helpful:

(a) Nature of Release:

Real life releases may be continuous or instantaneous and be idealized as either point or line sources. For example, an instantaneous point source situation occurs in cases such as an explosion. In the numerical solutions a continuous release has been assumed due to its closeness to many real life situations such as stacks and spills of volatile materials.

(b) Sampling Time:

During experimental studies the values of sigmas depend heavily on sampling time for the same plume under the same atmospheric conditions. The results for a 10 min. average and a two hour average plume can differ by as much as a factor of 2. For an instantaneous plume boundaries are quite irregular, while a 10 min. average plume will have a more regular and much wider boundary (a two hour plume is still wider). Away from the source large turbulent wind eddies play a dominant role in diffusing the cloud and the effect of smaller eddies diminishes gradually.

Therefore, one may require a large sampling time to get a steady-state picture of large fluctuations. The numerical solutions given here apply to the

steady-state case and so effectively model a (large) time-averaged plume.

(c) Release Height:

Releases in practical applications are usually made above ground. Due to generally prevailing emission control regulations elevated releases are much more common.

The numerical results are from an elevated source ( $h_s = 100\text{m}$ ). The release heights for experimental curves are discussed below. The application of  $\sigma$ -curves to buoyant plumes is given in section 4.3.7.4.

(d) Terrain Features:

Experiments are conducted under widely varying terrain conditions such as open fields, flat deserts, low/rough hills, low woods, rolling terrains and dense scrub. For the numerical results the surface roughness is a specified parameter: in this case equivalent to smooth mud flats.

(e) Velocity Field:

One interesting point which may be helpful to note is that in most field experiments on dispersion, conditions such as uniform sky cover and constant wind direction during the sampling time are favored. A steady state wind field with no change in velocity with downwind distance has been used for numerical work.

#### 4.3.6.1 BNL/ASME Dispersion Parameters Vrs. Numerical Results:

BNL  $\sigma$ -curves are plotted for distances ranging from 10m to 60km using wind gustiness as a measure of atmospheric stability based on 15 years of field experiments. Most of these studies involve the emission of very small oil fog droplets from a source 108m above ground.  $\sigma_y$  data are based on actual measurements while  $\sigma_z$  is derived using

$$\sigma_z = \frac{q}{C \sigma_y \bar{U} \pi} e^{-F}$$

where, F is an adjustment term for the Gaussian equation and C is measured concentration.  $\bar{U}$  has invariably been assumed constant (however it should increase with height).

ASME recommended coefficients are the same as obtained during BNL experiments.

The points which should be mentioned about BNL curves are:

- (a) values of  $\sigma$ 's are based on one hour averages from 108m releases
- (b) for large downwind distances ( $> 10$ km) experimental curves are extrapolated.

On comparing the present numerical results with experimental BNL curves for  $\sigma_y$  (Figures 4.1, 4.3 and 4.4), one may observe that the numerical values of  $\sigma_y$  are greater than the experimental values for downwind distances up to about 500m - 1000m. After this the numerical values are lower but beyond about  $10^4$ m they are trying to "catch" the experimental curves. The "catch-up" process is due to cross-wind shear effects discussed later on. These figures also show that the rate of increase of

$\sigma_y$  depends on atmospheric stability. The maximum rate is for a stable atmosphere while the minimum rate is for strong instability conditions; this situation leads to higher numerical values for  $\sigma_y$  as compared to experimental values during stable conditions for large downwind distances (of the order of 100km).

For unstable and neutral atmospheres numerical values for  $\sigma_z$  are higher in the initial portion of plume development. Numerical  $\sigma_z$  results for stable conditions are also higher in value than the BNL results. The difference between the Pasquill curve and the BNL curve is explained by Singer and Smith (1965) as

- (a) in stable cases  $\sigma_z$  is a very gentle function of distance, and only with precise data may one determine the difference between a straight line (BNL curve) and a curved plot (Pasquill curve)
- (b)  $\bar{U}$  is held constant with distance.

#### 4.3.6.2 Pasquill Curves Vrs. Numerical Results:

A family of  $\sigma$ -curves were suggested by Pasquill (1961) based on available experimental data and theoretical expectations. Later studies indicated that Pasquill curves fit the experimental data for the Prairie Grass experiments (see Barad, 1968). The curves are based on smoke-plume elevation  $H_{sp}$  (visible portion) and angular spread  $\theta$  using the relations:

$$\sigma_z = H_{sp} / 2.14$$

and

$$\sigma_y = \frac{\theta \cdot x}{4.28} \tag{4.31}$$

The numerical coefficient 2.14 is just the 10% ordinate of the normal error curve. A comparison of Pasquill curves (from Figure A.2 and A.3 of Slade, 1968) and numerical values (Figure 5.9 to 5.12) shows that numerical values are higher than experimental values for downwind distances up to the order of a km (because of less turbulence near ground). Afterwards the numerical curves are lower than the Pasquill curves except for  $\sigma_z$  under stable and near-neutral atmospheric conditions. The generally higher experimental values of sigmas are rather curious because Pasquill curves are based on three minute averages from ground level releases!

#### 4.3.6.3 TVA Dispersion Coefficients Vrs. Numerical Curves:

Carpenter et. al. (1971) presented dispersion coefficients for the use in dispersion models (Coning dispersion, Inversion Break up dispersion and Trapping) using 20 years of comprehensive field surveillance and documentation of emissions from TVA power plants. The study included a varied range of unit sizes, stack heights and meteorological conditions. The average potential temperature gradient with height was used as an indicator for atmospheric stability.

Sigmas are calculated by employing the relation

$$\sigma = \frac{\text{Area}}{C_{\text{peak}} \cdot \sqrt{2\pi}} \quad (4.32)$$

where the area is equal to the base times the average height of concentration profile along the axis and  $C_{\text{peak}}$  is the maximum concentration in that profile.

In a number of cases  $\sigma_z$  is calculated using

$$C_{\max} = \frac{q}{2\pi\sigma_y\sigma_z\bar{U}} \quad (4.33)$$

and thus, the distribution is considered Gaussian i.e.

$$C = C_{\max} e^{-\frac{1}{2} \left(\frac{x}{\sigma}\right)^2} \quad (4.34)$$

T.V.A. results for unstable cases are not available.\* For other stabilities numerical values are lower than TVA values except for  $\sigma_z$  in stable conditions. In the case of  $\sigma_y$  numerical values are trying to "catch" TVA curves due to cross-wind shear effects. In this case TVA values show a lower trend at large downwind distances. Since the TVA plumes are from hot industrial stacks, the initial large values may have been caused by strong vertical mixing due to the self generated turbulence of these plumes. During stable conditions TVA  $\sigma_z$  values show relatively little increase with distance and this reflects very small values of vertical turbulence. TVA curves are 3 - 5 minute averages for 100m stacks.

#### 4.3.6.4 Sutton Coefficients Vrs. Numerical Results:

Sutton (1947) used virtual diffusion coefficients ( $C_y$  and  $C_z$ ) to obtain sigmas.

$$C_y^2 = \frac{4\nu^n}{(1-n)(2-n)\bar{u}^n} \left( \frac{v'}{\bar{u}^2} \right)^{1-n}$$

$$C_z^2 = \frac{4\nu^n}{(1-n)(2-n)\bar{u}^n} \left( \frac{w'}{\bar{u}^2} \right)^{1-n} \quad (4.35)$$

where  $\nu$  is the kinematic viscosity of the air and  $u'$ ,  $w'$  are eddy velocities across wind and in the vertical respectively.

\* In fact these cases are lumped with neutral cases. Also, TVA curves represent nearly instantaneous situations.

$$\text{and } 2\sigma_i^2 = C_i^2 x^{2n} \quad i = y \text{ or } z \quad (4.36)$$

Here  $n$  relates to the diffusing power of the turbulence and is normally determined by the vertical transfer of momentum as indicated by the shear of the wind near the surface.  $n$  lies between 0 - 1 (very turbulent to low turbulence conditions).

The numerical estimates are generally higher than the Sutton values for a neutral case. Sutton's equations for sigmas have not been confirmed for non-neutral stability. Sutton curves are based on 3 minute averages from ground level releases and then extrapolated for 100m release.

#### 4.3.6.5 Conclusion of 4.3.6.1 to 4.3.6.4:

In summary, the correlation between the numerical results and the various experimental results is satisfactory if we keep in mind the limitations of both the numerical and the experimental approaches. Because of this agreement between computed and experimental results, and in view of the differences between the various experimental  $\sigma$ -curves, it seems justifiable to not only obtain  $\sigma$ -curves theoretically but also to generate  $\sigma$ -graphs for any arbitrary release height. This is one of the purposes of this study and something which is not possible using experimental data alone.

#### 4.3.6.6 Predicted Sigmas for any Arbitrary Release Height:

The dispersion coefficients are dependent on stability, release height, surface roughness, K-profiles, height of mixing layer, etc. Experimental curves given by Pasquill and others are given as a function of stability and some are valid for ground level releases and others for

100m release, and for the surrounding experimental terrain. It is both time consuming and expensive to obtain sigmas for a release height from field studies. However, numerical modelling enhances our ability to remove these restrictions and allows us to obtain  $\sigma$ -curves for any release height and any surface roughness. In this section the discussion is restricted to  $\sigma$ -curves for any release height and the influence of surface roughness on sigmas is deferred till section 4.3.7.3.

The basic approach as discussed elsewhere in this report is essentially to perform numerical experiments after correlating basic  $\sigma$ -curves to experimental curves (the latter part has been done in an earlier section).

Qualitatively, the effect of varying release height on sigmas will depend on the following factors:

(a) The Value of K in the Vicinity of the Plume Element:

Atmospheric turbulence plays an important role in the diffusion of a cloud or plume. Since atmospheric turbulence is parameterized by "K" in our model, and since  $K = K(z)$ ,  $\sigma$ -values and how  $\sigma$  varies with downwind distance must depend on the cloud/plume height relative to the chosen K-profile. As the height of the release point above the surface layer increases, the value of K reduces and a lower value of  $\sigma$  for very high releases as compared to moderate releases will be observed.

(b) Cross-wind Shear Effect:

Due to the turning of the wind with height, plume elements are sheared and the value of  $\sigma$  is changed

from the value when no shear exists. Further the effect of this shear will be more pronounced for releases in Ekman layer (i.e. above the surface layer) and for those parts of clouds or plumes released within the surface layer which penetrate the Ekman layer. This will further modify the values of  $\sigma'_y$ 's (since  $\sigma'_z$ 's are not sensitive to this effect). Under neutral or stable conditions this effect is in the opposite direction to affect "a" and, for  $\sigma'_y$ , will tend to compensate for the effect of decreasing K with height.

(c) Surface Roughness:

As the release height is increased, the initial portion of the plume (away from the ground) will be less affected by surface roughness. Elevated releases will therefore, be less sensitive to surface roughness variations than near-ground-level releases.

Figures 4.7 to 4.10 give the results of numerical computations for different release heights in graphical form. The curves are given for 50m, 100m, 200m, 300m and 500m release heights using the same environmental parameters used earlier.

In the case of the vertical spread of the plume, the values of  $\sigma_z$  decrease as the release height is increased from 100m to 500m under all atmospheric stability conditions (neutral as well as non-neutral). For example, for the unstable case numerical results show a decrease of  $\sigma_z$  value by 45% for a 500m release when compared to a 100m release. For a release height below 100m (50m was used here) the  $\sigma_z$  values are lower

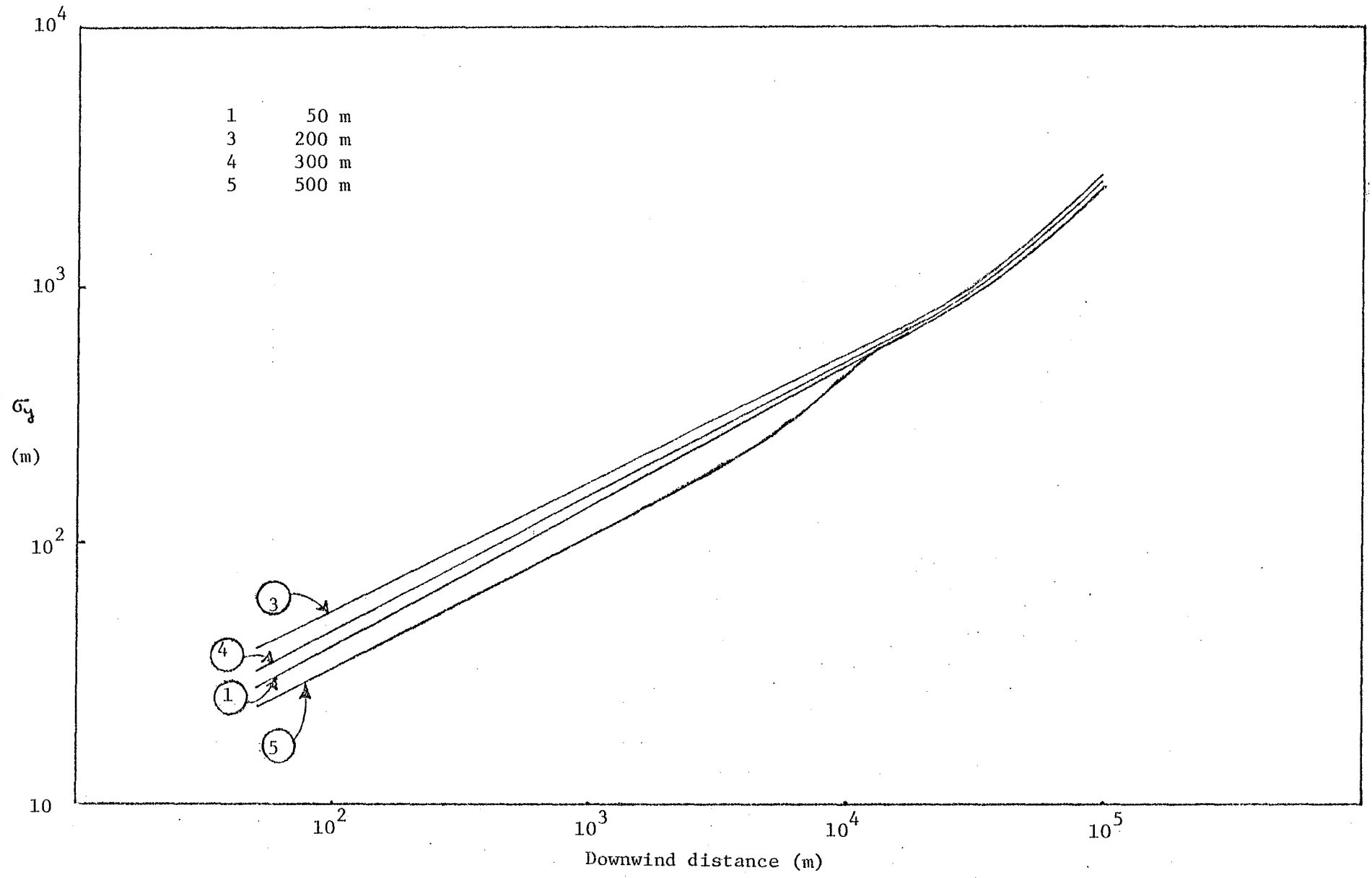


Figure 4.7:  $\sigma_y$  FOR ELEVATED RELEASES IN AN UNSTABLE ATMOSPHERE

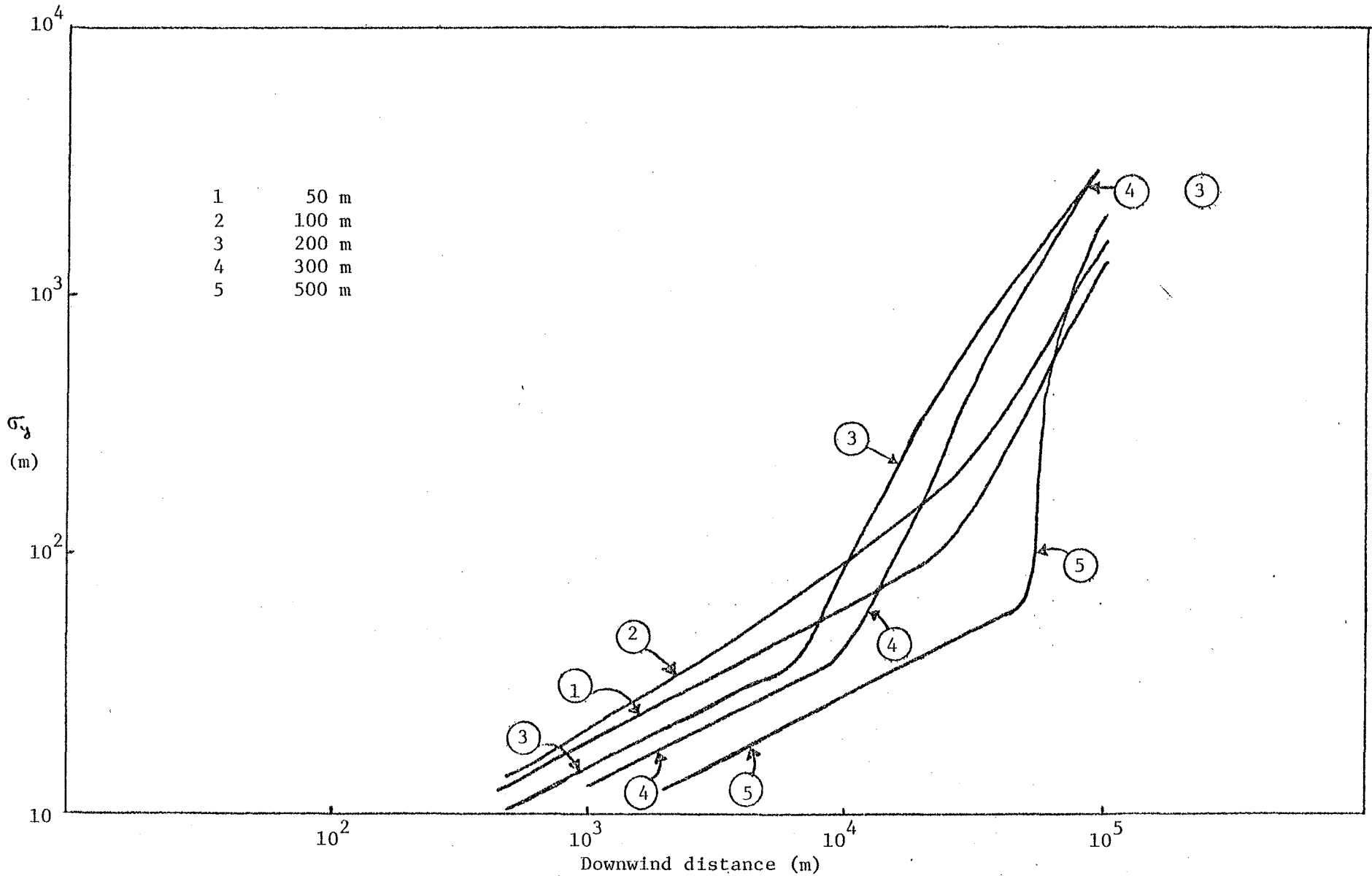


Figure 4.8:  $\sigma_y$  FOR ELEVATED RELEASES IN A STABLE ATMOSPHERE

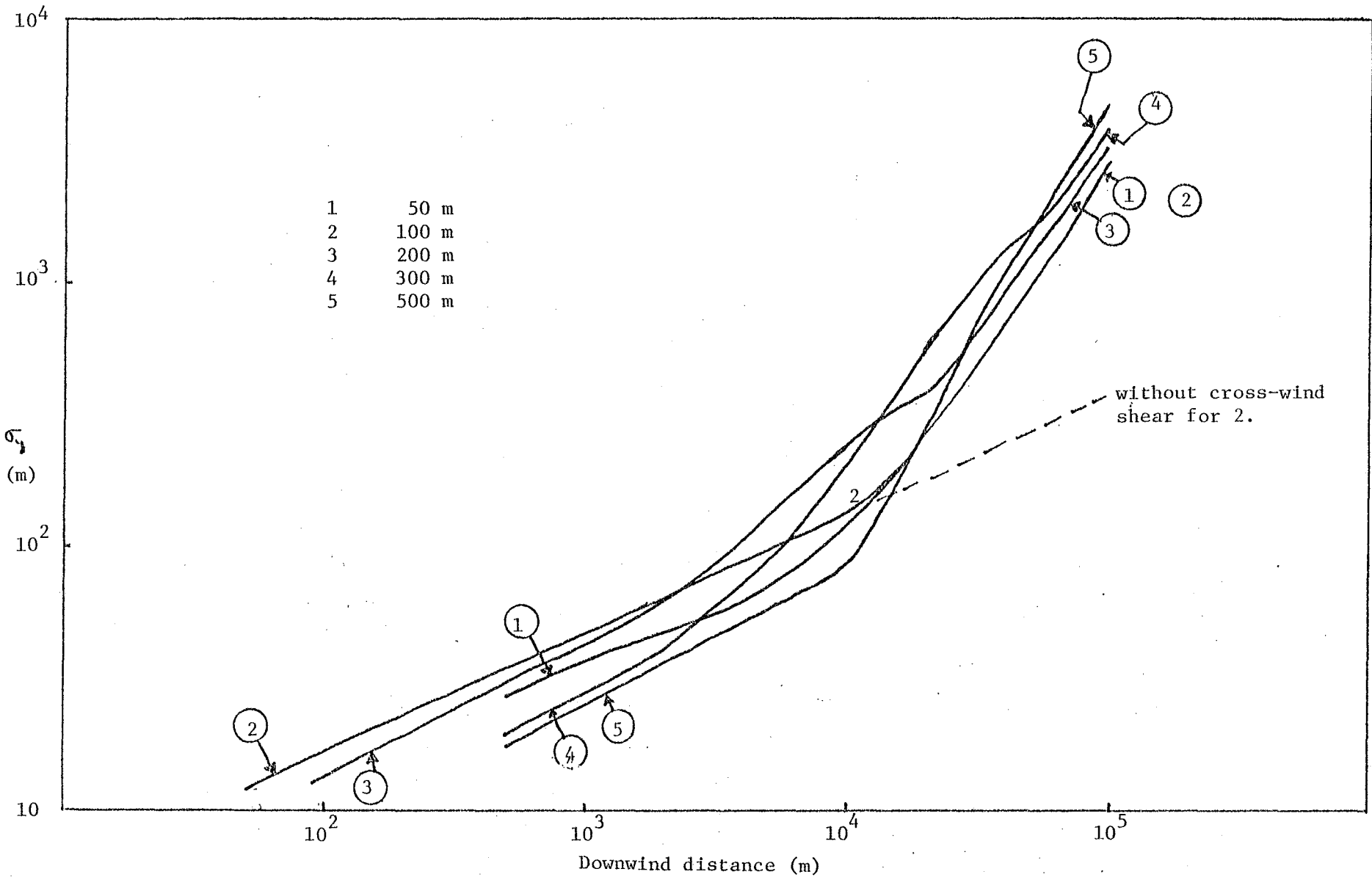


Figure 4.9:  $\sigma_y$  FOR ELEVATED RELEASES IN A NEUTRAL ATMOSPHERE

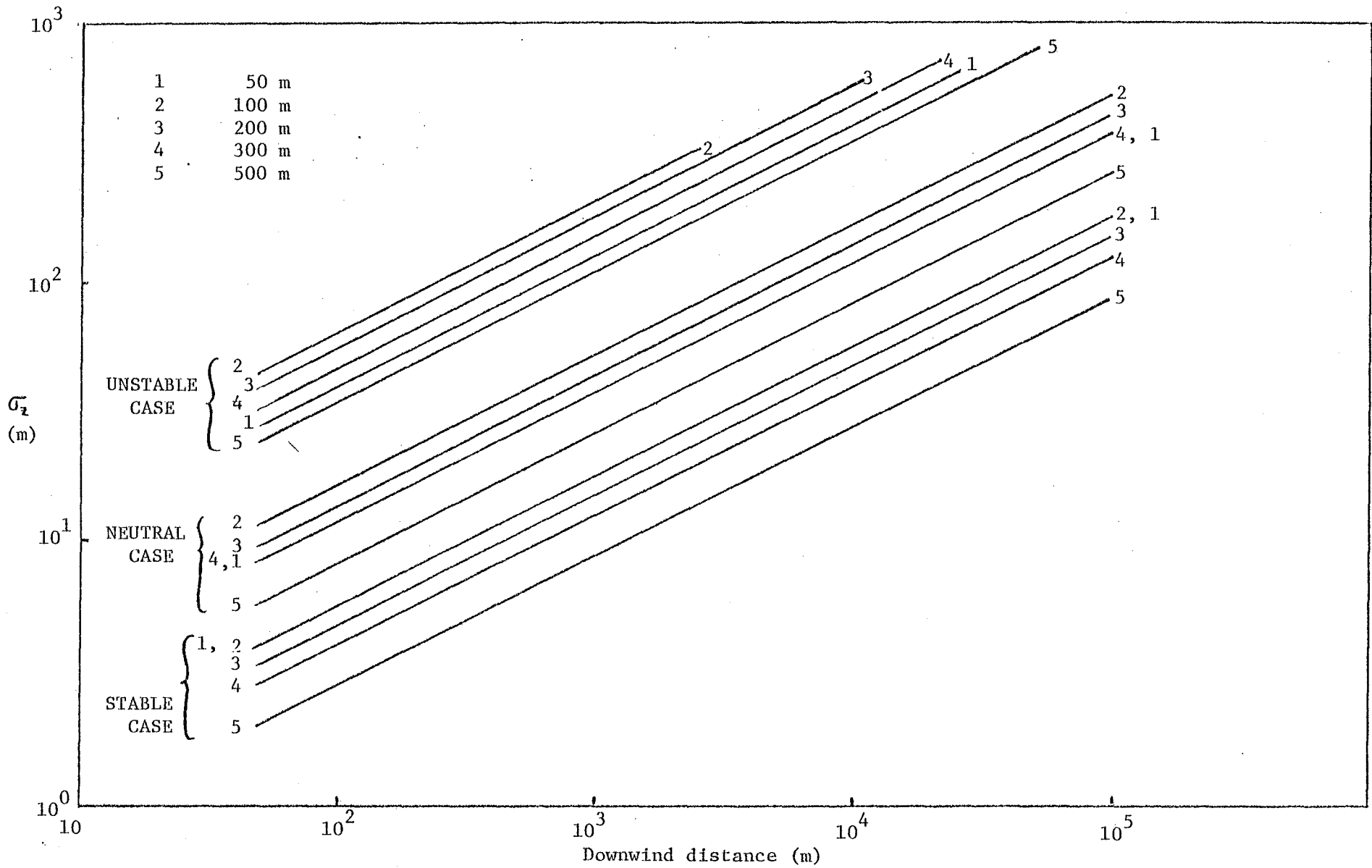


Figure 4.10:  $\sigma_z$  FOR ELEVATED RELEASES

than for 100m release values (this is due to a lower level of turbulence).

The trends for  $\sigma_y$  are not the same as those of  $\sigma_z$  because of cross-wind shear effects. The magnitude of change in  $\sigma_y$  from no shear conditions is further complicated by an earlier observation that the effects of wind shear are dependent on stability as well as the degree of shear. From figures 4.8 and 4.9 it is clear that maximum deviations in  $\sigma_y$  from no wind shear situation is under stable conditions and is for a 500m release. Both the cases are physically justified: stable conditions are associated with large wind shears and 500m release plume is subject to maximum shear (due to a large change in the wind direction at higher elevations in comparison to lower layers) for the cases considered. As far as the absolute value of  $\sigma_y$  is concerned, at 100km  $\sigma_y$  is maximum for a 300m release followed by 200m, 500m, 100m, and 50m releases under stable conditions.

One interesting point which may be observed by comparing/extrapolating the curves given in figures 4.7 and 4.8 is that at large downwind distances the stable plume disperses more than the unstable plume. For example in the case of 200m and 300m releases this occurs at  $x \geq 70$ km. This may be due to the effect of cross-wind shear effect - as stable conditions are associated with large wind shear. This result has not been observed in experimental studies, but such studies do not extend to such large downwind distances. It would be interesting to search for this effect in, for example, satellite photographs of urban plumes. The numerical value of  $x \geq 70$  km is an underestimate because of abrupt slope changes in numerically computed  $\sigma_y$  curves.

#### 4.3.6.7 Cross-wind Shear Effects:

The dispersion of the plume is affected by the change in direction of the mean wind and the effects of sigmas may be studied from Figures 4.1 - 4.6

and 4.7 - 4.10. In earlier sections several attempts were made to explain the behaviour of the plume using this fact. The cross-wind shear effects depend on the height of release of effluents as well as on the atmospheric stability (which in turn determines the turbulence transfer mechanism - K-profiles and associated velocity field.) The observed effects are:

(a) Horizontal Dispersion ( $\sigma_y$ )<sup>\*</sup>:

The downwind distance at which shear effects are first dominant (viz. at the point  $x_s$  which is evident as a slope change in the graphs) is a function of atmospheric stability for a particular release height. Pasquill (1969: Figure 2) has also obtained a fairly sharp "transition" point from theoretical considerations. One gets a sharper transition when, at the transition point  $x_s$ , a larger part of the plume remains in the outer layer. This is more likely in stable cases because greater shear means smaller  $x_s$  (as observed in numerical experiments) and hence less overall growth at this point.

The cross-wind shear effects are felt much earlier during stable conditions as compared to unstable cases (except for a 500m release). For a 100m release height  $x_s \sim 5\text{km}$  for a stable case and  $x_s \sim 10\text{km}$  for an unstable case, while under neutral conditions the "transition" point lies between these two values.  $x_s$  shifts depending upon the release height. Surprisingly, this point for a 50m release lies between a 300m release and a 500m release. Here, the behaviour of a 500m release may be explained on the basis that it is already close to top of the strong shear zone (relative to a 50m release) and the plume soon gets significantly out of shear zone.

Cross-wind shear effects are much larger under stable conditions than under unstable conditions. This is due to the larger wind shears which are associated with more stable conditions. This result agrees with the experimental observations of Brown and Michael (1974).

\* See Appendix-D for a discussion on abrupt slope changes in  $\sigma_y$  curves.

From the analysis of data from Studsvik, Sweden (obtained from Dr. Högstrom) and Hanford, Washington, Pasquill (1969) concluded that during stable conditions, significant shearing of the plume occurred beyond about 2 to 3km downwind (however the effect of enhancing the plume spread was not important within 5km from an elevated source (release height = 87m), and within about 12km for a ground-level source). From Figure 4.8 this distance is approximately 5km. Results using numerical velocity profiles (discussed in the following section) indicate  $x_s$  as 8km. Due to these effects  $\sigma_y$  is not proportional to  $x^{\frac{1}{2}}$  as constant K theory ( $\sigma^2 \propto x$ ) predicts.  $\sigma_y$  increases much more rapidly than  $x^{\frac{1}{2}}$ .

The variation in  $\sigma_y (= \sigma_t + \Delta_s)$  can be seen to consist of two parts:

(i) a first portion where  $\sigma_t$  is determined by horizontal turbulence

(ii) a second portion ( $\Delta_s$ ) where shear effects dominate

(Note: Shear effects begins to overtake the turbulence effects on  $\sigma_y$  as the plume moves downwind.)

(b) Vertical Dispersion ( $\sigma_z$ ) :

Cross-wind shear effects are negligible under all atmospheric conditions. This is due to the fact that the change in wind direction is in the x-y plane and is not in the x-z plane. The author is not aware of any experimental study in which cross-wind shear effects on  $\sigma_z$  have been observed.

#### 4.3.7 Numerical results for Sigmas using Numerically Computed Velocity Field:

In section 4.3.6, the discussion was limited to the sigmas obtained using empirical velocity profiles. As indicated earlier, to keep the model

as a future research tool, the numerically computed velocity field (obtained in Chapter 2) is fed in as an input in order to obtain more detailed information on the  $\sigma$ -curves and the limitations of the results given in section 4.3.6.

#### 4.3.7.1 Numerical and Experimental Sigmas

Numerical sigmas for a 100m release are compared in Figures 4.12 to 4.17 with the experimental values of Pasquill, TVA, Sutton and BNL/ASME curves, as was done in an earlier section using an empirical velocity field. The numerical sigmas differ from the sigmas of section 4.3.6 (empirical sigmas) due to the fact that the solutions of a baroclinic boundary layer for velocity (see Figure 4.11 for a summary) and the data given in Table 4.4 are used. There are minor quantitative differences between numeric sigmas\* and empirical sigmas\*. These are due basically to differences in the K-profiles. For example the PBL height for section 4.3.6 was set as 1000m for each stability conditions while here it is adjusted with stability based on our experience of velocity field computations. The same is the case with the residual K at the top ( $\delta$ ): for empirical calculations  $\delta$  was set to zero while the values of  $\delta$  were adjusted for numerical velocity field in order to satisfy the boundary conditions at the top of PBL. The value of  $\delta$  is important in cases where release is in the free field (release height > PBL height).

Once again the agreement between the numerical values and the available experimental curves is good. The detailed interpretation is similar to that for section 4.3.6 and the reader is referred to that section. The important points are discussed below.

From the results it is clear that  $\sigma_y$  is significantly affected

---

\* The term numerical sigmas is used for sigmas obtained using a numerically computed velocity field while the term empirical sigmas is used for sigmas obtained using an empirical velocity field.

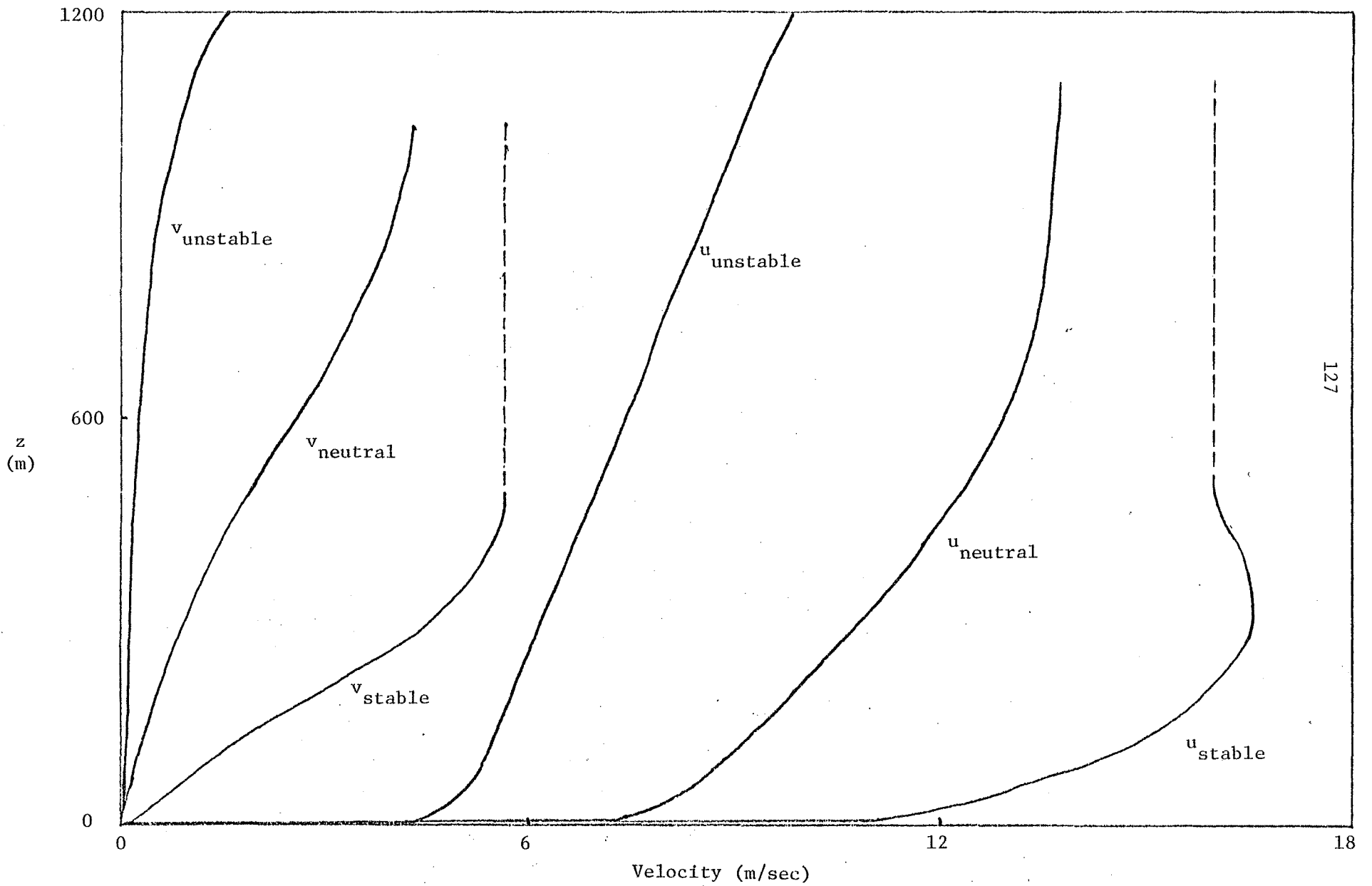


Figure 4.11: VELOCITY PROFILES FOR NUMERICAL  $\sigma$  - CALCULATIONS

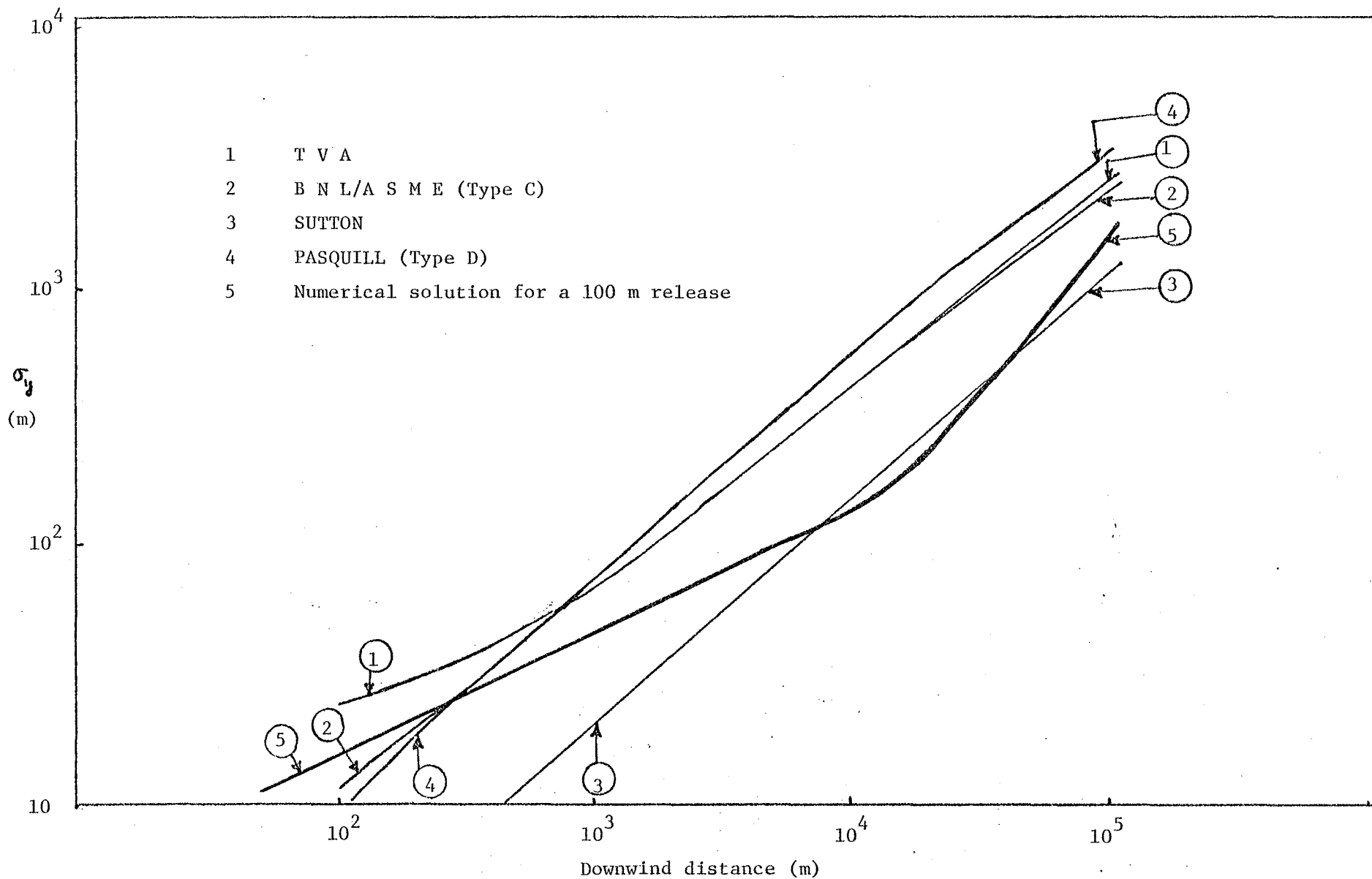


Figure 4.12: COMPARISON OF EXPERIMENTAL AND NUMERICAL  $\sigma_y$  USING NUMERICAL VELOCITY PROFILES (NEAR-NEUTRAL ATMOSPHERE)

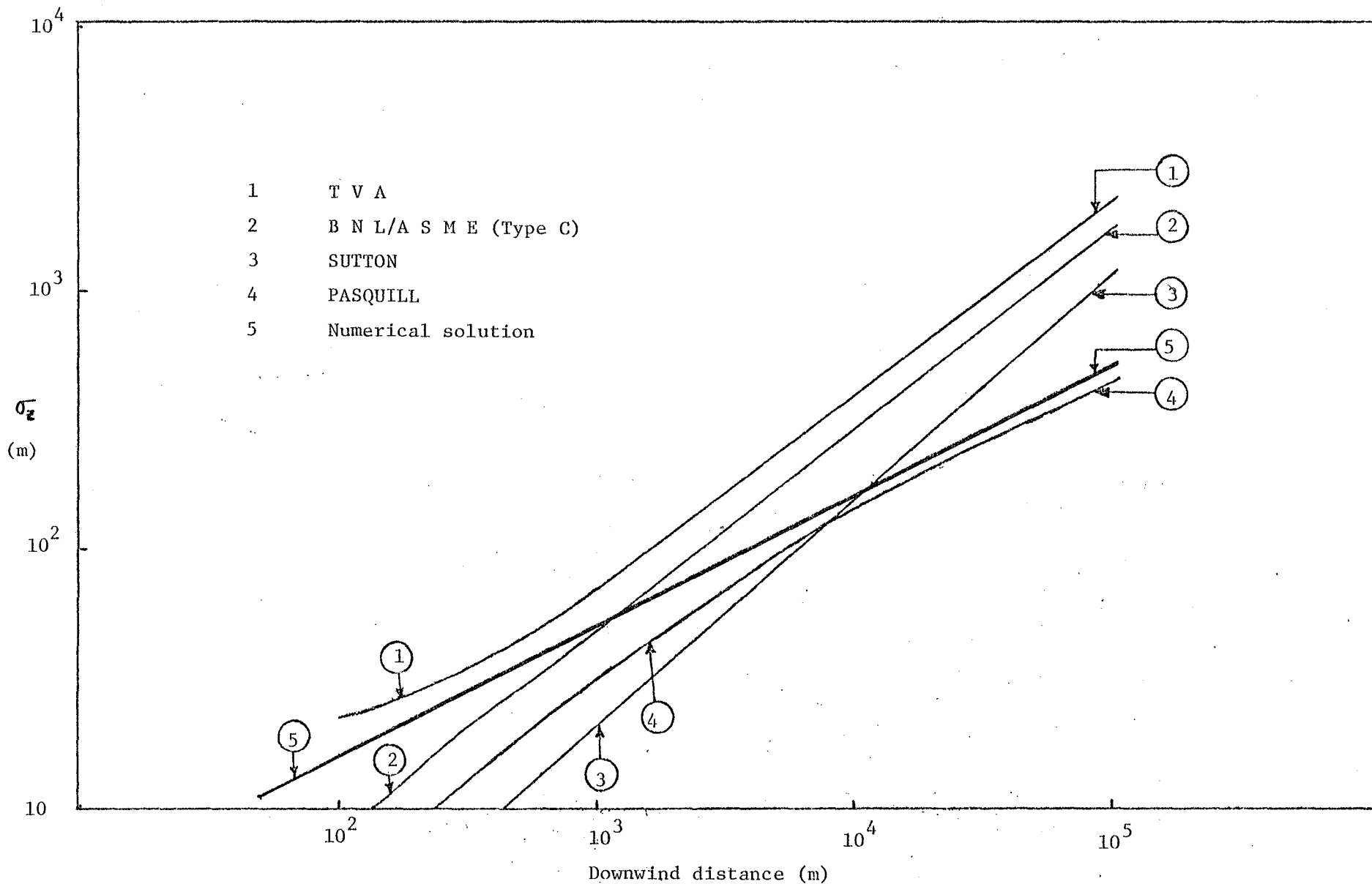


Figure 4.13: COMPARISON OF EXPERIMENTAL AND NUMERICAL  $\sigma_z$  USING NUMERICAL VELOCITY PROFILES (NEAR-NEUTRAL ATMOSPHERE)

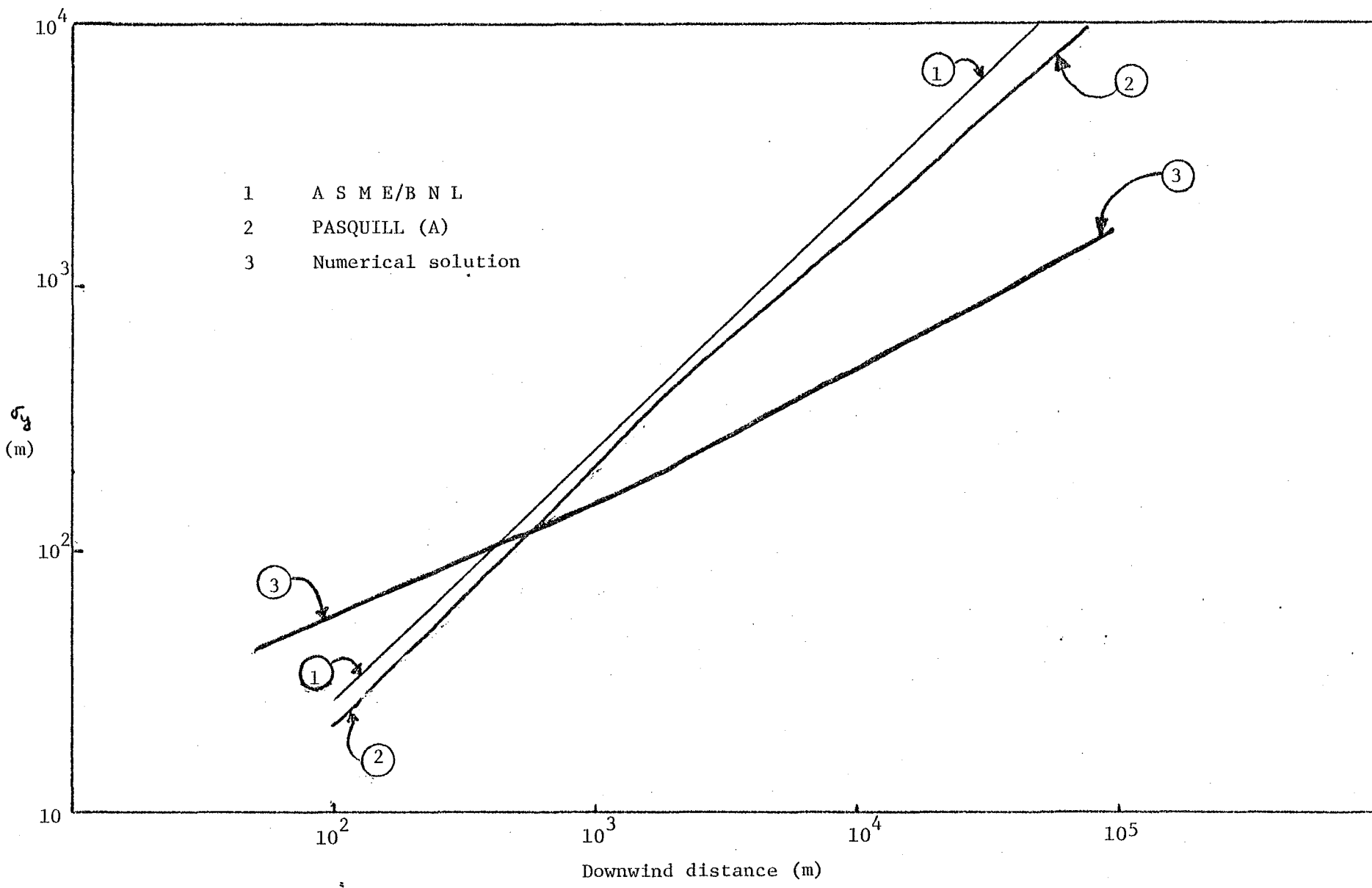


Figure 4.14: COMPARISON OF EXPERIMENTAL AND NUMERICAL  $\sigma_y$  USING NUMERICAL VELOCITY PROFILES (UNSTABLE ATMOSPHERE)

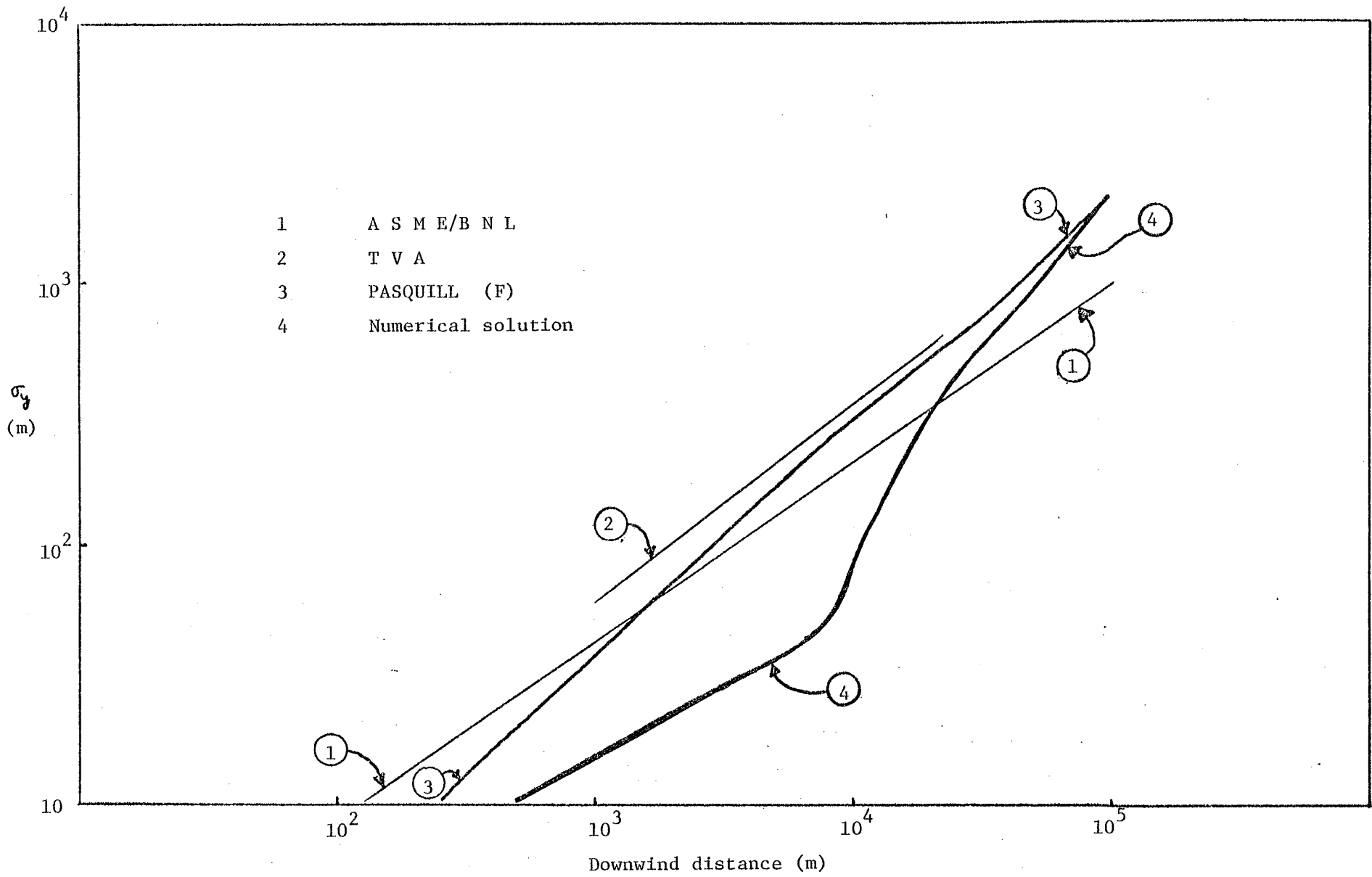


Figure 4.15: COMPARISON OF EXPERIMENTAL AND NUMERICAL  $\sigma_y$  USING NUMERICAL VELOCITY PROFILES (STABLE ATMOSPHERE)

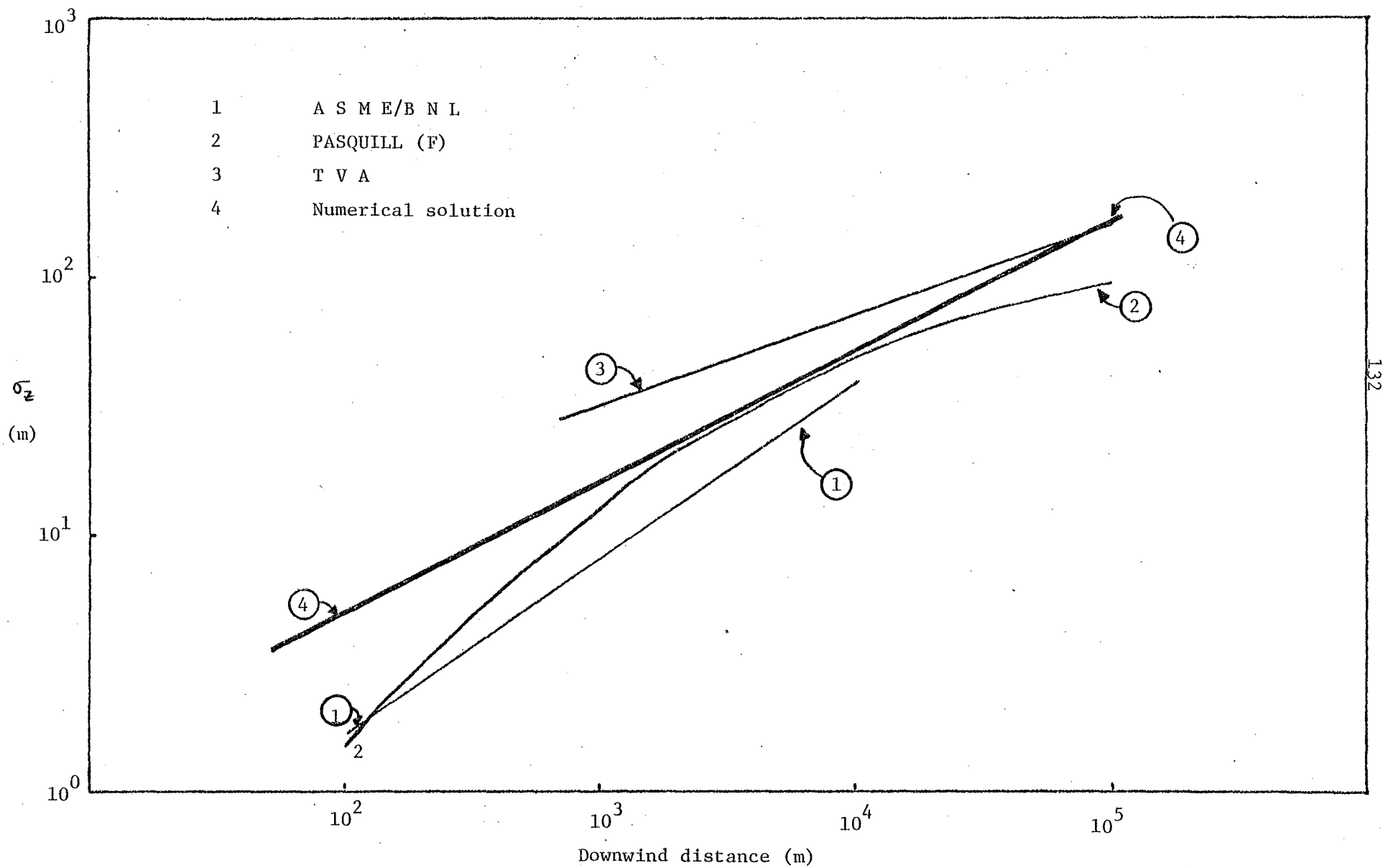


Figure 4.16: COMPARISON OF EXPERIMENTAL AND NUMERICAL  $\sigma_z$  USING NUMERICAL VELOCITY PROFILES (STABLE ATMOSPHERE)

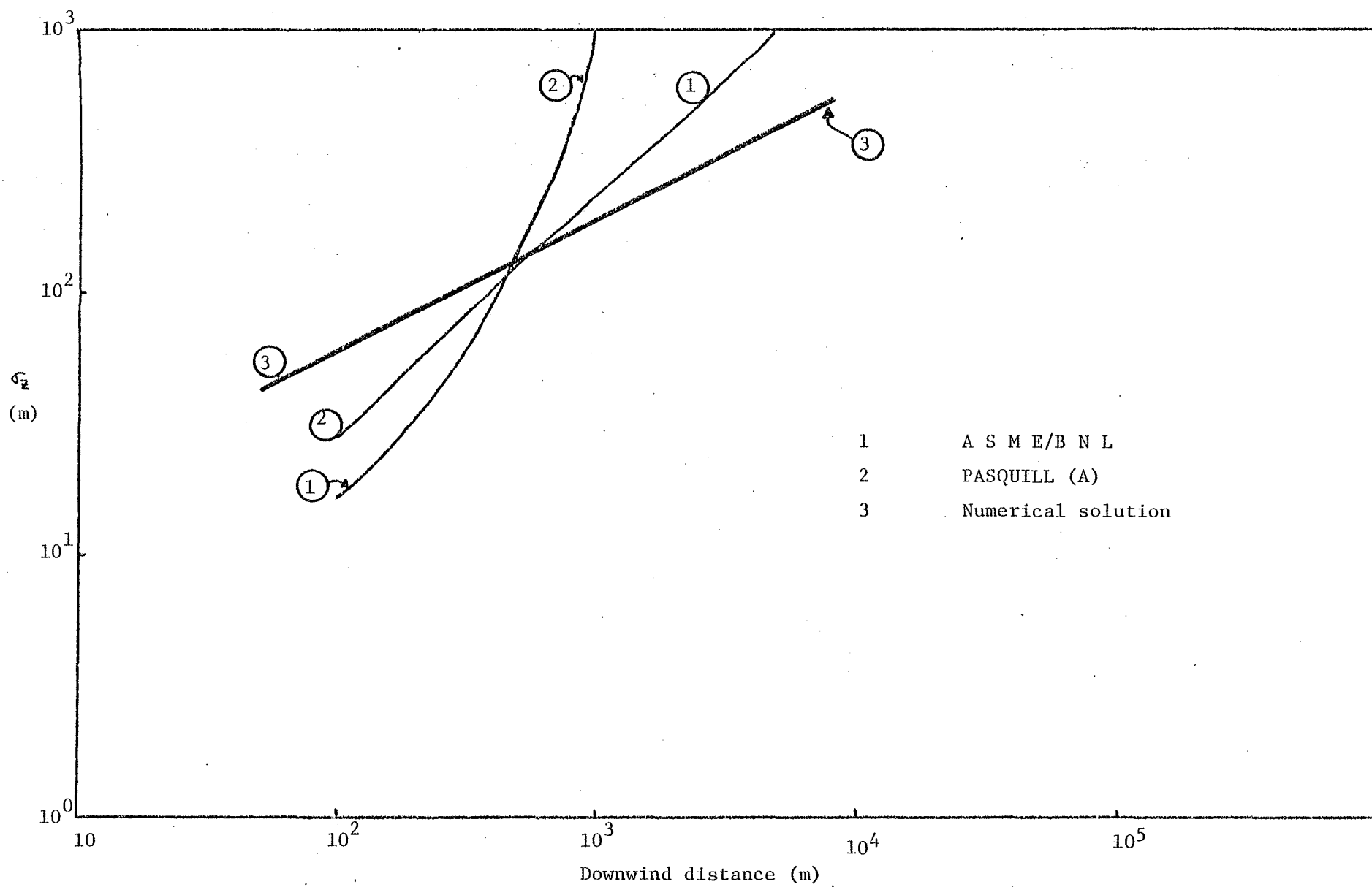


Figure 4.17: COMPARISON OF EXPERIMENTAL AND NUMERICAL  $\sigma_z$  USING NUMERICAL VELOCITY PROFILES (UNSTABLE ATMOSPHERE)

Table 4.4: INPUT VARIABLES FOR "TOTAL" NUMERICAL  $\sigma$ -CURVES

Height of PBL (m)	1200	Unstable
	1000	Neutral
	450	Stable
$\frac{h}{H}$	0.1 (Maximum h = 100 m)	
Surface Roughness $z_o$	0.01 m	
$\delta$ (m <sup>2</sup> /sec)	4.0	Unstable
	0.1	Neutral
	0.6	Stable
$p^1$	1.1	Unstable case
	1.5	Near-neutral case
	1.9	Stable case
$U_*^2$	0.313 m/sec	Stable case
	0.196 m/sec	Unstable case
	0.308 m/sec	Near-neutral case
$\alpha_o^3$	9.0°	Unstable case
	17.0°	Near-neutral case
	19.0°	Stable case
L	-10.0	Unstable case
	$\infty$	Near-neutral case
	134.0	Stable case

<sup>1</sup> Following Misra (1976)

<sup>2</sup> See Chapter 2 for the formula

<sup>3</sup> From PBL modelling (Chapter 2)

by the change in the direction of wind as noted earlier. This agrees qualitatively with the experimental work of Crozier and Seely (1955), who conclude that cross-wind shear has an important effect on  $\sigma_y$ .

#### 4.3.7.2 The Effect of Release Height on Dispersion Coefficients:

$\sigma$ -curves generated by performing numerical experiments as discussed in section 4.3.6. The results are given in Figures 4.18 to 4.21 for 50m, 100m, 200m and 500m release heights. Input parameters are listed in Table 4.4.

The effect of varying release height will depend on the particular K-value in the neighbourhood of the plume element, the cross-wind shear effect and the surface roughness. Cross-wind shear is discussed briefly below while surface roughness effects are discussed in the next section.

From Figures 4.18 to 4.20, it is clear that the cross-wind shear effect on  $\sigma_y$  is more dominant under stable conditions than under unstable cases. This is due to the larger wind shears associated with greater stability and is consistent with the observations of Brown and Michael (1974). The fact that no wind shear effect is noticeable for a 500m release in the stable atmosphere case is due to the fact that the source is above the top of the PBL (here, PBL height = 450.0m for stable conditions).

In general, numeric-sigmas agree qualitatively with empirical sigmas and there are only minor quantitative differences. Because of these similarities one may ask: what is the real value of the numerical modelling of the PBL velocity field? First of all detailed modelling has helped us to see the role of PBL variables such as PBL height and the residual value of K on sigmas. These effects can easily be incorporated in empirical-

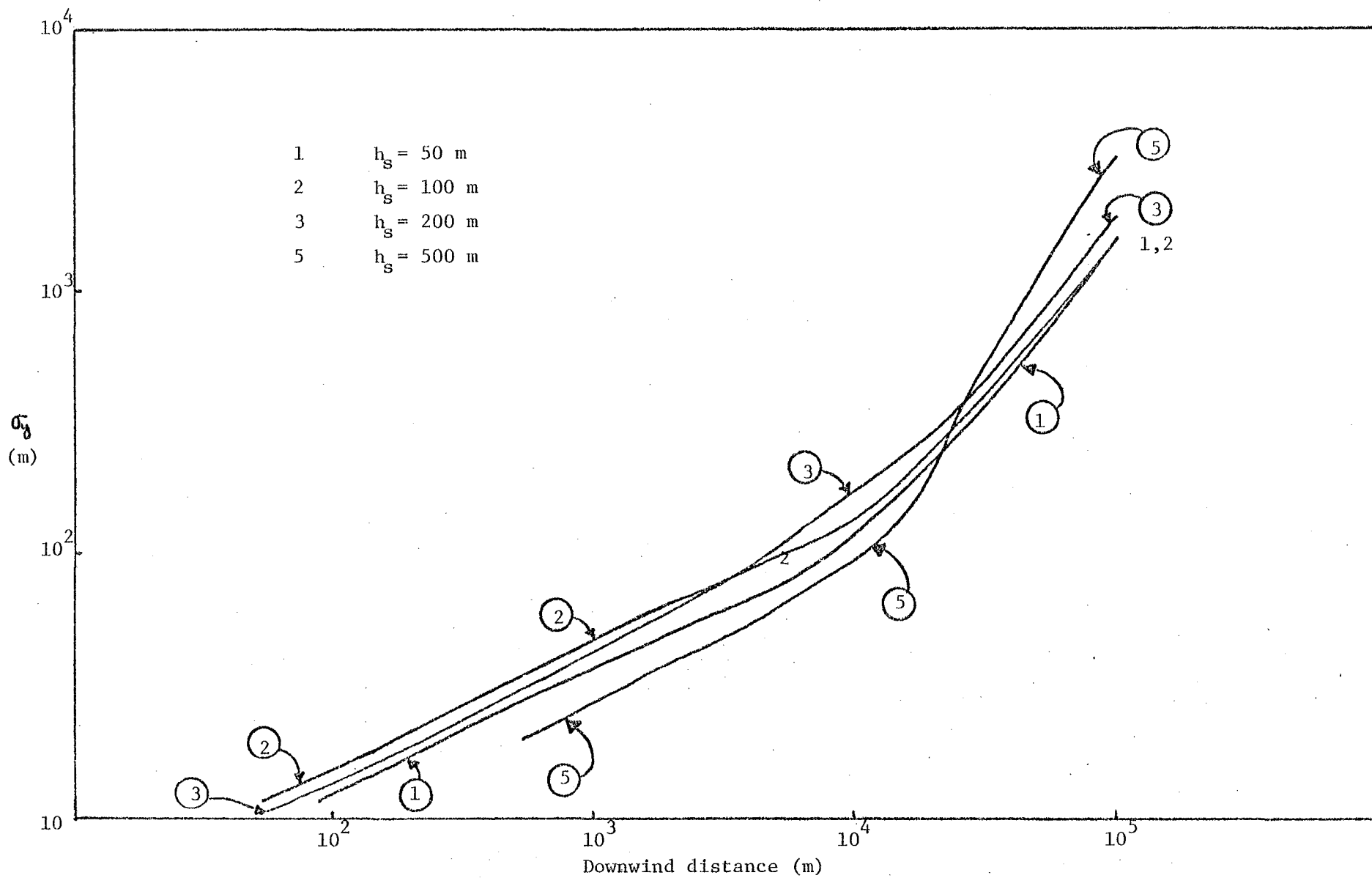


Figure 4.18:  $\sigma_y$  FOR ELEVATED RELEASES USING NUMERICAL VELOCITY PROFILES (NEAR-NEUTRAL ATMOSPHERE)

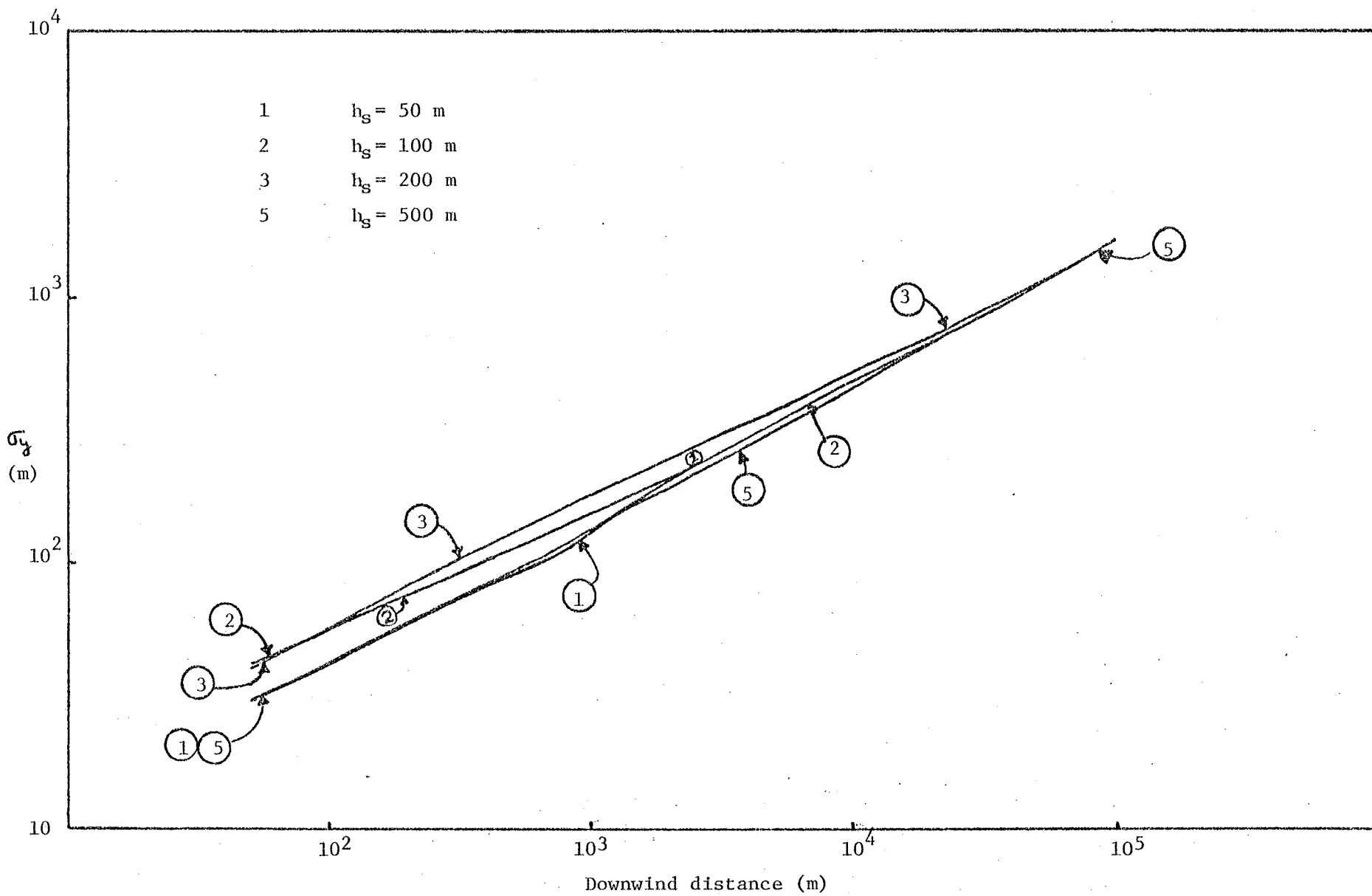


Figure 4.19:  $\sigma_y$  FOR ELEVATED RELEASES USING NUMERICAL VELOCITY PROFILES ( UNSTABLE ATMOSPHERE )

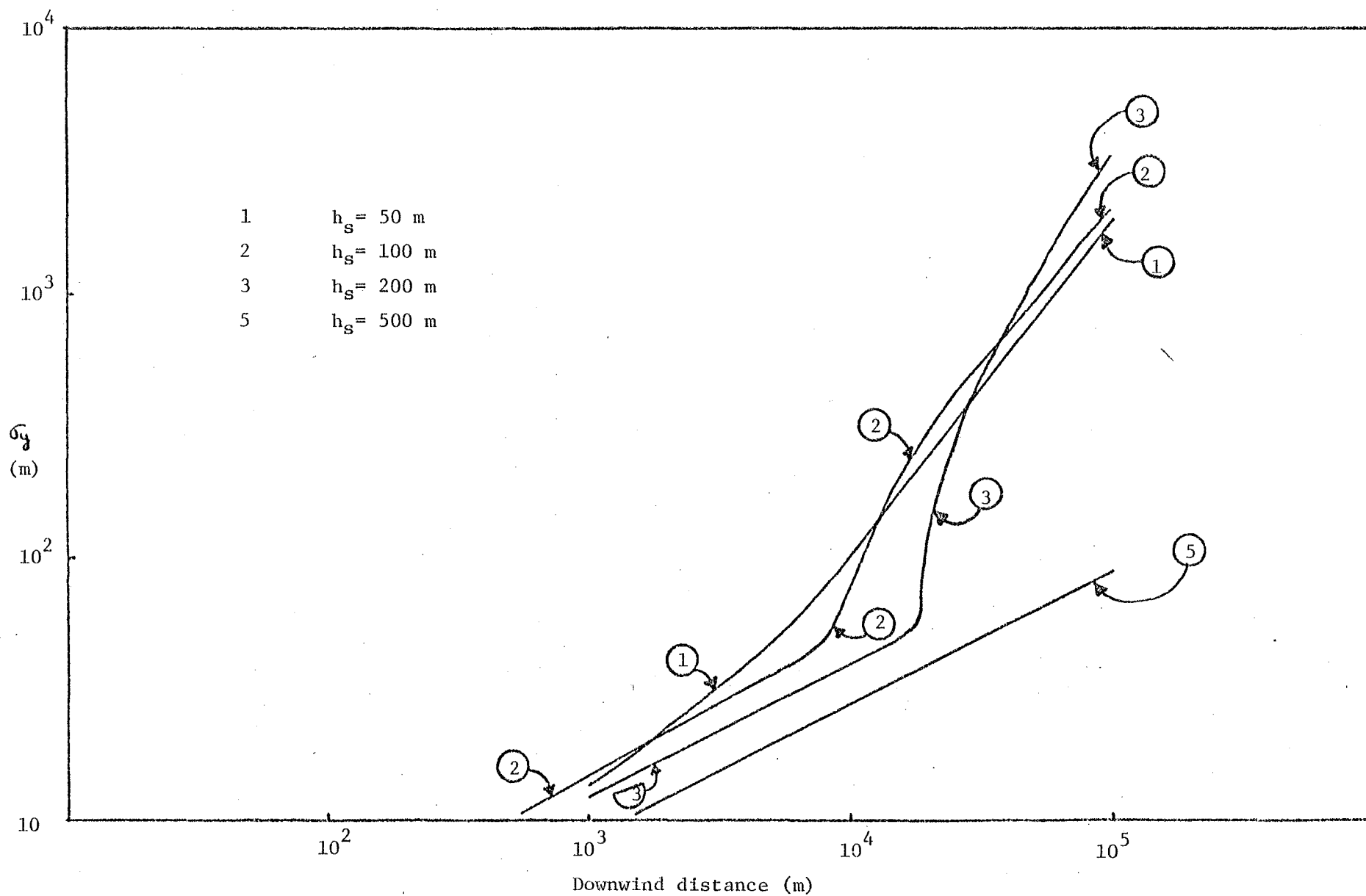


Figure 4.20:  $\sigma_y$  FOR ELEVATED RELEASES USING NUMERICAL VELOCITY PROFILES ( STABLE ATMOSPHERE )

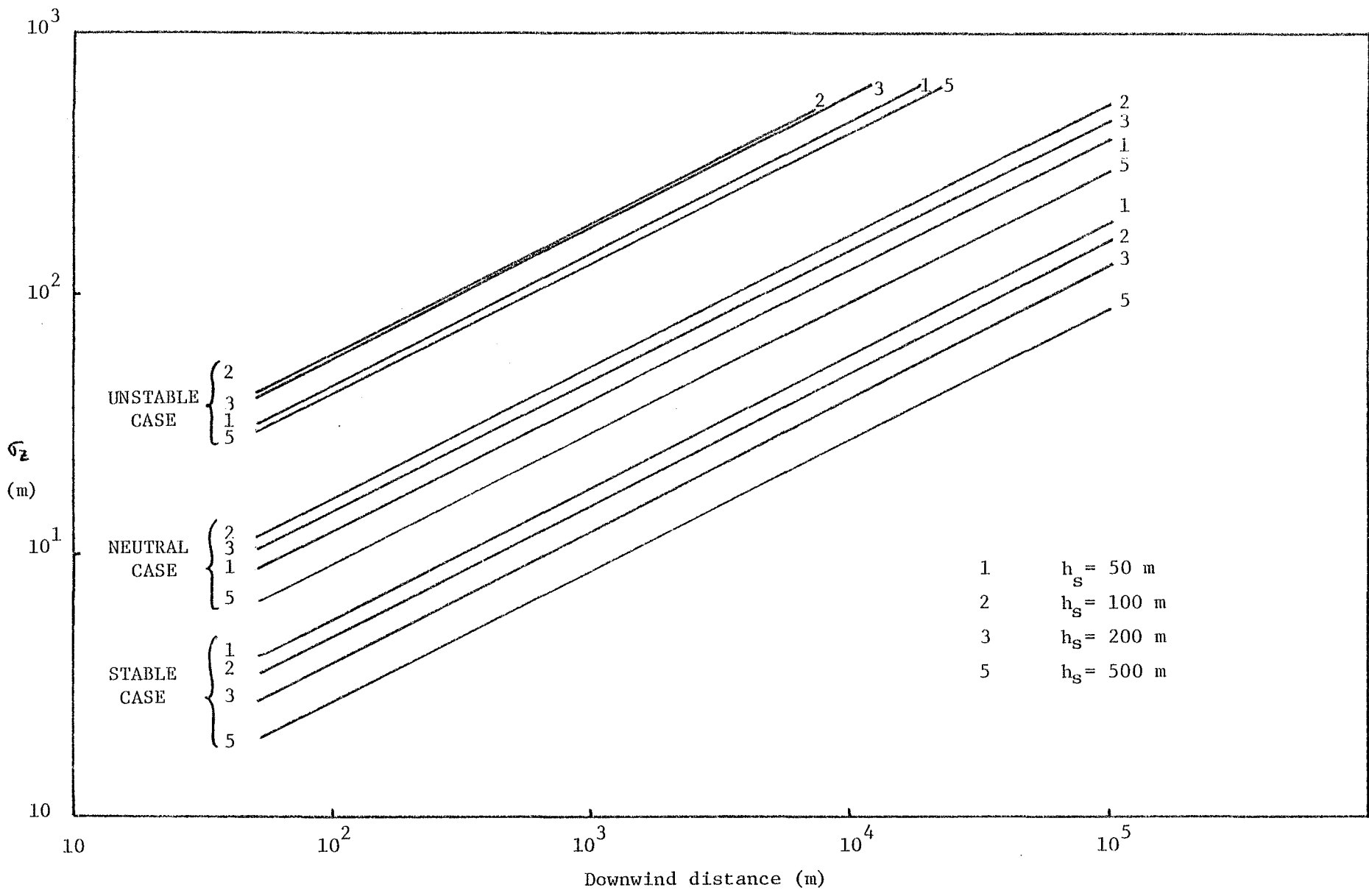


Figure 4.21:  $\sigma_z$  FOR ELEVATED RELEASES USING NUMERICAL VELOCITY PROFILES

$\sigma$  model. Secondly, with an empirical velocity field it is impossible to study the effects of surface roughness on  $\sigma$  variation. In general there is insufficient information on the  $u$  and  $v$  components of the velocity field. One must, therefore, use detailed PBL modelling to resolve the issue. Thirdly, for assessment studies detailed information on  $u$  and  $v$  may not be available and usually, only general features of a site are given - in such cases predictive PBL models of this type are required.

#### 4.3.7.3 Effects of Surface Roughness, $z_0$ :

From a physical point of view, it is obvious that sigmas for near-ground releases will be more affected by surface roughness than sigmas for releases far away from the ground. In addition increased surface roughness effects are similar to increasing the instability of the atmosphere. Greater surface roughness increases the level of mechanical turbulence, while increased instability increases the level of thermally generated turbulence.

Numerical results for a near-neutral case using  $z_0$  ranging from 0.01m to 1.1m are plotted in Figures 4.22 to 4.25. Two typical release heights 50m and 500m are considered. The curves confirm the above points. For a 50m release at 1km from the source, the numerical value of  $\sigma_y$  for a 1.1m surface roughness increases by 90% from that of a 0.01m rough surface. Associated velocity profiles are given in Figure 4.26 and are obtained using the PBL model described in Chapter 2.

One interesting point to note from Figures 4.22 to 4.25 is the shift in the point at which cross-wind shear effects on  $\sigma_y$  are first important. This point moves closer to the source as the roughness increases. From the above discussion, one might have thought otherwise. However, the shift may be easily explained from the fact that increasing

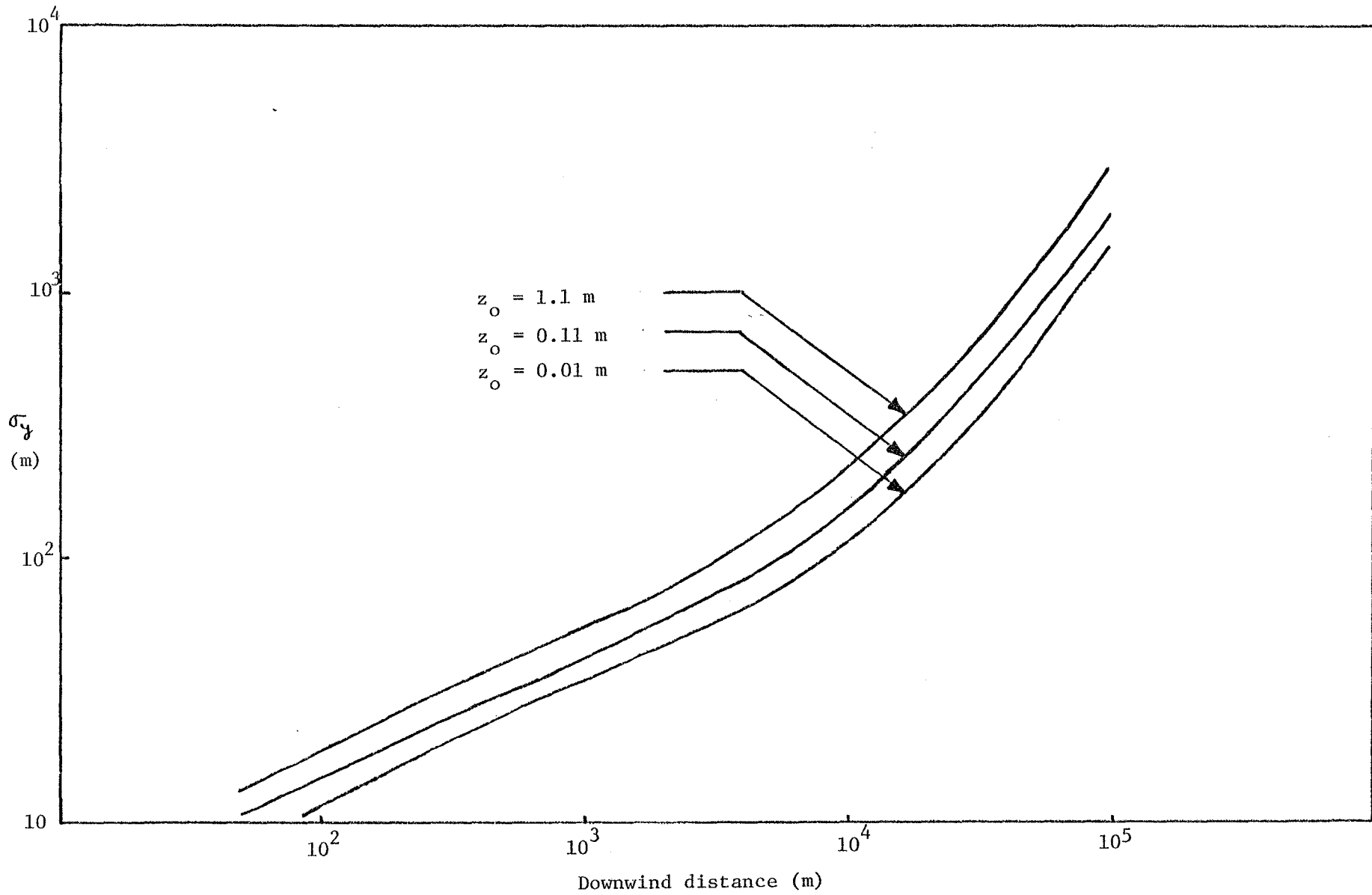


Figure 4.22: EFFECT OF SURFACE ROUGHNESS ON  $\sigma_y$  FOR A 50 m RELEASE HEIGHT ( NEAR-NEUTRAL ATMOSPHERE )

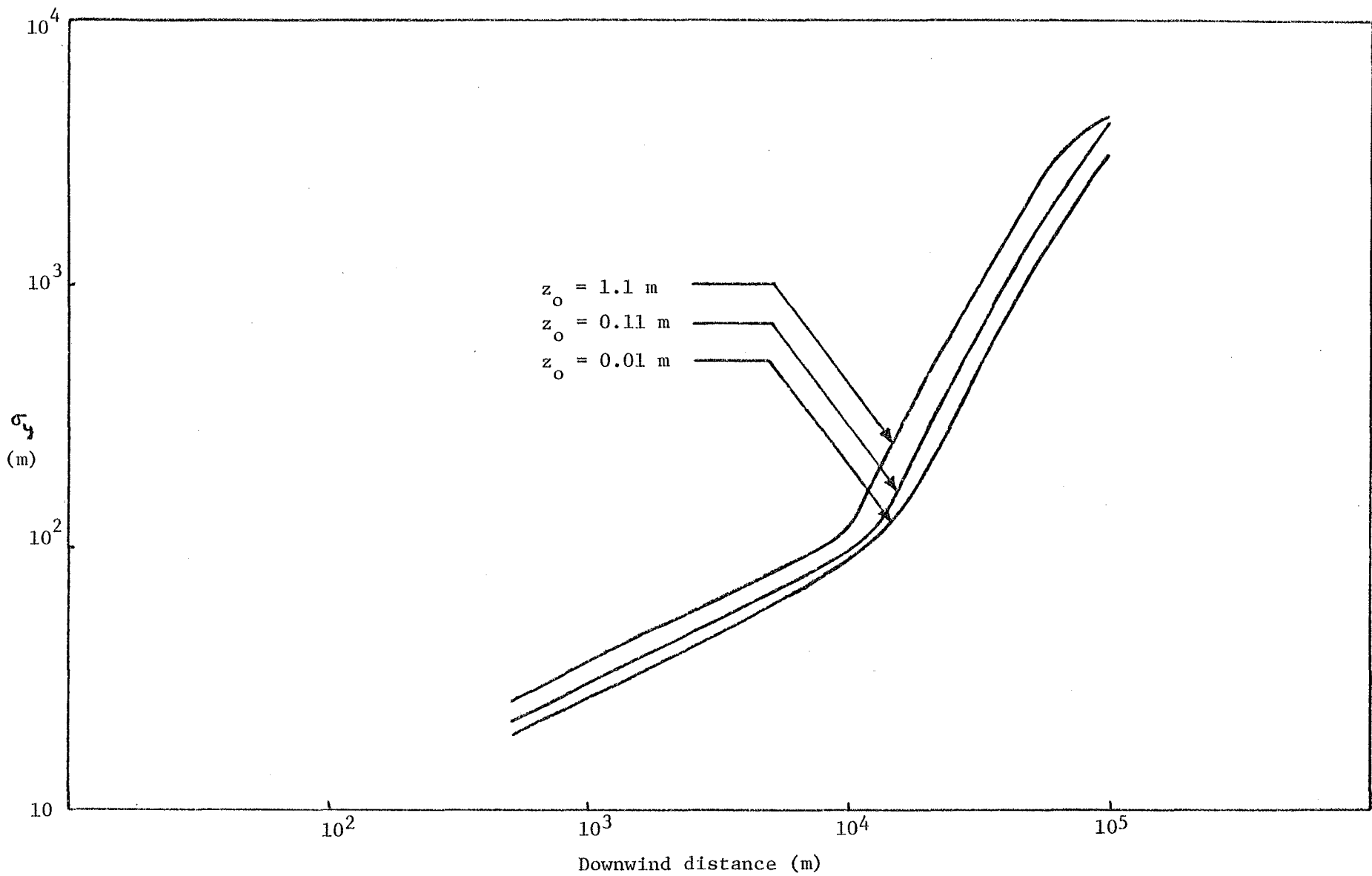


Figure 4.23: EFFECT OF SURFACE ROUGHNESS ON  $\sigma_y$  FOR A 500 m RELEASE HEIGHT ( NEAR-NEUTRAL ATMOSPHERE )

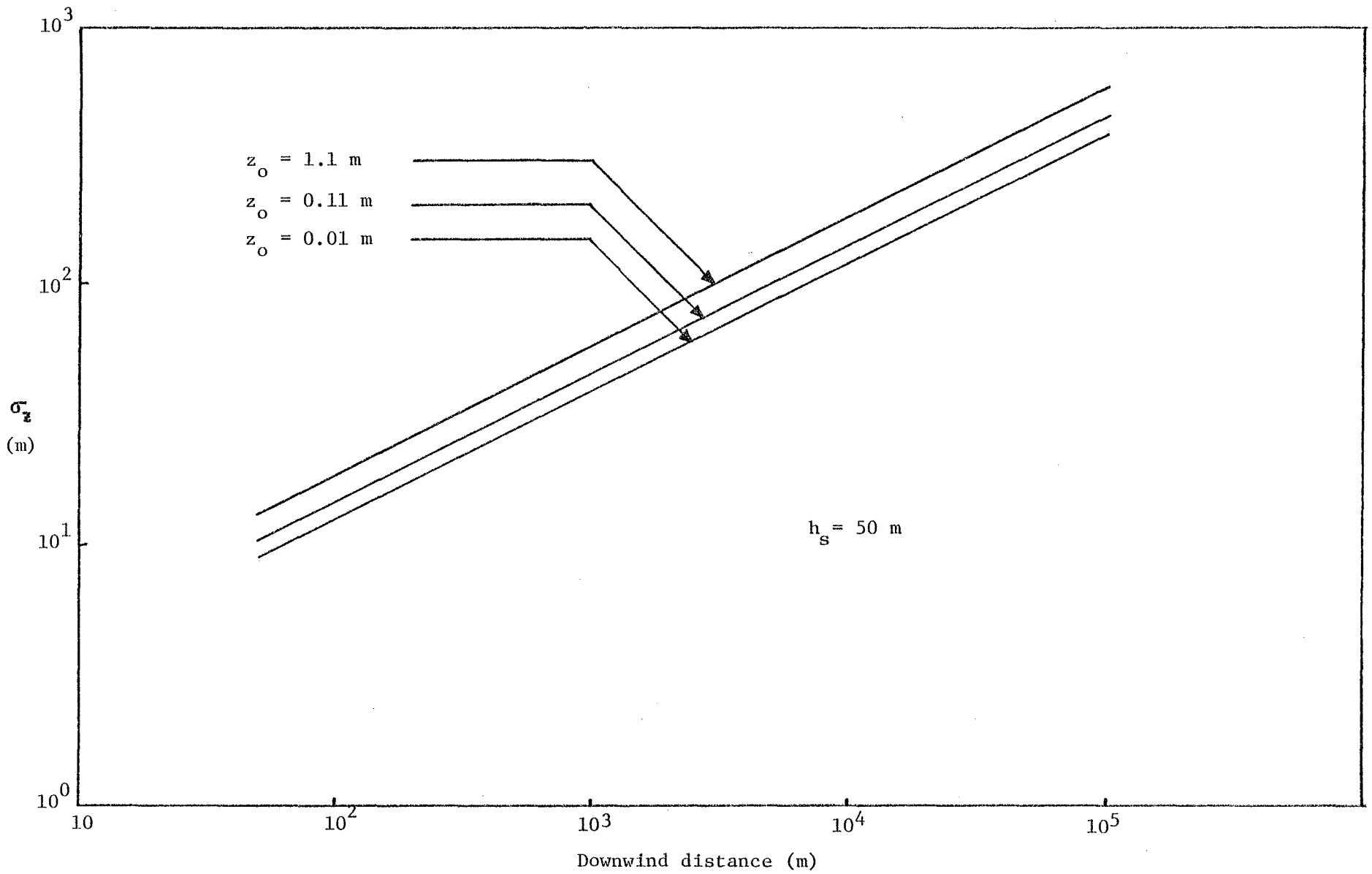


Figure 4.24:  $\sigma_z$  FOR VARYING SURFACE ROUGHNESSES ( NEAR-NEUTRAL ATMOSPHERE )

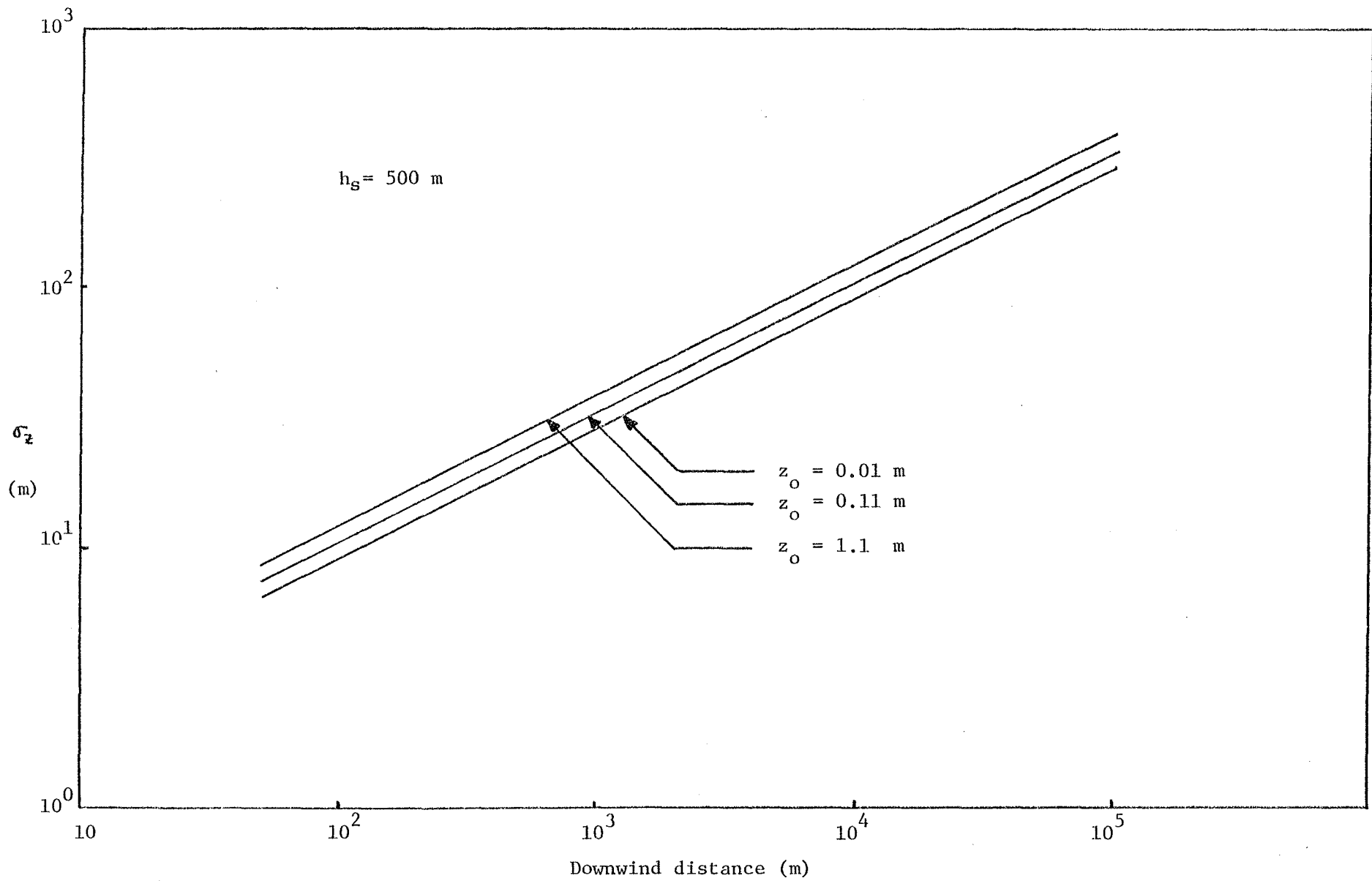


Figure 4.25:  $\sigma_z$  FOR VARYING SURFACE ROUGHNESSES ( NEAR-NEUTRAL ATMOSPHERE )

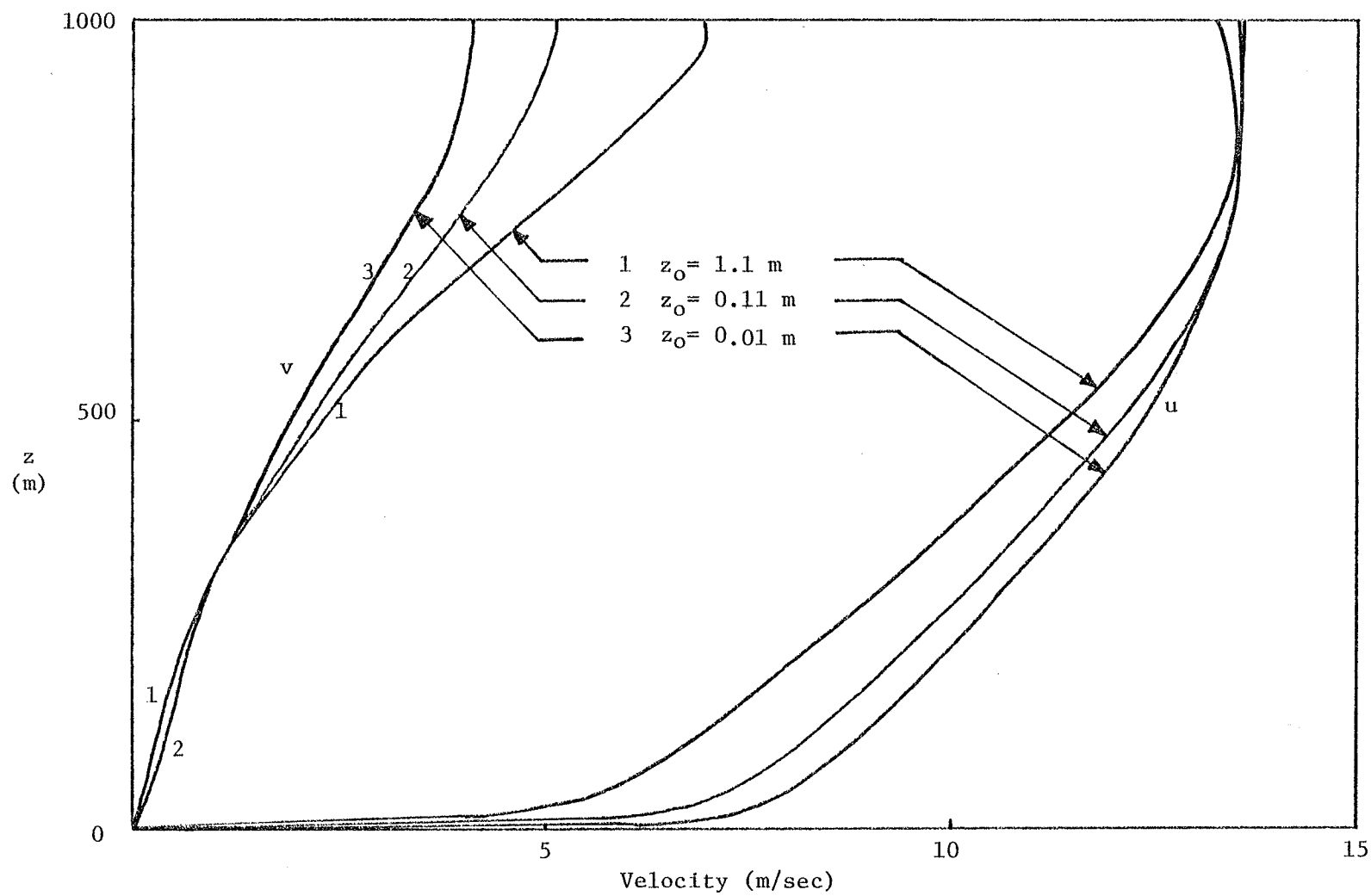


Figure 4.26: VELOCITY PROFILES FOR VARYING SURFACE ROUGHNESS CONDITIONS

surface roughness means large wind shears for a given atmospheric stability. Therefore, for the point at which cross-wind shear effects are first important, the effect should be similar to a situation in which we are going from an unstable atmosphere to a stable atmosphere. This leads to a shift towards the source (see section 4.3.6) and in accord now with Figures 4.22 to 4.25.

Further Pasquill (1976) pointed out that

- (i) the effect of surface roughness on  $\sigma_z$  is represented basically through the friction velocity and the theoretical dependence on  $\sigma_z$  on surface roughness has not been comprehensively verified by observations,
- (ii) the effect of surface roughness on  $\sigma_y$  follows

$$\frac{\sigma_{y2}}{\sigma_{y1}} = \left(\frac{z_{o2}}{z_{o1}}\right)^{0.2}$$

The results given in Figures 4.22 and 4.23 roughly follow this trend.

#### 4.3.7.4 Application of $\sigma$ -Curves to Buoyant and Non-buoyant Plumes, and to Limited mixing conditions:

So far the discussion has been general in nature, limited to elevated releases irrespective of the buoyant or non-buoyant nature of the plume. However, the results are equally valid for both types of plumes if the "effective stack height" method is used for source location. For non-buoyant plumes the "effective" source location will be the true stack height while for buoyant plumes the "effective" source location is composed of true stack height and the plume rise (as used in existing Gaussian Plume Models: see Figure 4.27).

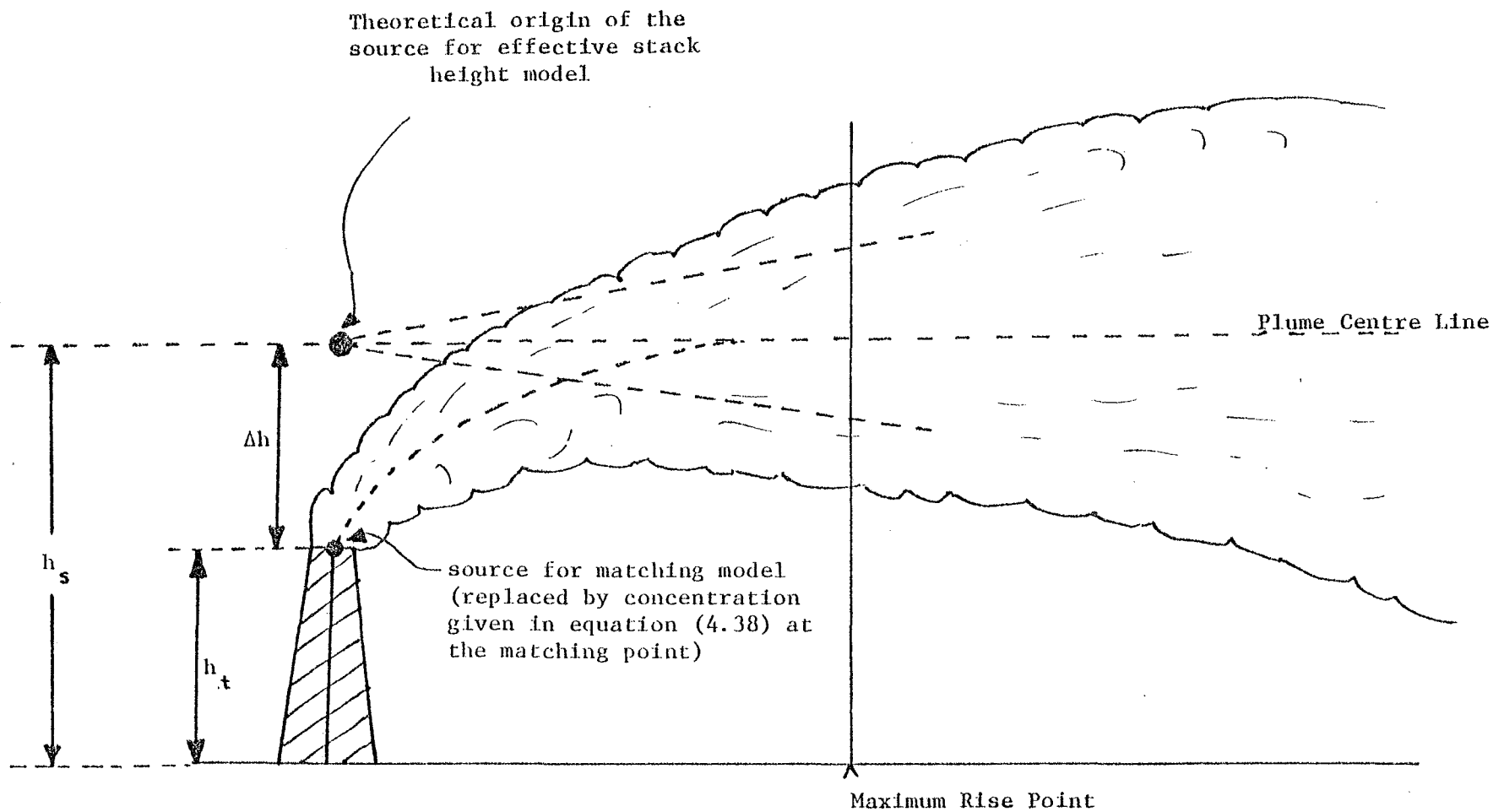


Figure 4.27: SOURCE FOR EFFECTIVE STACK HEIGHT AND MATCHING MODELS

For limited mixing conditions, vertical diffusion is limited by a stable layer. This limits the numerical value of  $\sigma_z$  to the so-called mixing height. Therefore, as an approximation a constant value of  $\sigma_z$  (for curves given in Figures 4.10 and 4.21) is suggested from a point (downwind distance) where  $\sigma_z =$  mixing height.

#### 4.3.7.5 General Assessment of Experimental Data and Numerical Results:

From the earlier discussions, it is evident that the quality of  $\sigma$ 's produced by the numerical model is comparable to the experimental curves. One of the major drawbacks with the experimental approach is that it is very expensive. This limits the sampling grid and the number of observations. Other shortcomings in the diffusion experiments are:

1. Non-homogeneous Turbulence Conditions:

The real atmosphere never approaches vertical homogeneity and even horizontal homogeneity is quite rare. The theories which are used to extract information from raw dispersion data are only valid for homogenous turbulence. Development of theories under non-homogeneous conditions for experimental work will be an interesting area for further investigation.

2. Complex topographic features in particular cases limit the applicability of measurements to general situations.

3. Sampling and Tracer Release Time:

Release and sampling time varies from a few minutes to a few hours. Limited number of experiments have

been conducted to collect data over a variety of release and sampling times.

#### 4. Deposition of Pollutants:

The earth's surface is neither a perfect absorber nor a perfect reflector of pollutants or tracers. Since it is difficult to determine the effects of tracer deposition during diffusion experiments, the results of concentration measurements are not truly representative of the ideal situation (i.e. zero or total deposition depending on the type of experiment).

The numerical approach provides results under realistic and arbitrary atmospheric and meteorological conditions. The models developed in this thesis are flexible enough to be "tuned" for site-specific purposes. One point that can be raised in favor of numerical implementation is relatively less manpower is required to do the job once the models are ready.

The numerical results given in this section and section 4.3.6 clearly indicate that the dispersion coefficients may be obtained as functions of atmospheric stability, height of release and the surface roughness. The results therefore provide a physically realistic extension of the available (experimentally based)  $\sigma$ -curves which are widely used for an initial environmental impact evaluation.

One of the main points is that the experimental  $\sigma$ -curves can not handle variable source height. This is because the effect of shear on  $\sigma_y$  is determined in a very complicated way by stability and release height. One would need a whole new set of curves for each height and

such curves are just NOT available. The only thing near are isolated elevated release curves which are most probably site-specific and therefore of limited use for new power plants. Another thing this model does is put in the height of PBL as a parameter: this is important if release height is comparable to PBL height.

#### 4.3.8 Solution of C-D Equation:

In the previous sections the C-D equation was solved indirectly by solving the concentration-moments. A direct solution of the C-D equation was also performed.

As indicated in the literature survey, a number of authors have obtained numerical solutions to the C-D equation. One of the problems with these computer results is that there is generally a wide difference between these results and the results obtained from Gaussian Plume models for ground level concentrations. One way to narrow this gap is to improve the numerical results by treating the source in a more realistic way than the currently used method. This point will be discussed in detail in this section.

##### 4.3.8.1 Current Method of Treating Source Term Q:

Pollutant source strengths are usually specified as mass units per unit time. The source term Q in the C-D equation, however, has dimensions of mass/unit time/unit volume.

The usual way (see for example Lantz, 1972, Ragland and Dennis, 1975) to overcome this difficulty is to divide the mass per unit time source strength (q) by the grid-block volume or control volume i.e.;

$$Q = \frac{q}{\Delta x \cdot \Delta y \cdot \Delta z} \quad (4.37)$$

The source is then placed at the effective stack height.

The basic disadvantage of this approach is that, for each grid space setting, a different value of  $Q$  is obtained.

#### 4.3.8.2 Proposed Method to Treat Source Term $Q$ :

An alternative approach is to use the Entrainment theory up to the point where the plume has reached its asymptotic rise or atmospheric turbulence starts dominating over plume's own turbulence and then use the C-D equation with an initial concentration of

$$C = \frac{q}{\pi R_m^2 V_m} \quad (4.38)$$

(where,  $V_m$  and  $R_m$  are plume centreline speed and radius of "matching" height  $z_m$ ) distributed over a circle of radius  $R_m$ . This effectively replaces the source term by an equivalent boundary area source condition. This method of treating source terms in atmospheric diffusion calculations has not been used before and is an original contribution of this thesis. This method is referred to as the "area source matching technique" below.

#### 4.3.8.3 Comparison of Numerical Solutions and Gaussian Model:

The numerical scheme (described in Appendix D) has been applied to the case  $K = \text{constant}$  and  $U = \text{constant}$  to facilitate comparison with the Gaussian theory. (Gaussian dispersion theory makes these approximations in order to obtain an analytic solution.) The variables are listed in Table 5.5.1. The information on number of grid blocks, computer core capacity, computing time, etc. is also given in this table.

Figure 4.28 shows a comparison of ground level centreline normalized concentrations (normalization is done using  $C_{\max}$ ) from a single

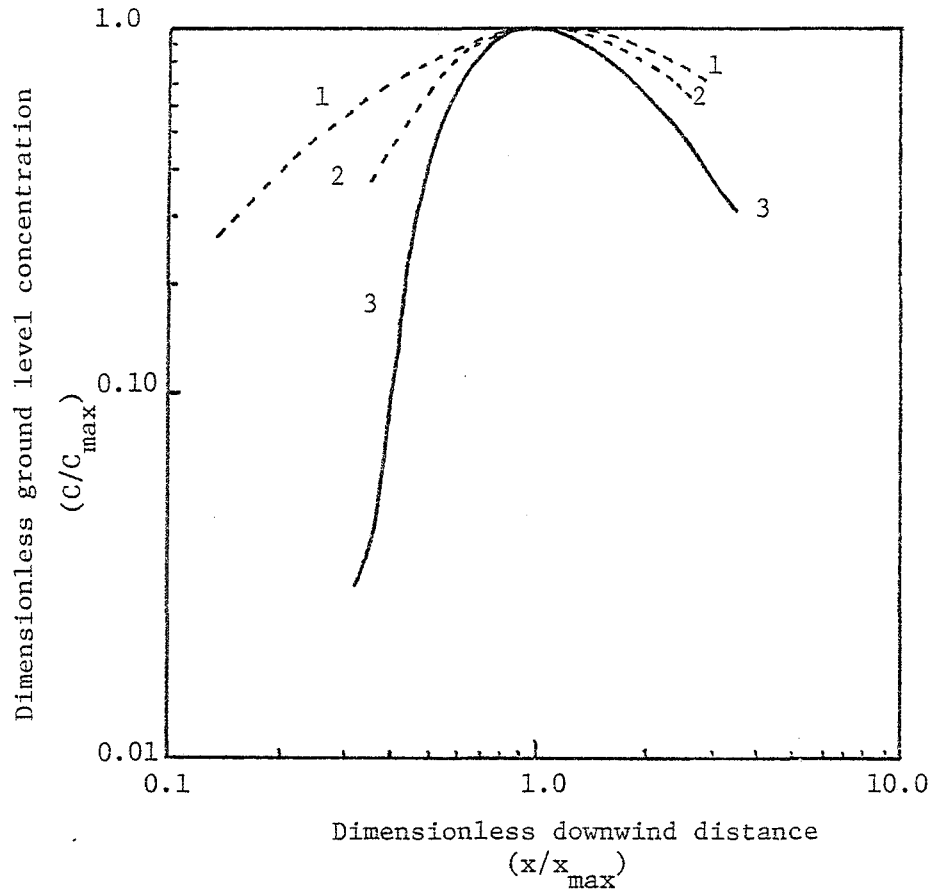


Figure 4.28: COMPARISON OF NUMERICAL SOLUTIONS  
WITH PASQUILL/GAUSSIAN PLUME MODEL

- 1 ---- Numerical solution using  $Q=q/\Delta x.\Delta y.\Delta z$   
( $K_y=K_z=8 \text{ m}^2/\text{sec}$ ;  $K_x=0.0$ )
- 2 ---- Numerical solution using "matching" technique
- 3 ——— Gaussian Plume Model (Neutral Case)

Table 4.5: DATA FOR C-D EQUATION SOLUTION USING ADI SCHEME

No. of Grid Blocks	= 20 X 20 X 20 = 8000 for section 4.3.8.1 = 30 X 20 X 20 = 12000 for section 4.3.8.2
Grid:	Irregular
Compiler:	Fortran H
Core Capacity Required:	230K for "set up made" 120K/160K for "execution made"
Computing time for Steady State Solution	3 min (for 4.3.8.1) 7 min (for 4.3.8.2)
Time Step	10 sec. for $T < 50.0$ 20 sec. for $50 < T < 100.0$ 50 sec. for $100 < T < 200.0$ 100 sec. for $T > 200.0$
Eddy Diffusivity	$K_x = 0.0$ $K_y = K_z = 8 \text{ m}^2/\text{sec}$
Wind Speed	= 7 m/sec
Source Strength	= 10 gm/sec
Downwind Distance at the Matching Point	= 200 m
Radius at the Matching Point	= 15 m
Neutral Case	$\sigma_y = 0.32 x^{0.78}$ $\sigma_z = 0.22 x^{0.78}$

source ( $h_s = 100\text{m}$ ) obtained from the Gaussian Plume model with those obtained from the numerical model using the usual source term and from the "area source matching technique" proposed above.

The differences between the usual numerical (using  $Q = q/\Delta x \Delta y \Delta z$ ) and Gaussian models are considerable. This gap is substantially reduced if the proposed "area source matching" method is used.

Thus, the use of entrainment theory along with the C-D equation is a potential useful approach for further research work.

## CHAPTER 5

## CONCLUDING REMARKS

The purpose of this study was to analyze and to improve existing methods for predicting dispersion phenomenon from elevated releases in the Planetary Boundary Layer. This objective has been achieved by a modular approach to the problem. The system under consideration was broken into its components and then each segment was studied. The major conclusions for each module considered in the analysis are given below:

(a) Plume Rise Theory:

A numerical analysis of various approximations used in current plume rise theories of wet and dry plumes was made. Interesting conditions were obtained regarding the range of validity for the following commonly-used approximations:

- (i) the Boussinesq approximation is good for temperature differences  $\leq 200^{\circ}\text{C}$  between the plume and the atmosphere and should not be used where such differences are large. This is due to enhanced entrainment in the no Boussinesq approximation case as compared to the Boussinesq approximation (i.e. an overestimate of plume rise in the Boussinesq approximation case).
- (ii) the maximum effect of the Boussinesq approximation on the visible plume length is under unstable and humid atmospheric conditions.

- (iii) horizontal drag effects ( $c_d$ ) have a negligible influence on plume rise and growth.
- (iv) solid particulate matter should not be ignored if the plume is "heavy" ( $\psi > .03$  gm/gm) and the temperature difference between the atmosphere and the plume is small.
- (v) the Briggs (see Briggs, 1969) form of the energy equation is preferred over the Slawson and Csanady (see Slawson and Csanady, 1971) form if an approximate form of the Energy equation has to be used. This is based on the proposed no Boussinesq approximation form of the Energy equation.

(b) Wind Structure:

A set of "new" K-profiles was used to model atmospheric turbulence realistically. These profiles were based on recent experimental evidence and on theoretical developments in Boundary Layer Meteorology. Computed wind profiles compared favourably with the Wangara data (see Clarke and Hess, 1974). The values of the parameters A and B which arise in Rossby-number similarity theory were evaluated and found to lie within the limits of experimental data. Finally, the velocity profiles for a baroclinic atmosphere were obtained (by direct use of K-profiles) for use in diffusion calculations, thus keeping the same model of turbulence throughout the development.

(c) Sigmas for Elevated Releases:

A model was developed for estimating sigmas using a

Moment-Concentration method and the K-theory. The model is capable of generating  $\sigma$ -curves (numerically) from a knowledge of source conditions. The results were tested against the published experimental curves of Pasquill, Sutton, BNL/ASME and TVA. The aim of this portion of the project was to extend current Gaussian Plume models for tall stacks to cover an arbitrary release height.  $\sigma$ -curves were calculated numerically as functions of atmospheric stability, height of release and surface roughness.

Numerical results also showed that the dispersion of the plume is affected by the turning of the wind. Specifically, in the case of horizontal spread ( $\sigma_y$ ) the cross-wind shear effects depend on the height of release of effluents as well as on the atmospheric stability (see section 4.3.6.7) while in the case of vertical spread ( $\sigma_z$ ) the effects are negligible under all atmospheric conditions.

(d) Solution of C-D Equation:

An alternative method for treating the source term in the numerical solutions of C-D equation was developed. This method is based on the fact that, in the initial portion of growth, atmospheric turbulence contributes very little towards the diffusion of the plume. At the point where atmospheric turbulence starts to be responsible for the mixing of the plume an area source may be used. This area source is introduced as a concentration boundary condition. It was found that this method gave results which were more compatible with those of simpler Gaussian

models than are similar results obtained using the conventional method where source =  $q/(\text{Volume of grid})$ .

Predictive air quality models are never really completed.

There are always old sections to be replaced by new sections, replacements which may become necessary because of new experimental observations and/or new theoretical developments in the areas involved. Keeping this in mind future work on the model developed here may be carried out as follows:

- (i) experimental evaluation of the K-profiles (eddy viscosity and eddy diffusivity) used in the model.
- (ii) direct measurements of  $\sigma_y$  and  $\sigma_z$ , and ground level concentration for elevated releases along with the velocity field.
- (iii) extension of the Moment-Concentration method to study transient behaviour (this may be important under fumigation pollution conditions).
- (iv) further study of alternative methods to calculate down-wind concentration fields and dispersion parameters ( $\sigma_y$  and  $\sigma_z$ ).

It is hoped that the results of this study will be useful in the preparation of the analytical portions of Environmental Impact Statements for industries and for new or existing energy centres.

## APPENDIX A

AN INCLINED MODEL FOR A NEUTRAL ATMOSPHERE  
FOR MAXIMUM GROUND LEVEL CONCENTRATION

The model described in the main text uses  $\Delta h = \text{constant}$ .

Under neutral atmospheric conditions the "2/3-power law" may be used to describe the mean path of buoyancy dominated plumes. In order to derive an expression for maximum ground level concentration by incorporating  $\Delta h \neq \text{constant}$ , the following steps are taken:

Using equation (4.8) and (4.9), differentiating (4.8) with respect to  $x$ , and letting  $\frac{\partial C}{\partial x} = 0$ , one obtains the following condition for maximizing  $C$

$$\frac{b+d}{x} = \frac{h_s}{a^2 2b} \left[ \frac{b}{x} \cdot h_s - \frac{\partial h_s}{\partial x} \right] \quad (\text{A-1})$$

Now,

$$h_s = h_t + \Delta h = h_t + C_1 \frac{x^{2/3}}{U} \quad (\text{A-2})$$

$$\therefore \frac{\partial h_s}{\partial x} = 2/3 \frac{C_1}{U} x^{-1/3} \quad (\text{A-3})$$

From (A-1) and (A-3), one obtains

$$x_{\max} = \left\{ \frac{(b - 2/3) h_s^2 + 2/3 h_s h_t}{a^2 (b + d)} \right\}^{1/2b} \quad (\text{A-4})$$

Equations (A-2) and (A-4) may be solved iteratively to obtain a solution for  $x_{\max}$ .

For ground level releases ( $h_t = 0$ ), a closed form for  $x_{\max}$  may be derived and can be put in the following form:

$$x_{\max} = \left\{ \frac{(b - 2/3)}{a^2 (b + d)} \right\}^{3/6b - 4} \left( \frac{C_1}{U} \right)^{6/6b - 4} \quad (\text{A-5})$$

From equation (A-5) one may observe that for BNL and TVA values of the parameter  $b$ , positive results of  $x_{\max}$  are obtained, while Pasquill and Turner  $b$ -values yield negative values of  $x_{\max}$ . This is due to the values of  $b (< 2/3)$ . For Pasquill and Turner curves values are for near ground level releases. Thus, the plume is restrained from spreading due to ground and this results in a low value of  $b$  ( $\sigma_z$  exponent).

Physically, equation (A-5) can yield a positive value of  $x_{\max}$  only if the downward spread of pollutant at some downwind point is more rapid than the dilution effects due to lateral dispersion and the general decrease in ground-level concentration due to buoyant plume rise. It is interesting that a positive value of  $x_{\max}$  is possible for this rather extreme case of ground level release. It indicates that the effects of buoyant plume rise on  $x_{\max}$  for general release points may be quite significant (as we know from the work of Csanady, 1973). Further analysis of this model is left for future research.

## APPENDIX B

## THOMAS ALGORITHM

Matrix form of equations given in figure D-1 (Appendix D) may be written as:

$$[A]\vec{c} = \vec{d} \quad (1)$$

If matrix A can be expressed as

$$A = [L][U] \quad (2)$$

where,

$$[L] = \begin{bmatrix} & & 0 \\ & \diagdown & \\ 0 & & \end{bmatrix} \quad \text{and} \quad [U] = \begin{bmatrix} \diagdown & & 0 \\ & \diagdown & \\ 0 & & \end{bmatrix}$$

$$[L][U]\vec{c} = \vec{d}$$

Let  $\vec{g} = [U] \vec{c}$

$\therefore [L]\vec{g} = \vec{d}$

Now, solve  $\vec{g}$  by forward substitution and solve  $\vec{c}$  by backward substitution.

## APPENDIX C

COMPARISON OF  $\sigma_y$  AND  $\sigma_z$  FOR A CONSTANT DIFFUSIVITY ( $K = \text{CONSTANT}$ )  
AND CONSTANT WIND FIELD (MEAN VALUE =  $U$ ) CASE

Downwind Distance (m)	$\sigma_y$ and $\sigma_z$ Numerical Model	$\sigma_y$ and $\sigma_z$ using $\sigma^2 = 2K \cdot \frac{x}{U}$
100	14.14	14.14
200	20.00	20.00
500	31.62	31.62
1000	44.72	44.72
1500	54.77	54.77
2000	63.25	63.25
2500	70.71	70.71
3000	77.46	77.46
4000	89.44	89.44

Note: The results are identical indicating that the program is working O.K.

## APPENDIX D

A Discussion on Abrupt Slope Changes in Numerically  
Computed  $\sigma_y$  curves

In this appendix, an attempt has been made to explain two points which one may observe in numerically computed  $\sigma_y$  curves given in Figures 4.1, 4.3, 4.4, 4.7, 4.8, 4.9, 4.12-4.15 and 4.18-4.20.

- (i) abrupt slope changes at the point where cross-wind shear effect are first dominant
- (ii) large values of slopes under stable and neutral conditions.

The abrupt slope changes are due to the K-profile and happens when the plume gets to have a significant portion above A (see Figure D-1). A more realistic profile would be as dashed and would therefore show a more gradual change of slope i.e. slope change is realistic; but is over emphasized by the choice of K-profile.

Table 1 provides an approximate value of the exponents in  $\sigma_y$  variation ( $\sigma_y \sim x^s$ ) from the point where cross-wind shear effects are first important. The theoretical results given by Corrsin (1953), Saffman (1962) and Smith (1965) shows  $\sigma \propto x^{3/2}$  for horizontal relative diffusion in shear flows. Hanna (1975) found that between 100 and 400 sec. spreading of tetroon pairs was close to (travel time)<sup>3/2</sup>. Thus the value of  $s$  given in Table D-1 is overestimated relative to the previous studies. The reasons are:

- (i) due to abrupt slope changes as explained in previous paragraph.
- (ii) Uncertainties in estimation of  $K$  in upper part of boundary layer
- (iii) for small values of  $K$  ( $K \rightarrow 0$ ), the theory is not valid as shown by Saffman (1962).

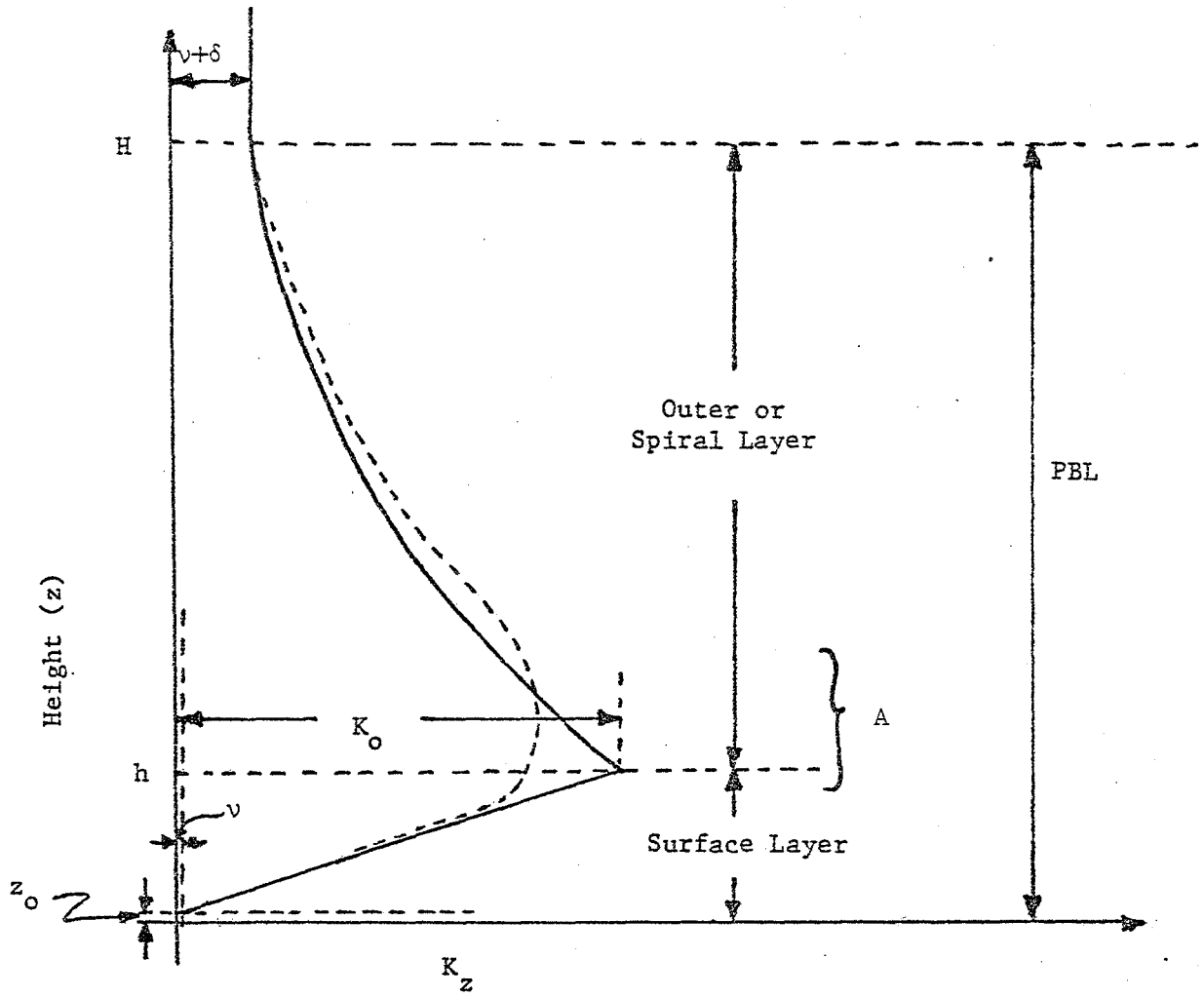


Figure D.1: K-PROFILES (SEE FIGURE 2.1)

TABLE D-1: Approximate Values of  $s$  in  $\sigma_y \sim x^s$  for Cross-Wind Shear Dominated Region

Empirical  $\sigma$ -curves

RELEASE HEIGHT	UNSTABLE	STABLE	NEUTRAL
50 m		1.7	1.3
100 m		0.7 $x < 30$ km 1.7 $x > 30$ km	1.3
200 m	0.8	1.9	1.4
300 m		2.2	1.3
500 m		8.1	1.9

Numerical  $\sigma$ -curves

RELEASE HEIGHT	UNSTABLE	STABLE	NEUTRAL
50 m	negligible	1.2	1.3
100 m	cross-wind	1.6	1.3
200 m	shear effect	2.8	1.3
500 m	for the	no wind shear	1.7
	range	observed for	
	considered	the range	
		considered	

From Table D-1, the values of  $s$  are more than 1.5 in stable cases and for a 500 m release height in neutral cases. Both the situations can be easily explained from the above points:

- (a) Stable cases: main reason is (iii); others (i) and (ii)
- (b) neutral case (500 m release): main reasons are (i) and (ii)

## APPENDIX E

## NUMERICAL SCHEME FOR THE SOLUTION OF 3-D C-D EQUATION

Various numerical schemes are available for the solution of partial differential equations (PDE). Alternating Direction Implicit methods (ADI) are powerful tools for the solution of multi-dimensional parabolic and elliptic PDE's. The ADI schemes originally introduced by Peacemear and Rachford (1955) and Douglas (1962) are intended to simplify the solution of the system of equations. The method reduces a problem of higher dimension to a series of one-dimensional problems. Hence, we only need to solve a series of tridiagonal systems of equations. A scheme similar to that given by Douglas is used in this thesis.

Equation:

$$\frac{\partial C}{\partial t} + \nabla \cdot (CV) = \frac{\partial}{\partial x} \left( K_x \frac{\partial C}{\partial x} \right) + \frac{\partial}{\partial y} \left( K_y \frac{\partial C}{\partial y} \right) + \frac{\partial}{\partial z} \left( K_z \frac{\partial C}{\partial z} \right) + Q$$

(a) Convection Term:

This term (i.e.  $\nabla \cdot (CV)$ ) is treated in the following way:

$$\nabla \cdot (CV) = \frac{\partial(UC)}{\partial x} + \frac{\partial(VC)}{\partial y} + \frac{\partial(WC)}{\partial z}$$

where,

$$\frac{\partial(UC)}{\partial x} \text{ is approximated as } \frac{U_{i+1} C_{i+1} - U_{i-1} C_{i-1}}{2 \cdot \Delta x}$$

This allows equal fluxes between the elements and thus automatically satisfies conservation of mass.

The finite difference approximation of  $\frac{\partial(UC)}{\partial x}$ , in general,

can be written as

$$\delta_x(UC) = \frac{- (1 - B) U_{i-1} C_{i-1} + (1 - 2B) U_i C_i + B U_{i+1} C_{i+1}}{\Delta x}$$

where,  $B = 0, \frac{1}{2}, 1$  correspond to backward [ $O(\Delta x)$ ; of the order  $\Delta x$ ], central [ $O(\Delta x)^2$ ], and forward [ $O(\Delta x)$ ] finite difference approximations respectively.

$B = \frac{1}{2}$  corresponds to the Central Approximation of Convection (CAC) discussed by Raithby (1976) while  $B = 0$  (for  $U > 0$ ) and  $B = 1$  ( $U < 0$ ) are equivalent to the UAC (Upstream Approximation of Convection).

For versatility and possible comparison between different schemes, the computer program for the diffusion equation used here has been written in the general form involving the parameter  $B$ . The reason for this is because the "optimum" scheme can be either CAC or UAC or a combination of both depending on the grid Peclet number (Velocity·Grid length/ $K$ ). Here "optimum" means minimizing errors due to the discretization process.

(b) ADI Scheme:

The difference equations may be written in the following way:

Step 1: Move forward in time in the x-direction

$$\begin{aligned} \frac{C_{n+1}^* - C_n}{\Delta t} + \delta_x \left( \frac{(UC^*)_{n+1} + (UC)_n}{2} \right) + \delta_y (VC)_n + \delta_z (WC)_n \\ = \delta_x^2 \left( \frac{C_{n+1}^* + C_n}{2} \right) + \delta_y^2 (C_n) + \delta_z^2 (C_n) + Q_n \end{aligned}$$

The  $i, j, k$  are suppressed.

Step 2: Same operation in y-term

$$\begin{aligned}
& \frac{C_{n+1}^{**} - C_n}{\Delta t} + \delta_x \left( \frac{(UC^*)_{n+1} + (UC)_n}{2} \right) + \delta_y \left( \frac{(VC^{**})_{n+1} + (VC)_n}{2} \right) \\
& + \delta_z (WC)_n = \delta_x^2 \left( \frac{C_{n+1}^* + C_n}{2} \right) + \delta_y^2 \left( \frac{C_{n+1}^{**} + C_n}{2} \right) \\
& + \delta_z^2 (C_n) + Q_n .
\end{aligned}$$

Step 3: Same operation in z-term

$$\begin{aligned}
& \frac{C_{n+1} - C_n}{\Delta t} + \delta_x \left( \frac{(UC^*)_{n+1} + (UC)_n}{2} \right) + \delta_y \left( \frac{(VC^{**})_{n+1} + (VC)_n}{2} \right) \\
& + \delta_z \left( \frac{(WC)_{n+1} + (WC)_n}{2} \right) = \delta_x^2 \left( \frac{C_{n+1}^* + C_n}{2} \right) + \delta_y^2 \left( \frac{C_{n+1}^{**} + C_n}{2} \right) \\
& + \delta_z^2 \left( \frac{C_{n+1} + C_n}{2} \right) + Q_n
\end{aligned}$$

Rearranging the expression obtained in Step 1, we get:

$$\begin{aligned}
& \left( \frac{1}{\Delta t} + \frac{\delta_x (U_{n+1})}{2} - \frac{\delta_x^2}{2} \right) C_{n+1}^* = \delta_x^2 \left( \frac{C_n}{2} \right) - \delta_x \left( \frac{(UC)_n}{2} \right) \\
& + (\delta_y^2 - \delta_y (V_n)) C_n + (\delta_z^2 - \delta_z (W_n)) C_n + \frac{1}{\Delta t} C_n + Q_n
\end{aligned}$$

or,

$$\begin{aligned}
& (\delta_x^2 - \delta_x (U_{n+1}) - \frac{2}{\Delta t}) C_{n+1}^* = -[\delta_x^2 - \delta_x (U_n) \\
& + 2(\delta_y^2 - \delta_y (V_n)) + 2(\delta_z^2 - \delta_z (W_n)) + \frac{2}{\Delta t}] C_n - 2 \cdot Q_n
\end{aligned}$$

Subtracting the expression of Step 1 from Step 2, we obtain:

$$\begin{aligned} & \frac{C_{n+1}^{**} - C_{n+1}^*}{\Delta t} + \delta_y \left( \frac{(UC_{n+1}^{**}) + (VC)_n}{2} \right) - \delta_y (VC)_n \\ &= \delta_y^2 \left( \frac{C_{n+1}^{**} + C_n}{2} \right) - \delta_y^2 (C_n) \end{aligned}$$

or,

$$\begin{aligned} & (\delta_y^2 - \delta_y (V_{n+1}) - \frac{2}{\Delta t}) C_{n+1}^{**} = (-\frac{2}{\Delta t}) C_{n+1}^* \\ & + (\delta_y^2 - \delta_y (V_n)) C_n \end{aligned} \tag{E-2}$$

Similarly, Step 3 and Step 1 yield

$$(\delta_z^2 - \delta_z (W_{n+1}) - \frac{2}{\Delta t}) C_{n+1} = -(\frac{2}{\Delta t}) C_{n+1}^{**} + (\delta_z^2 - \delta_z (W_n)) C_n$$

where,

$$\delta_x^2 C_{ijk} = \frac{K_{x_{i+\frac{1}{2}}} \left( \frac{C_{i+1} - C_i}{\Delta x^+} \right) - K_{x_{i-\frac{1}{2}}} \left( \frac{C_i - C_{i-1}}{\Delta x^-} \right)}{\left( \frac{\Delta x^+ + \Delta x^-}{2} \right)}$$

$$K_{x_{i \pm \frac{1}{2}}} = (K_{x_i} + K_{x_{i \pm 1}}) / 2$$

$$\Delta x^+ = x_{i+1} - x_i, \quad \Delta x^- = x_i - x_{i-1}$$

The scheme is stable and self-consistent with no convection term.

The stability of the scheme with a convection term (either using CAC or UAC) and a source term is a debatable point. However, numerical results may be obtained by specifying a particular grid size.

(c) Boundary Conditions and Solution Method:

The boundary conditions should be physically realistic and consistent with the finite difference scheme. The background concentration is set to zero i.e.

$$C(x, y, z) = 0 \quad \text{at } t = 0$$

Turbulent fluxes across the boundaries are assumed to be zero:  
i.e.

$$\frac{\partial C}{\partial x} = \frac{\partial C}{\partial y} = \frac{\partial C}{\partial z} = 0 \quad \text{at all boundaries}$$

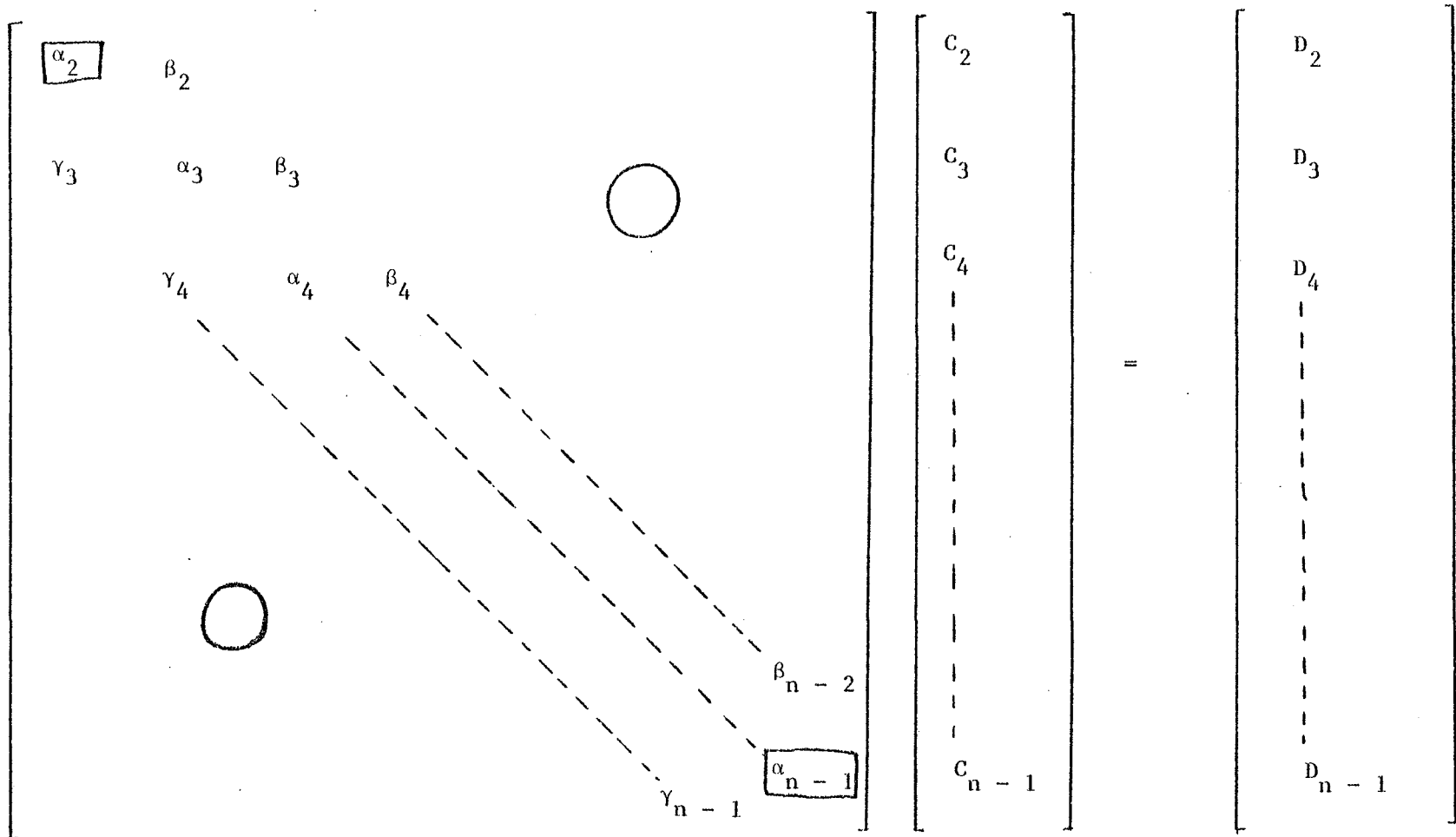
This is discretized by using forward differences: viz;

$$\frac{\partial C}{\partial x} = \frac{C_{i+1} - C_i}{\Delta x}$$

and similar expressions for  $\frac{\partial C}{\partial y}$  and  $\frac{\partial C}{\partial z}$

Equations (E-1), (E-2) and (E-3) represent a tridiagonal system of equations (see figure E-1) and may be solved by the Thomas Algorithm. While performing computations using equations (E-1) and (E-2), intermediate solutions are obtained for each grid line in the x-and y-directions. On the other hand the solution of equation (E-3) yields the result for every grid line in the z-direction. The direction of computation is altered in each step (x-direction to y-direction to z-direction). Some of the elements of the matrix are changed to accommodate the boundary conditions (see figure E-1).

Figure E-1 MATRIX FORM OF EQUATIONS



Elements effected by B.C.

$$\alpha_2 = \alpha_2 + \gamma_2$$

$$\alpha_{n-1} = \alpha_{n-1} + \beta_{n-1}$$

## REFERENCES

## CHAPTER I

Carpenter, S.B. et.al., 1971, Principal Plume Dispersion Models: TVA Power Plants, J. Air Pollut. Control. Ass., Vol. 23, pp. 491-495.

Wigley, T.M.L. and P.R. Slawson, 1975, The Effect of Atmospheric Conditions on the Length of Visible Cooling Tower Plumes, Atmos. Environ., Vol. 9., pp. 437-495.

## CHAPTER II

Batchelor, G.K., 1950, Application of the Similarity Theory of Turbulence to Atmospheric Diffusion, QJRMS, 76, pp. 133-146.

Blackadar, A.K., 1962, The Vertical Distribution of Wind and Turbulent Exchange in a Neutral Atmosphere, J. Geophys. Res., 67, pp. 3095-3102.

Blackadar, A.K. and J. Ching, 1965, Wind Distribution in a Steady State Planetary Boundary Layer of the Atmosphere with Upward Heat Flux, Final Rept., Contract AF. (604)-6641, Dept. of Meteorology, Penn. State University, pp. 23-44.

Blackadar, A.K. and H. Tennekes, 1968, Asymptotic Similarity in Neutral Barotropic PBL, J. Atmos. Sci., Vol. 25, pp. 1015-1022.

Brown, R.A., 1974, Analytical Methods in PBL Modelling, Chapter 8 John Wiley Inc. & Sons, N.Y.

Businger, J.A., 1973, Turbulent Transfer in the Atmosphere Surface Layer, Workshop on Micrometeorology, AMS, pp. 67-100.

Clarke, R.H., 1970, Observational Studies of the Atmospheric Boundary Layer, QJRMS., Vol. 96, pp. 91-114.

Clarke, R.H. and G.D. Hess, 1974, Geostrophic Departure and the Functions A and B of Rossby-Number Similarity Theory, Boundary Layer Meteor., Vol. 7, pp. 267-287.

Csanady, G.T., 1967, On the Resistance Law of a Turbulent Ekman Layer, J. Atmos. Sci., Vol. 24, pp. 467-471.

Csanady, G.T., 1972, Geostrophic Drag, Heat and Mass Transfer Coefficient for the Diabetic Ekman Layer, J. Atmos. Sci., Vol. 29, pp. 488-496.

- Deardroff, J.W., 1970, A Three Dimensional Numerical Investigation of the Idealized Planetary Boundary Layer, Geophys. Fluid. Dyn., Vol. 1, pp. 377-410.
- Deardroff, J.W., 1972, Numerical Investigation of Neutral and Unstable Planetary Boundary Layers, J. Atmos. Sci., Vol. 29, pp. 91-115.
- Deardroff, J.W., 1973, Three-Dimensional Numerical Modelling of the Planetary Boundary Layer, Chapter 7, Workshop on Micro-meteorology, American Meteorological Society, pp. 271-311.
- Donaldson, C.P., 1973, Construction of a Dynamic Model of the Production of Atmospheric Turbulence and the Dispersal of Atmospheric Pollutants, ibid, pp. 313-392.
- Dyer, A.J. and B.B. Hicks, 1970, Flux-gradient Relationships in the Constant Flux Layer, QJRMS, Vol. 96, pp. 715-721.
- Dyer, A.J., 1974, A Review of Flux-Profile Relationships, Bound. Layer Meteor., Vol. 7, pp. 363-372.
- Ekman, V.W., 1905, On the Influence of the Earth's Rotation on Ocean Currents, Arkiv., Math. Astros. Fyjik, Vol. 2, II.
- Estoque, M.A., 1963, A Numerical Model of the Atmospheric Boundary Layer, J. Geophys. Res., Vol. 68, pp. 1103-1113.
- Estoque, M.A. and C.M. Bhuralkar, 1970, A Method for Solving the Planetary Boundary Layer Equations, Boundary Layer Meteor., Vol. 1, pp. 169-194.
- Estoque, M.A., 1973, Numerical Modelling of the Planetary Boundary Layer, AMS Workshop on Micrometeorology, pp. 217-270.
- Gill, A.E., 1967, The Turbulent Ekman Layer, Department of Applied Mathematics and Theoretical Physics, University of Cambridge.
- Haltiner, G.J. and F.L. Martin, 1957, Dynamical and Physical Meteorology, McGraw-Hill, N.Y.
- Hanna, S.R., 1969, Characteristics of Winds and Turbulence in the Planetary Boundary Layer, U.S. Department of Commerce, ESSA, Air Resources Laboratories Tech. Memo, No. 8, 61 pp., Oak Ridge Tennessee.
- Hanna, S.R., 1969, The Thickness of the Planetary Boundary Layer Atmos. Environ., Vol. 3, pp. 519-536.
- Holton, J.R., 1972, An Introduction to Dynamic Meteorology, Academic Press, N.Y.
- Howroyd, G.C. and P.R. Slawson, 1975, The Characteristics of a Laboratory Produced Turbulent Ekman Layer, Boundary Layer Meteorol., Vol. 8, pp. 201-220.

- Huang, C.H. 1975, The Dynamic Atmospheric Structure and the Velocity Defect Profiles in the Boundary Layer of a Neutral Atmosphere, Boundary-Layer Meteor., Vol. 9, pp. 391-409.
- Kazanskii, A.B. and A.S. Monin, 1960, A Turbulent Regime Above the Ground Atmosphere Layer, Izv. Akod. Navkssr. Ser. Geophys., Vol. I, pp. 165-168.
- Kazanskii, A.B. and A.S. Monin, 1961, On the Dynamical Interaction Between the Atmosphere and the Earth's Surface, Bull. Acad. Sci. USSR, Ser. Geophys., Vol. 5, pp. 786-788.
- Krishna, K., 1968, A Numerical Study of the Diurnal Variation of Meteorological Parameters in the Planetary Boundary Layer, Mon. Wea. Rev., Vol. 96, pp. 269-276.
- Lettau, H.H., 1959, Wind Profile, Surface Stress and Geostrophic Drag Coefficients, Advances in Geophysics, Vol. 6, Atmospheric Diffusion and Air Pollution, pp. 241-256, Academic Press, N.Y.
- Lettau, H.H., 1962, Theoretical Wind Spirals in the Boundary Layer of a Barotropic Atmosphere, Beltr. Phys. Atmos., Vol. 35, pp. 195-212.
- Lettau, H.H. and B. Davidson, 1957, Exploring the Atmosphere's First Mile, Vol. 1, pp. 578, Pergamon.
- Lumley, J.L. and B. Khajeh-Nouri, 1974, Computational Modelling of Turbulence Transport, Advan. Geophys. 18 A, Academic Press, N.Y., pp. 169-192.
- Misra, P.K., 1975, Improved Techniques for Large Scale Dispersion, Unpublished Ph.D. thesis, University of Waterloo, Waterloo.
- Misra, P.K., 1976, A Variable-K Planetary Boundary Layer Model, Atomic Energy of Canada Ltd., Pinawa, Manitoba, AECL - 5396, Jan.
- Moore, D.J., 1975, A Simple Boundary Layer Model for Predicting Time Mean Ground Level Concentrations of Material Emitted from Tall Chimneys (unpublished).
- Ohmstede, W.D. and J.R. Appleby, 1964, Numerical Solution of the Distribution of Wind and Turbulence in the PBL, Meteor, Res. Note No. 8, DA Task 1-A-0-11001-B-021-08. USAE RDAA MET - 5-64, pp. 43.
- Prandtl, L., 1932, Meteorologische Anwendung der Stromungslehre, Beitr. Phys. Atmos., Bjerkness Festschrift, Vol. 188.
- Priestley, C.H.B., 1954, Convection from a Large Horizontal Surface, Australian J. Phys., Vol. 6, pp. 279-290.
- Sasmori, T., 1970, A Numerical Study at Atmospheric and Solid Boundary Layers, J. Atmos. Sci., Vol. 27, pp. 1122-1137.

- Spiegel, E.A. and G. Veronis, 1960, On the Boussinesq Approximation for a Compressible Fluid, Astrophys. J., Vol. 131, pp. 442-447.
- Swinbank, W.C., 1974, The Geostrophic Drag Coefficient, Boundary-Layer Meteor., Vol. 7, pp. 125-127.
- Taylor, P.A., 1969, On Planetary Boundary Layer Flow Under Conditions of Neutral Thermal Stability, J. Atmos. Sci., Vol. 26, pp. 427-431.
- Taylor, P.A., 1970, A Model of Airflow Above Changes in Surface Heatflux Temperature and Roughness for Neutral and Unstable Conditions, Boundary-Layer Meteor., Vol. 1, pp. 18-39.
- Taylor, P.A. and Y. Delage, 1971, A Note on Finite Differencing Schemes for the Surface and Planetary Boundary Layers, Boundary-Layer Meteor., Vol. 2, pp. 108-131.
- Wagner, N.K., 1966, A 2-D, Time Dependent Numerical Model of Atmospheric Boundary-Layer Flow Over Inhomogeneous Terrain, Ph.D. Thesis, University of Hawaii.
- Wanagaard, J.C. and O.R. Cote, 1974, A Planetary Boundary Layer Model, Symposium on Atmospheric Diffusion and Air Pollution, Santa Barbara, Calif., Sep. 9-13, AMS, pp. 23-24.
- Wipperman, F., 1970, The Two Constants in the Resistance Law for a Neutral Barotropic Boundary Layer of the Atmosphere, Beiträge zur Physik der Atmosphäre, 43 Band, pp. 133-140.
- Wipperman, F., 1972, Baroclinic Effects on the Resistance Law of the Planetary Boundary Layer of the Atmosphere, Beiträge Phys. Atmos., Vol. 45, pp. 244-259.
- Wipperman, F., 1973, The Planetary Boundary-Layer of the Atmosphere, Deutscher Wetterdienst Offenbach A.M.

### CHAPTER III

- Briggs, G.A., 1969, Plume Rise, AEC Critical Review Series.
- Briggs, G.A., 1975, Plume Rise Predictions, Lectures on Air Pollution and Environmental Impact Analysis, AMS, Chapter-3, pp. 59-111.
- Bringfelt, B., 1969, A Study of Buoyant Chimney Plumes in Neutral and Stable Atmospheres, Atmos. Environ., Vol. 3, pp. 609-623.
- Cadle, R.C., 1975, Volcanic Emissions of Halides and Sulfur Compounds to the Troposphere and Stratosphere, Journal of Geophysical Research, Vol. 80, #12, pp. 1650-1652.

- Csanady, G.T., 1971, Bent-Over Vapor Plumes, J. Appl. Meteor., Vol. 10, pp. 36-42.
- Csanady, G.T., 1973, Effect of Plume Rise on Ground Level Pollution, Atmos. Environ., Vol. 7, pp. 1-16.
- Hanna, S.R., 1972, Rise and Condensation of Large Cooling Tower Plumes, J. Appl. Meteor., Vol. 11, pp. 793-799.
- Hanna, S.R., 1976, Predicted and Observed Cooling Tower Plume Rise and Visible Plume Length at the John F. Amos Power Plant, Atmos. Environ., Vol. 10, pp. 1043-1052.
- Moore, D.J., 1966, Physical Aspects of Plume Models, Int. J. Air - Water Poll., Vol. 10, pp. 411.
- Morton, B.R., G.I. Taylor and J.S. Turner, 1956, Turbulent Gravitational Convection from Maintained and Instantaneous Sources, Proc. Roy. Soc., Vol. A23, pp. 1.
- Morton, B.R., 1957, Buoyant Plumes in a Moist Atmosphere, J. Fluid Mech., Vol. 2, pp. 127-144.
- Morton, B.R., 1971, The Choice of Conservation Equations for Plume Models, J. Geophysical Res., Vol. 76, No. 30, pp. 7409-7416.
- Ooms, G., 1972, A New Method for the Calculation of the Plume Path of Gases Emitted by a Stack, Atmos. Environ., Vol. 6, #12, pp. 899-909.
- Pratte, B.D. and W.D. Baines, 1967, Profiles of the Round Turbulent Jet in a Crossflow, Proc. A.S.C.E.J. Hydraulics Div., Vol. 93, No. HY6, pp. 53-64.
- Priestley, C.H.B. and F.K. Ball, 1955, Continuous Convection from an Isolated Source of Heat, QJRMS, Vol. 81, pp. 144-157.
- Richards, J.M., 1971, Simple Expression for the Saturation Vapour Pressure of Water in the Range  $-50^{\circ}$  to  $140^{\circ}$ , J. Phys. Serv., D4, L15-L18.
- Richards, J.M., 1973, The Stability of Wet and Dry Bent-Over Plumes J. Appl. Meteor., Vol. 12, pp. 133-139.
- Schmidt, W., 1941, Turbulent Propagation of a Stream of Heated Air, Z. Angew. Math. Mech., Vol. 21, pp. 351-363.
- Slawson, P.R. and G.T. Csanady, 1967, On the Mean Path of Buoyant, Bent-Over Chimney Plumes, J. Fluid Mech., Vol. 2B, pp. 311-322.
- Slawson, P.R. and G.T. Csanady, 1971, The Effect of Atmospheric Conditions on Plume Rise, J. Fluid Mech., Vol. 47, pp. 33-49.

- Slawson, P.R. and T.M.L. Wigley, 1975, Drift Analysis for the Hartsville Nuclear Power Plant,
- Spiegel, E.A. and G. Veronis, 1960, On the Boussinesq Approximation for a Compressible Fluid, Astrophys. J., Vol. 131, pp. 442-447.
- Strauss, W., 1966, Industrial Gas Cleaning, Pergamon.
- Weil, J.C., 1974, The Rise of Moist, Buoyant Plumes, J. Appl. Meteor., Vol. 13, pp. 435-443.
- Weir, A., et. al., 1976, Factors Influencing Plume Opacity, Environmental Science and Technology, Vol. 10, #6, pp. 539-544.
- Westlin, P.R., D.L. Brenchley and P.J. Smith, 1972, An Empirical Study of the Length of Cooling Tower Plumes, Air Pollution Control Assoc., 65th Annual Meeting, Miami Beach, Florida.
- Wigley, T.M.L. and P.R. Slawson, 1971, On the Condensation of Buoyant, Moist, Bent-Over Plumes, J. Appl. Meteor., Vol. 10, pp. 253-259.
- Wigley, T.M.L. and P.R. Slawson, 1972, A Comparison of Wet and Dry Bent-Over Plumes, J. Appl. Meteor., Vol. 11, pp. 335-340.
- Wigley, T.M.L., 1974, Comments On: A Simple but Accurate Formula for the Saturation Vapour Pressure Over Liquid Water, J. Appl. Meteor., Vol. 13, pp. 608.
- Wigley, T.M.L., 1975, Condensation in Jets, Industrial Plumes and Cooling Tower Plumes, J. Appl. Meteor., Vol. 14, pp. 78-86.
- Wigley, T.M.L., 1975, A Numerical Analysis of the Effect of Condensation on Plume Rise, J. Appl. Meteor., Vol. 14, No. 6, pp. 1105-1109.

## CHAPTER IV

- Aries, R., 1956, On the Dispersion of a Solute in a Fluid Flowing Through a Tube, Proc. Roy. Soc. (London), A235, pp. 67-77.
- Barad, M.L. (Ed.), 1958, Project Prairie Grass, A Field Program in Diffusion, Geophysical Research Papers, No. 59, Vols. I and II, Report AF CRC-TR-58-235, Air Force Cambridge Research Center.
- Berlyand, M.E. (Ed.), 1973, Air Pollution and Atmospheric Diffusion, John Wiley & Sons, N.Y.

- Berlyand, M.E., 1972, Investigation of Atmospheric Diffusion Providing a Meteorological Basis for Air Pollution Control, Atmos. Environ., Vol. 6, pp. 379-388.
- Brown, R.M. and P. Michael, 1974, Measured Effect of Shear on Plume Dispersion, Symposium on Atmospheric Diffusion and Air Pollution, (AMS), Sept. 9-13, Santa Barbara, Calif., pp. 246-250.
- Businger, J.A., 1973, Turbulent Transfer in the Atmospheric Surface Layer, AMS Workshop on Micrometeorology, pp. 67-100.
- Carpenter, S.B., et. al., 1971, Principal Plume Dispersion Models: TVA Power Plants, J. Air. Pollut. Control Assoc., Vol. 23, pp. 491-495.
- Crozier, W.D. and B.K. Seely, 1955, Concentration Distributions in Aerosol Plumes Three to Twenty Two Miles from a Point Source, Trans. Amer. Geophys. Union, Vol. 36, pp. 42.
- Csanady, G.T., 1968, Diffusion in an Ekman Layer, J. Atmos. Sci., Vol. 26, pp. 414-426.
- Csanady, G.T., 1972, Crosswind Shear Effects on Atmospheric Diffusion, Atmos. Environ. Vol. 6, #3, pp. 221-232.
- Csanady, G.T., 1973, Effect of Plume Rise on Ground Level Pollution, Atmos. Environ., Vol. 7, pp. 1-16.
- Csanady, G.T., 1973, Turbulent Diffusion in the Natural Environment, Reidel.
- Danard, M.B., 1972, Numerical Modelling of Carbon Monoxide Concentrations Near Highways, J. Appl. Meteor., Vol. 11, No. 6, pp. 947-957.
- Draxler, R.R., 1976, Determination of Atmospheric Diffusion Parameters, Atmos. Environ., Vol. 10, pp. 99-105.
- Egan, B.A. and J.R. Mahoney, 1972, Numerical Modelling of Advection and Diffusion of Urban Area Source Pollutants, J. Appl. Meteor., Vol. 11, pp. 312-322.
- Gillani, N.V. and R.B. Husar, 1975, Mathematical Modelling of Air Pollution - A Parametric Study, Proceedings of the Second Federal Conference on the Great Lakes, Argonne National Laboratory, U.S.A., March 25-27.
- Gifford, F.A., 1976, Turbulent Diffusion-Typing Schemes: A Review, Nuclear Safety, Vol. 17, #1, pp. 68-86.
- Hino, M., 1968, Computer Experiment on Atmospheric Diffusion Over a Complicated Topography, Atmos. Environ., Vol. 2, pp. 541-558.

- Hogstrom, U., 1964, An Experimental Study on Atmospheric Diffusion, Tellus, Vol. 16, pp. 205-251.
- Hosker, R.P., 1974, A Comparison of Estimation of Procedures for Over-Water Plume Dispersion, AMS Symposium on Atmos. Diffusion and Air Pollution, pp. 281-287.
- Lantz, R.B., 1972, Application of Three Dimensional Numerical Model to Air Pollutant Calculations, APCA Annual Meeting (65th), Miami, Fla., June 18-22, 1972 paper no. 72-141.
- Lebedeff, S.A. and S. Hameed, 1975, Study of Atmospheric Transport Over Area Sources by an Integral Method, Atmos. Environ., Vol. 9, pp. 333-338.
- MacCready, P.B., L.B. Baboolad, and P.B.S. Lissaman, 1974, Diffusion and Turbulence Aloft Over Complex Terrain, AMS Symposium on Atmos. Diffusion and Air Pollution, pp. 218-225.
- Pasquill, F., 1961, The Estimation of the Dispersion of Wind Borne Material, Met. Mag., Vol. 90, pp. 33-49.
- Pasquill, F., 1962, Atmospheric Diffusion, D.V.M. Co. Ltd., N.Y.
- Pasquill, F., 1962, Some Observed Properties of Medium-Scale Diffusion in the Atmosphere, QJRMS, Vol. 88, pp. 70-79.
- Pasquill, F., 1969, The Influence of the Turning of the Wind with Height on Crosswind Diffusion, Phil. Trans. Roy. Soc., London, Vol. A265, pp. 173-181.
- Pasquill, F., 1971, Atmospheric Dispersion of Pollution, QJRMS, Vol. 97, pp. 369-395.
- Pasquill, F., 1976, Atmospheric Dispersion Parameters in Gaussian Plume Modelling Part II, PB-258-036, EPA.
- Paulson, C.A., 1970, The Mathematical Representation of Wind Speed and Temperature Profiles, JAM, Vol 9, pp. 857-861.
- Ragland, K.W. and R.L. Dennis, 1975, Point Source Atmospheric Diffusion Model with Variable Wind and Diffusivity Profiles, Atmos. Environ., Vol. 9, pp. 175.
- Ragland, K.W., 1976, Worst-Case Ambient Air Concentrations from Point Sources Using the Gaussian Plume Model, Atmos. Environ., Vol. 10, pp. 371-374.
- Randerson, D., 1970, A Numerical Experiment in Simulating the Transport of SO<sub>2</sub> Through the Atmosphere, Atmos. Environ., Vol 4, pp. 615-632.
- Roberts, O.F.T., 1923, The Theoretical Scattering of Smoke in a Turbulent Atmosphere, Proc. Roy. Soc., A Vol. 245, pp. 640.

- Roffman, A. and R. Grimble, 1974, A Time-Dependent Air Quality Model with Terrain Corrections, Symposium on Atmospheric Diffusion and Air Pollution, AMS, Sept. 9-13, Santa Barbara, Calif., pp. 311-316.
- Rounds, W., 1955, Solutions of the Two-Dimensional Diffusion Equations, Trans. Amer. Geo. Union, Vol. 36, No. 2, pp. 395.
- Runca, E. and Sardei, F., 1975, Numerical Treatment of Time Dependent Advection and Diffusion of Air Pollutants, Atmos. Environ., Vol. 9, pp. 69-80.
- Saffman, P.G., 1962, The Effect of Wind Shear on Horizontal Spread from an Instantaneous Ground Source, QJRMS, Vol. 88, pp. 382-393.
- Sethuraman, S., R.M. Brown, and J. Tichler, 1974, Spectra of Atmospheric Turbulence Over the Sea During Stably Stratified Conditions, AMS Symposium on Atmos. Diffusion and Air Pollution, pp. 71-76.
- Shir, C.C., 1970, A Pilot Study in Numerical Techniques for Predicting Air Pollutant Distribution Downwind from a Linestack, Atmos. Environ., Vol. 4, pp. 387.
- Slade, D.H. (Ed.), 1968, Meteorology and Atomic Energy, U.S. Atomic Energy Commission/Division of Technical Information.
- Smith, F.B., 1965, The Role of Wind Shear in Horizontal Diffusion of Ambient Particles, QJRMS, Vol. 91, pp. 318-329.
- Smith, F.B., 1972, A Scheme for Estimating the Vertical Dispersion from a Source near Ground, Proceedings NATA/CCMS third meeting.
- Smith, M.E. and I.A. Singer, 1965, An Improved Method for Estimating Concentrations and Related Phenomena from a Point Source Emission, USAEC Report BNL-9700, Brookhaven National Laboratory.
- Sutton, O.G., 1947, The Theoretical Distribution of Airborne Pollution from Factory Chimneys, QJRMS, Vol. 73, pp. 426-436.
- Sutton, O.G., 1952, Micrometeorology, McGraw-Hill, N.Y.
- Tyldesley, I.B. and C.E. Wallington, 1965, The Effect of Wind Shear and Vertical Diffusion on Horizontal Dispersion, QJRMS, Vol. 91, pp. 158-174.
- Turner, D.B., 1970, Workbook of Atmospheric Dispersion Estimates PB-191-482, U.S. Department of Health, Education and Welfare.
- Weil, J.C., 1974, Comparison Between Measured and Model-Estimated Ground-Level SO<sub>2</sub> Concentrations Downwind from the Dickerson Power Plant, Martin Marietta Laboratories.

Whaley, H., 1972, The Derivation of Plume Dispersion Parameters from Measured 3-D Data, Research Report R254, Department of Energy, Mines and Resources, Mines Branch, Ottawa.

#### CHAPTER V

Briggs, G.A., 1969, Plume Rise, AEC Critical Review Series.

Clarke, R.H. and G.D. Hess, 1974, Geostrophic Departure and the Functions A and B of Rossby-Number Similarity Theory, Boundary Layer Meteor., Vol. 7, pp. 267-287.

Slawson, P.R. and G.T. Csanady, 1971, The Effect of Atmospheric Conditions on Plume Rise, J. Fluid Mech., Vol. 47, pp. 33-49.

#### APPENDIX

Corrsin, S. 1953: Remarks on turbulent heat transfer, Proc. First Iowa Symp., University of Iowa, Iowa City, 5-30.

Douglas, J., 1962, Alternating Direction Methods for Three Space Variables, Numerische Mathematik, Vol. 4, pp. 41-63.

Hanna, S.R. 1975: Relative diffusion of tetroon pairs during convective conditions. Paper presented at First Conf. Regional and Mesoscale Modeling, Analysis and Prediction, Las Vegas, Nev. AMS.

Peaceman, D.W. and H.H. Rachford, 1955, The Numerical Solution of Parabolic and Elliptic Differential Equations, J. Soc. Ind. Appl. Math., Vol. 3, pp. 28-41.

Raithby, G.D., 1976, A Critical Evaluation of Upstream Differencing Applied to Problems Involving Fluid Flow, Computer Methods in Applied Mechanics and Engineering, Vol. 3, pp. 75-103.

Raithby, G.D., 1976, Skew Upstream Differencing Schemes for Problems Involving Fluid Flow, Computer Methods in Applied Mechanics and Engineering, Vol. 9, pp. 153-164.

## Conditions of Use

Kumar, A., 1978. Pollutant dispersion in the planetary boundary layer. Syncrude Canada Ltd., Edmonton, Alberta. Professional Paper 1978-1. 182 pp.

Permission for non-commercial use, publication or presentation of excerpts or figures is granted, provided appropriate attribution (as above) is cited. Commercial reproduction, in whole or in part, is not permitted without prior written consent.

The use of these materials by the end user is done without any affiliation with or endorsement by Syncrude Canada Ltd. Reliance upon the end user's use of these materials is at the sole risk of the end user.